NASA TECHNICAL NOTE

NASA TN D-8378

EFFECTS OF ROTOR MODEL DEGRADATION ON THE ACCURACY OF ROTORCRAFT REAL-TIME SIMULATION

Jacob A. Houck and Roland L. Bowles

Langley Research Center
Hampton, Va. 23665

NATIONAL AERONAUTICS AND SPACE ADMINISTRATION • WASHINGTON, D. C. • DECEMBER 1976

1. Report No.	2. Government Accession No.	3. Recipient's Catalog No.
NASA TN D-8378		

4. Title and Subtitle
EFFECTS OF ROTOR MODEL DEGRADATION ON THE ACCURACY OF ROTORCRAFT REAL-TIME SIMULATION

5. Report Date
December 1976

6. Performing Organization Code

7. Author(s)
Jacob A. Houck and Roland L. Bowles

8. Performing Organization Report No.
L-11083

9. Performing Organization Name and Address
NASA Langley Research Center
Hampton, VA 23665

10. Work Unit No.
745-01-01-01

11. Contract or Grant No.

12. Sponsoring Agency Name and Address
National Aeronautics and Space Administration
Washington, DC 20546

13. Type of Report and Period Covered
Technical Note

14. Sponsoring Agency Code

15. Supplementary Notes
Part of the information presented herein was included in a thesis entitled "Computational Aspects of Real-Time Simulation of Rotary Wing Aircraft" submitted by Jacob Albert Houck in partial fulfillment of the requirements for the degree of Master of Science, The George Washington University, Hampton, Virginia, May 1976.

16. Abstract

A study was conducted to determine the effects of degrading a rotating blade element rotor mathematical model to meet various real-time simulation requirements of rotorcraft. Three methods of degradation were studied: reduction of number of blades, reduction of number of blade segments, and increasing the integration interval, which has the corresponding effect of increasing blade azimuthal advance angle. The three degradation methods were studied through static trim comparisons, total rotor force and moment comparisons, single blade force and moment comparisons over one complete revolution, and total vehicle dynamic response comparisons. Recommendations are made concerning model degradation which should serve as a guide for future users of this mathematical model, and in general, they are in order of minimum impact on model validity: (1) reduction of number of blade segments, (2) reduction of number of blades, and (3) increase of integration interval and azimuthal advance angle. Extreme limits are specified beyond which the rotating blade element rotor mathematical model should not be used.

17. Key Words (Suggested by Author(s))	18. Distribution Statement
Rotor mathematical model degradation Real-time simulation Rotary wing Helicopters	Unclassified - Unlimited Subject Category 05

19. Security Classif. (of this report)	20. Security Classif. (of this page)	21. No. of Pages	22. Price*
Unclassified	Unclassified	90	$4.75

* For sale by the National Technical Information Service, Springfield, Virginia 22161

EFFECTS OF ROTOR MODEL DEGRADATION ON THE ACCURACY OF ROTORCRAFT REAL-TIME SIMULATION*

Jacob A. Houck and Roland L. Bowles
Langley Research Center

SUMMARY

A study was conducted to determine the effects of degrading a rotating blade element rotor mathematical model to meet various real-time simulation requirements of rotorcraft. Three methods of degradation were studied: reduction of number of blades, reduction of number of blade segments, and increasing the integration interval, which has the corresponding effect of increasing blade azimuthal advance angle. The three degradation methods were studied through static trim comparisons, total rotor force and moment comparisons, single blade force and moment comparisons over one complete revolution, and total vehicle dynamic response comparisons. Recommendations are made concerning model degradation which should serve as a guide for future users of this mathematical model, and in general, they are in order of minimum impact on model validity: (1) reduction of number of blade segments, (2) reduction of number of blades, and (3) increase of integration interval and azimuthal advance angle. Extreme limits are specified beyond which the rotating blade element rotor mathematical model should not be used.

INTRODUCTION

In view of the expanding interest in helicopter research and development in the past decade at the Langley Research Center, several real-time man-in-the-loop helicopter simulation programs have been developed for the Langley real-time simulation (RTS) facility. (See ref. 1.) The simulations have been used as analytical tools for man and vehicle performance evaluation and in support of flight-test programs. These studies have included flight director development, development and evaluation of advanced heads-up computer-generated displays, route structure development for intercity transportation, evaluation of terminal area navigation and approach procedures, motion-visual research, and mathematical model research and development. The rotorcraft mathematical models employed in these studies have varied from simple linear perturbation models to full force and moment models including rotating blade element rotor models.

An effort to adapt and evaluate a helicopter mathematical model for real-time simulation, including a state-of-the-art rotor model, was initiated in 1974

*Part of the information presented herein was included in a thesis entitled "Computational Aspects of Real-Time Simulation of Rotary Wing Aircraft" submitted by Jacob Albert Houck in partial fulfillment of the requirements for the degree of Master of Science, The George Washington University, Hampton, Virginia, May 1976.

to support the rotor research planned at the Langley Research Center. This model (ref. 1) represents the Rotor Systems Research Aircraft (RSRA). The RSRA is a flying test platform to be used in the evaluation of advanced rotor and control systems. The RSRA mathematical model was derived from a general helicopter simulation model which has been used extensively in nonreal time in the design of helicopters and compound vehicles. The model is basically a total-force nonlinear large-angle representation in six rigid body degrees of freedom. In addition, rotor blade flapping, lagging, and hub rotational degrees of freedom are represented. Each simulated component of the aircraft (fig. 1) is modularized within the mathematical model. This characteristic allows easy manipulation of the aircraft's configuration.

The main problem encountered when using this mathematical model for real-time man-in-the-loop simulation studies is obtaining real-time operation while using the full rotating blade element rotor model (actual number of blades and a representative number of segments for each blade). Real-time operation is reached when the computer execution time for the active portion of the program is less than or equal to the prescribed integration time interval. In the past this has been accomplished by degrading the model in various ways. The purpose of this paper is to investigate the various methods of rotor and total vehicle model degradation. This investigation includes the effects due to reducing the number of blades, reducing the number of blade segments, varying the integration interval in size which, in turn, varies the azimuthal advance angle, and combinations of the three methods. This study provides data on the effects of degrading the rotating blade element model to meet real-time computer requirements for the simulation of rotorcraft.

SYMBOLS AND ABBREVIATIONS

Measurements and calculations were made in the U.S. Customary Units. They are presented herein in the International System of Units (SI) with the equivalent values in the U.S. Customary Units given parenthetically except in computer-generated figures. When two symbols for a concept are given, the second symbol denotes the computer symbol.

b		blade
i		integers
n		total number of data points
p_b	PB	body-axis roll rate, degrees per second
$\dot{p}_b$	PBD	body-axis roll acceleration, radians per second^2
s		blade segment
Δt		integration interval, seconds
x_a	XA	lateral cyclic control position, percent of total travel

x_b	XB	longitudinal cyclic control position, percent of total travel
x_c	XC	collective control position, percent of total travel
x_i		value of ith data point, dimensionless
x_p	XP	tail rotor pedal control position, percent of total travel
y_i		nondimensional distance along blade at ith station
α		angle of attack, degrees
β	BR	blade flap angle, degrees
ζ	XLAG	blade lag angle, degrees
θ	THET	pitch attitude, degrees
μ		mean value
σ		standard deviation
ϕ	PHI	roll attitude, degrees
$\Delta\Psi$		azimuthal advance angle, degrees
Ω		rotor rotational speed, radians per second or revolutions per minute

Subscripts:

INB(n)	inboard end
OUTB(n)	outboard end

Abbreviations:

CDC	Control Data Corporation
IFR	instrument flight rules
NASA	National Aeronautics and Space Administration
VTOL	vertical take-off and landing

ROTOR MODEL DESCRIPTION

The following brief description of a blade element model for an articulated rotor system is provided. The total rotor forces and moments are developed from a combination of the aerodynamic, mass, and inertia loads acting on each simulated blade. For each blade simulated, the flapping and lagging

degrees of freedom are represented. In addition, when the rotor speed governor is disengaged, the rotor shaft degree of freedom is released. Blade element theory is used to determine the aerodynamic loads. Blade inertia, mass, and weight effects are fully accounted for in the model. The elemental aerodynamic loads, dependent on local blade angle of attack and velocity vector, are calculated for each blade segment and are summed along each blade. The blade segment definition is based on the assumption of equal annuli area and is defined in the appendix. The mass and ineria loads, dependent on blade and aircraft motion, are added to the aerodynamic loads for each blade. This summation gives the shear loads on the blade root hinge pins. Total rotor forces are obtained by summing all the blade hinge pin shears with regard to azimuth. Rotor moments result from the offset of the hinge shears from the center of the shaft. Blade flapping and lagging motion are determined from aerodynamics and inertia moments about the hinge pins. Interference effects from the rotor onto the fuselage and empennage are accounted for. The following basic assumptions are made in the rotor representation:

(1) No account is taken of rotor blade or airframe flexibility.

(2) Air mass flow degree of freedom through the rotor can be represented by applying a simple lag to the calculation of downwash. The only nonuniform flow is due to increases in forward speed which cause a redistribution of the uniform flow from the front to the back of the disk.

(3) Simple sweep theory can be applied to determine the aerodynamic effects of yawed flow on the blade element, from unyawed flow blade data.

(4) Quasi-static aerodynamic loads are assumed.

(5) The flapping and lagging blade hinges were assumed coincident.

For a more detailed treatment of the rotor model and computer program structure, the reader is directed to the appropriate sections in reference 1.

PROBLEM DESCRIPTION

This section provides an insight into the difficulties encountered with the use of this rotor mathematical model, and the methods utilized to overcome these problems. This section and the next describe the detailed study covered in this paper to evaluate these methods.

Problems have arisen in the past when using the rotating blade element model for man-in-the-loop real-time simulation applications primarily because of the inadequate computing bandwidth of current computers. In order to use this model at all, gross degradation of the rotor representation and/or integration interval size were required. This was done so that the computer execution time for the active part of the program would be less than or equal to the desired integration interval and, in other words, would achieve real-time execution. The mathematical model was developed in a nonreal-time mode to insure validity of the rotor model (see ref. 1). In the nonreal-time mode, the rotor is represented by the actual number of blades, a representative number of blade segments

to represent the blade loading adequately, the actual rotor rotational rate, and a sufficiently small azimuthal advance angle, that is, a small integration interval size. Since this type of representation precludes the achievement of real-time execution, various combinations of reduced blades, blade segments, rotor rotational rate, and increased azimuthal advance angle are required to achieve real time while still retaining "satisfactory" static and dynamic comparisons with data from the nonreal-time model. The steps necessary to reduce the mathematical model of the rotor, which accounts for a large part of the computation time, for real-time operation are not routine; however, some general guidelines do exist, and they are used as a starting point for this study. The guidelines are a minimum number of three blades, three blade segments, and a maximum of 55° of azimuthal advance as presented in reference 2.

Figure 2 shows the effect of rotor rotational speed and azimuthal update on allowable program execution time in order to prevent computational divergence of the flapping equation of motion. This is represented by the relationship, $\Delta\Psi = 57.3\Omega\ \Delta t$. Several present and future helicopters are provided for comparison. As can be seen the maximum program execution time available for the RSRA vehicle, if given a 30° azimuthal advance, is approximately 25 milliseconds. This program execution time must now be matched to the computational speed of the digital computer which is used for the simulation study.

Figure 3 presents a rotorcraft vehicle with a five-bladed rotor model with a rotational rate of 200 rpm. An azimuthal advance angle of 30° was chosen for illustrative purposes. Program execution time has been normalized to unity for the CDC 6600 computer with the ICOPS RUN compiler. The CDC CYBER 175 with the NOS FTN compiler (optimization enabled) is represented at its tested bandwidth of 3.5 times faster than the CDC 6600. Minimum blade and blade-segment boundaries are presented. The cross-hatched area represents the combinations of blades and blade segments which can be modeled on the CDC 6600. Note that the five-blade five-blade-segment representation normally used (5b × 5s) is on the borderline of achieving real time for this azimuthal advance angle and leaves no execution time for additions to the program. It can be seen that the CDC CYBER 175 would be able to handle the representation easily.

The problem at hand is that of representing a rotorcraft vehicle on a digital computer in real time with an adequate rotor mathematical model for both objective and subjective tests and with the knowledge that additional computer requirements such as visual systems, complete cockpit requirements, landing-gear models, electronic flight control computer interfacing, etc., are normally included in man-in-the-loop simulations.

The purpose of this paper is to present an expanded systematic parametric study consisting of blade reduction, blade-segment reduction, integration interval increase (that is, azimuthal advance angle increase), and combinations of the three methods of degradation. Effects on both static and dynamic solutions are presented; thus, the best method of representing the rotor system under the constraints of real-time computer duty cycle time and accuracy of solution required is determined.

TECHNICAL APPROACH

In order to study the effects of reducing number of blades, number of blade segments, and increasing integration interval size, four types of tests were conducted. They consisted of vehicle static trim comparisons, total rotor force and moment comparisons (mean and standard deviation), blade parameter comparisons for a 360° sweep, and dynamic response comparisons for the total vehicle.

The rotor mathematical model was set up with five blades and ten blade segments. A rotor speed of 200 rpm was chosen so that for the integration intervals studied, the rotor blades would always assume the same azimuthal locations for each rotation. Finally, an integration interval of 1/240 second was chosen which, in turn, caused the blade azimuthal advance angle to be 5°. This description constitutes the baseline configuration and was used as a base to which all other configurations could be compared; however, the five-blade five-blade-segment rotor is considered the standard Langley configuration.

The rotor mathematical model was degraded systematically. The number of blade segments was held constant at five and integration interval constant at 1/240 second as the number of blades was reduced. The number of blades was then held constant at five as the number of blade segments was reduced. A separate configuration which consisted of three blades and three blade segments was used to study combination effects. In order to study the effect of integration interval size, a rotor mathematical configuration with five blades and five blade segments and another with three blades and three blade segments were selected. Intervals of 1/240 second ($\Delta\Psi = 5^\circ$), 1/30 second ($\Delta\Psi = 40^\circ$), and 1/20 second ($\Delta\Psi = 60^\circ$) were chosen. The 1/30- and 1/20-second intervals were chosen for the following reasons: 1/30 second is approximately the integration interval used at the Langley Research Center for real-time simulation and 1/20 second is approximately the integration interval used by other real-time simulation facilities. The appendix describes the methods used in degrading the rotor model. Table I details all configurations used in this study.

The static trim tests were set up in the following manner. The vehicle was started at an altitude of 152.4 m (500 ft) with the rotor mathematical model set for the desired configuration. The vehicle was then trimmed at various airspeeds over the airspeed range. Two airspeeds are presented for this comparison, that of 0 knot (hover), and 120 knots (cruise). While the vehicle was stabilized at each trim airspeed, all control positions and aircraft attitudes were recorded. These consisted of collective position, longitudinal and lateral cyclic positions, pedal position, vehicle pitch and roll attitudes, and vehicle angle of attack.

The total rotor force and moment tests were set up by starting the vehicle at the trim conditions determined in the static trim tests. The vehicle was flown in straight and level trimmed flight for 5 seconds during which all forces and moments from the rotor were recorded to determine their mean steady-state value,

$$\mu = \frac{1}{n}\sum_{i=1}^{n} x_i$$

The standard deviation

$$\sigma = \sqrt{\frac{\sum_{i=1}^{n} (x_i - \mu)^2}{n - 1}}$$

of each was also computed to give some insight into how steady the forces and moments were for the trim condition. A run of 5 seconds was chosen so that enough data would be available for the calculations, whereas the inherent total vehicle instabilities would not have had enough time to contaminate the results.

To determine the individual blade parameter data with respect to azimuthal position, the 360° blade sweep tests were set up by once again starting the vehicle at the previously determined trim conditions. The vehicle was then flown in straight and level trimmed flight long enough, approximately 0.3 second, for the index blade to make one complete revolution. During the 360° revolution, data were taken at each azimuthal position achieved by the blade. Data recorded consisted of the index blade forces and moments, and blade flapping and lagging motions.

The total vehicle dynamic response tests were set up by again starting the vehicle at the trim conditions determined previously in the static trim tests. The vehicle was then flown in straight and level trimmed flight. At 1 second into the flight, a 5-percent right lateral cyclic (0 percent equals full left stick, 100 percent equals full right stick) pulse was applied for 1 second and then the stick was returned to the trim position. The run continued until either 20 seconds had elapsed or the vehicle flew into the ground, pitched up to exactly 90° (this condition causes the computer program to sustain a fatal error due to the method used for computing the Euler angles), or the rotor blade flapping went unstable (this condition also causes a fatal error in the computer program). During the 20 seconds of the test run, all pertinent vehicle states were recorded. These consisted of the total vehicle body linear and angular accelerations, linear and angular velocities, body attitudes, and blade flapping and lagging motions. The lateral axis was chosen for the dynamic tests because of the low roll inertia relative to the pitch axis, and therefore it would show more sensitivity to changes in the integration interval.

RESULTS AND DISCUSSION

Static Trim Comparisons

The vehicle was started at an altitude of 152.4 m (500 ft) and was trimmed over the speed range for the various rotor configurations. The five-blade ten-blade-segment model is presented as the baseline for all comparisons. The five-blade five-blade-segment configuration presented in each case is the standard real-time rotor configuration used at Langley Research Center. Table II presents the effect of blade reduction on static trim. As can be seen, the largest

error occurs between the five-blade ten-blade-segment configuration and the five-blade five-blade-segment configuration which can be attributed to a blade-segment-reduction effect.

Table III presents the effect of blade-segment reduction on static trim. For the airspeeds considered, the largest errors occur in collective position (x_c) and roll attitude (ϕ) when compared with the baseline configuration. These errors can be attributed to a degradation in blade aerodynamic definition.

Table IV presents the effect of combination blade and blade-segment reduction on static trim for a fixed integration interval of 1/240 second. The two cases chosen were the configuration used for the man-in-the-loop simulation at Langley and a worst possible case. Comparing these results with those of tables II and III indicates that the error in the combination reduction case comes from the blade-segment-reduction effect.

Table V presents the effect of increasing integration interval, and therefore blade azimuthal advance angle, on static trim for two rotor configurations. The integration intervals presented and their corresponding azimuthal advance angles are 1/240 second ($\Delta\Psi = 5^\circ$), 1/30 second ($\Delta\Psi = 40^\circ$), and 1/20 second ($\Delta\Psi = 60^\circ$). As in the previous cases, collective position is the largest control position error and roll angle is the largest attitude error. However, for integration interval of 1/20 second, the rotor model has deteriorated to such an extent at 120 knots that obvious errors appear in all parameters.

Total Rotor Force and Moment Comparison

The total rotor force and moment tests were set up by starting the vehicle at the trim conditions determined for each rotor configuration in the static trim tests. The vehicle was then flown in straight and level flight for 5 seconds during which the rotor forces and moments were recorded so that a mean value and standard deviation could be determined for each; thus, a performance measure is provided to compare the rotor configurations. Figures 4 and 5 present the effect of blade reduction on total rotor forces and moments for the hover and 120-knot cases, respectively. The figures show the rotor thrust, horizonal force, side force, pitching moment, rolling moment, and torque plotted against number of blades. Reducing the number of blades has little effect on the mean values; however, differences in the standard deviations can be seen, the larger differences occurring for 120 knots. In general, as forward velocity increases and the number of blades is decreased, the standard deviation increases and indicates that larger internal oscillations are occurring in the rotor which is an n/rev amplitude amplification because of the reduced number of blades.

Figures 6 and 7 present the effect of blade segment reduction on total rotor forces and moments for the hover and 120-knot cases, respectively. The figures show the forces and moments plotted against number of blade segments. For both velocities, small differences occur in the standard deviation as the number of blade segments is reduced. Differences in mean value are small, the largest error occurring in torque at 120 knots. Thus, the primary effect of reduction of blade segments on the total rotor forces and moments is a corre-

sponding reduction in rotor torque which becomes more significant at each speed as velocity increases.

Figures 8 and 9 present the effect of increasing the integration interval, and therefore the azimuthal advance angle, on total rotor forces and moments for the hover and 120-knot cases, respectively. Two rotor configurations are plotted, five-blade—five-blade segments and three-blade—three-blade segments. For both velocity cases some differences occur in the mean values of the rotor forces and moments for the five-blade—five-blade-segment configuration when increasing the integration interval from 1/240 second ($\Delta\Psi = 5^{\circ}$) to 1/30 second ($\Delta\Psi = 40^{\circ}$), the largest difference being in the rotor torque. Although there are several noticeable differences in the standard deviations, their magnitude is relatively small. When increasing to an integration interval of 1/20 second ($\Delta\Psi = 60^{\circ}$), obvious errors occur in the mean values, extremely large errors occurring in the rotor moments, especially for 120 knots. Correspondingly, extremely large increases in the standard deviations occur. The three-blade—three-blade-segment configuration tends to follow the same trends; however, in general, this configuration shows larger differences in the standard deviation values, these larger differences being due to the additional combined effects of reducing the number of blades and blade segments.

360° Blade Sweep Comparison

The 360° blade sweep test was set up by starting the vehicle at the previously determined trim conditions. The index blade was allowed to make one complete revolution. During this revolution, data were taken at each azimuthal position achieved by the blade. Data recorded consisted of blade forces and moments, and blade flapping and lagging motions. Since reducing the number of blades has no meaning in this test (the index blade is always present in any configuration), no data are presented.

Figure 10 presents the effect of blade segment reduction on blade parameters for one revolution at 120 knots. Only very slight differences are apparent, the most prominent difference being a fairly constant reduction in torque over the entire 360° revolution. The data gathered for the hover case show no difference in any of the parameters except for a slight change in torque.

Figure 11 presents the effect of increasing integration interval to 1/30 second and 1/20 second on blade parameters for one revolution at 120 knots. For the case of integration interval of 1/30 second, slight differences exist in flap angle (β), thrust, pitching moment, and rolling moment. A constant bias exists in lag angle of approximately 0.5°. The largest error exists in torque which shows a relatively constant lower value except for a very small portion of the sweep where it assumes a higher value. For the hover case, only a slight difference in torque was apparent.

For the case of integration interval of 1/20 second, errors are apparent in all the parameters, only side force and horizontal force representing the baseline solution. The largest errors exist in lag angle which shows a relatively constant 4° bias, and torque which shows a value extremely lower than that of the baseline solution. For the hover case, slight differences appear in

all parameters except for lag angle which shows a bias of 1°, and torque which, in general, is below the baseline solution.

Dynamic Response Comparison

The total vehicle dynamic response tests were set up by starting the vehicle at the trim conditions determined previously in the static trim tests. At 1 second into the flight, a 5-percent 1-second lateral cyclic pulse was applied. During the test run, all pertinent vehicle states, such as linear and angular accelerations and velocities, body attitudes, and blade flapping and lagging motions, were recorded. Of these states, body roll acceleration ($\dot{p}_b$), body roll rate (p_b), roll angle (ϕ), and blade flap angle (β) are presented for illustration of the effects of the various mathematical model degradations. Each case presented is compared with the baseline rotor to illustrate these effects.

Time-history comparisons (ref. 1) of a five-blade—five-blade-segment rotor and five-blade three-blade-segment rotor with the five-blade—ten-blade-segment baseline rotor at the hover and 120-knot conditions show no difference.

Figure 12 presents the effect of blade reduction on vehicle dynamic response at 120 knots. The case represented is that of a three-blade five-blade-segment rotor compared with the baseline rotor. The effect of the reduction of number of blades is very apparent in the roll acceleration and roll rate curves. The mathematical model amplifies the rotor response when it scales the rotor forces and moments for the correct number of blades in the rotor system. The high-frequency oscillation in roll acceleration affects the roll rate but has an insignificant effect on roll attitude because of the small integration interval. The hover case shows the same effects, however, to a smaller degree.

Figure 13 presents the effect of combination blade and blade-segment reduction on vehicle dynamic response for 120 knots. It can be seen by comparing this figure with figure 12 and data in reference 1 that most of the difference between the three-blade—three-blade-segment rotor and the baseline rotor comes from the reduction in number of blades, and that blade-segment reduction has relatively no effect.

Figure 14 presents the effect of increasing integration interval from 1/240 second to 1/30 second on vehicle dynamic response at 120 knots. The rotor configuration considered is the five-blade—five-blade-segment rotor and again, it is compared with the baseline rotor. There is now an oscillation in roll acceleration which approaches 0.3 rad/sec^2. This effect is due to a combination of aerodynamic definition in the rotor and numerical solution and is analogous to a continual control input into the rotor model. As the vehicle goes to higher forward velocities, the amplitude of this oscillation will increase and more of its effect will filter through the body numerical integrators to roll rate and roll angle. The oscillation shown in figure 14 is apparent in roll rate and can just barely be seen in the roll angle. The average value of roll rate has been affected, and the vehicle has rolled to 15° some 2 seconds faster than the baseline vehicle. The blade flapping tends to smooth itself out in amplitude instead of following the anticipated response as depicted by the baseline rotor.

Figure 15 presents the data for the hover case. The same trends are apparent, but to a smaller extent.

Figure 16 presents the effect of increasing integration interval from 1/240 second to 1/30 second on vehicle dynamic response at 120 knots for the three-blade—three-blade-segment rotor. In this case the effect of reduced number of blades, reduced number of blade segments, and increased integration interval can be seen. As the rotor loads up at high speeds, the effects of blade reduction and integration interval continue to amplify each other until an oscillation in roll acceleration occurs which is as large as the effect of the pulse input, and in the final seconds of the run, the oscillation is double the pulse input. Thus, the vehicle equations of motion are continually experiencing pulse inputs. Again, the average roll rate value is higher than it should be, and the vehicle rolls 15° approximately 3 seconds faster than the baseline vehicle. The flap angle again tends to smooth out instead of following the anticipated response. Figure 17 presents the data for the hover case. The same trends are apparent, but to a smaller extent.

Figure 18 presents the effect of increasing integration interval from 1/240 second to 1/20 second on vehicle dynamic response at 120 knots for the five-blade—five-blade-segment rotor. One can easily see that the numerical solution and aerodynamic definition of the total model have broken down and are incorrect. Both the vehicle and rotor are highly unstable. The reader should note that the run was stopped at approximately 16 seconds to keep the computer program from sustaining a fatal error due to numerical divergence. Figure 19 presents the data for the hover case. Again, the reader can see the obvious breakdown of the numerical solution. This case looks somewhat better than the 120-knot case since the rotor aerodynamics at hover are less complex, and therefore are not as severely affected by the numerical instabilities.

Figure 20 presents the effect of increasing integration interval from 1/240 second to 1/20 second on vehicle dynamic response at 120 knots for the three-blade—three-blade-segment rotor. Again, as with the five-blade—five-blade-segment rotor, the vehicle and rotor both become unstable under these conditions, and the computer program sustained a fatal error at approximately 9 seconds into the run because the blade flap angle became unstable. Figure 21 presents the data for the hover case. Although this case looks better than the 120-knot case, it is obvious that the solution is again incorrect.

RECOMMENDATIONS FOR USING ROTATING BLADE ELEMENT MODEL FOR REAL-TIME SIMULATION

The following recommendations are made for using a rotating blade element model for the simulation of an articulated rotor system.

(1) Do not reduce the number of blade segments to less than three.

(2) Do not reduce the number of blades to less than three. A reduction to less than the actual number of blades when studying control systems or rotor systems should be critically examined.

(3) Do not increase integration interval to larger than 1/30 second.

(4) Do not increase azimuthal advance angle to larger than 40°. (Note that 1/30 second integration interval and 40° azimuthal advance angle correspond to each other exactly only at a rotor speed of 200 rpm.)

(5) If the model must be degraded, reduce blade segments first, blades second, and integration interval and azimuthal advance angle last.

(6) If any one of these factors must be degraded beyond the stated limits to reach real time, it is recommended that either a different rotor mathematical model be used or a faster computer be used.

CONCLUSIONS

This paper describes the results of a series of tests designed to examine the effects of degrading a rotating blade element rotor mathematical model of an articulated rotor system in order to fit the model within set computer timing constraints. The three methods of degradation studied were those of reduction of number of blades, reduction of number of blade segments, and increase of integration interval size and thus increase of blade azimuthal advance angle. The tests conducted consisted of static trim comparisons; total rotor force and moment comparisons; index blade force, moment, and angle comparisons for one 360° blade sweep; and, finally, total vehicle dynamic response comparisons for a lateral cyclic control pulse input.

Recommendataions are made concerning model degradation which should serve as a guide for future users of this mathematical model, and in general, they are in order of minimum impact on model validity: (1) reduction of number of blade segments, (2) reduction of number of blades, and (3) increase of integration interval and azimuthal advance angle. Extreme limits are specified beyond which the rotating blade element rotor mathematical model should not be used.

From the data collected the following conclusions were reached:

(1) Reducing blade segments does not appear to influence the solution to any great extent. This is due to the method used in determining the blade-segment locations which are based on equal annuli area.

(2) Reducing the number of blades has no effect on static trim data; however, the amplification of n/rev (n blades per revolution) amplitude affects dynamic response because of the rotor forces and moments oscillating over a wider band. Two effects result: (1) The rotor, and therefore the body, tends to respond to the number of blades simulated and to the tip path plane formed by them, and (2) the numerical integration formulas used in the integration of the body accelerations and rates tend to respond to the increased amplitude of the high-frequency content contained in the accelerations and rates.

(3) The worst single effect is that of increasing integration interval. This has the double effect of increasing blade azimuthal advance angle and affecting the numerical integrators. When the azimuthal advance angle is

increased, the number of points used to define the rotor forces and moments as the blades sweep out the tip path plane is reduced. This condition causes an unrepresentative definition of the aerodynamic data to occur. The second problem arises with the numerical integration formulas one must use for solution of the body equations of motion in real-time man-in-the-loop simulations. The faster formulas, computationally, are the ones which cannot stand large interval sizes and still retain their numerical accuracy and stability. And as would be expected, these two effects tend to couple and amplify each other.

(4) Because of the lack of rotor aerodynamic definition, these effects tend to amplify as the vehicle forward velocity increases and the rotor loads up. Thus, although some degradation might be acceptable at low speeds, it may not be suitable at all at higher speeds.

Langley Research Center
National Aeronautics and Space Administration
Hampton, VA 23665
November 24, 1976

APPENDIX

ROTOR MODEL DEGRADATION METHODS

The following sections describe the methods used in the degradation of the rotor mathematical model.

Blade Reduction

Once the number of blades to be simulated is chosen, the blades are evenly distributed around the disk by use of the following equation:

$$\Delta\Psi_b = \frac{360^\circ}{b_s}$$

where

$\Delta\Psi_b$ angle between adjacent blades, starting with blade 1 at 0°

b_s number of blades simulated

Then the forces and moments are calculated for the blades simulated. Next, the total rotor forces and moments for the rotor system are calculated in a manner represented by the following general equations:

$$F_T = \frac{b_{mr}}{b_s} \sum_{b=1}^{b=b_s} F_b$$

$$M_T = \frac{b_{mr}}{b_s} \sum_{b=1}^{b=b_s} M_b$$

where

F_T total rotor forces

F_b individual blade forces

M_T total rotor moments

M_b individual blade moments

b_{mr} actual number of blades

b_s number of blades simulated

APPENDIX

Blade-Segment Reduction

First, the number of blade segments (n_s) to be simulated is chosen. The positioning of these segments along the blades is determined by the following equations from reference 1 whose derivation is based on the assumption of equal annuli area. The reader is directed to sketch (a) for the definitions of the various blade-segment variables.

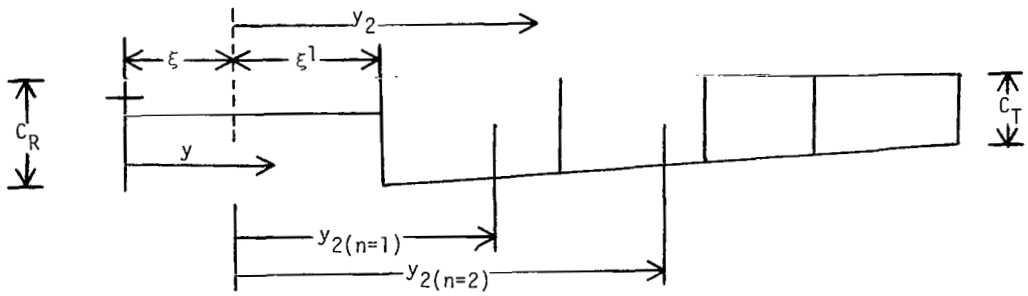

Sketch (a)

Distance to segment center of lift for first segment:

$$y_{2(n=1)} = \left\{\left[\frac{1 - (\xi + \xi^1)^2}{2n_s}\right] + (\xi + \xi^1)^2\right\}^{1/2} - \xi$$

where

ξ nondimensional distance from center of rotation to hinge

ξ^1 nondimensional distance from hinge to start of blade

Distance to segment center of lift for subsequent segments:

$$y_{2(n)} = \left\{\left[\frac{1 - (\xi + \xi^1)^2}{n_s}\right] + \left[\xi + y_{2(n-1)}\right]^2\right\}^{1/2} - \xi$$

Distance to inboard end of segment from center line:

$$y_{INB(n)} = \left\{\left[\xi + y_{2(n)}\right]^2 - \left[\frac{1 - (\xi + \xi^1)^2}{2n_s}\right]\right\}^{1/2}$$

Distance to outboard end of segment from center line:

$$y_{OUTB(n)} = \left\{\left[\xi + y_{2(n)}\right]^2 + \left[\frac{1 - (\xi + \xi^1)^2}{2n_s}\right]\right\}^{1/2}$$

Segment width:

$$\Delta y_{(n)} = y_{OUTB(n)} - y_{INB(n)}$$

Mean chord of segment:

$$C_{y(n)} = \left[\frac{y_{OUTB(n)} + y_{INB(n)} - 2(\xi + \xi^1)}{2(1 - \xi - \xi^1)}\right](C_T - C_R) + C_R$$

Integration Interval or Azimuthal Advance Angle Relationship

The user can determine either an integration interval or an azimuthal advance angle. Defining one uniquely defines the second by assuming a constant rotor speed.

$$\Delta\Psi = 57.3\Omega\ \Delta t$$

where

$\Delta\Psi$ azimuthal advance angle

Δt integration interval

Ω rotor rotational speed

REFERENCES

1. Houck, Jacob Albert: Computational Aspects of Real-Time Simulation of Rotary Wing Aircraft. M.S. Thesis, George Washington Univ., 1976. (Available as NASA CR-147932.)

2. Cooper, D. E.; and Howlett, J. J.: Ground Based Helicopter Simulation. Symposium on Status of Testing and Model Techniques for V/STOL Aircraft (Essington, Pa.), American Helicopter Soc., Oct. 1972.

TABLE I.- ROTOR MATHEMATICAL MODEL CONFIGURATIONS UTILIZED

Rotor speed, rpm	Number of blades	Number of blade segments	Integration interval, sec	Azimuthal advance angle, deg
*200	*5	*10	*$\frac{1}{240}$	*5
200	5	5	$\frac{1}{240}$	5
200	4	5	$\frac{1}{240}$	5
200	3	5	$\frac{1}{240}$	5
200	5	4	$\frac{1}{240}$	5
200	5	3	$\frac{1}{240}$	5
200	3	3	$\frac{1}{240}$	5
200	5	5	$\frac{1}{30}$	40
200	3	3	$\frac{1}{30}$	40
200	5	5	$\frac{1}{20}$	60
200	3	3	$\frac{1}{20}$	60

*This is the baseline configuration.

TABLE II.- EFFECT OF BLADE REDUCTION ON STATIC TRIM

[Integration interval of 1/240 second]

Rotor configuration*	x_c, percent	x_b, percent	x_a, percent	x_p, percent	θ, deg	ϕ, deg	α, deg
			Hover				
5b × 10s	53.046	58.420	54.458	55.901	6.765	-4.137	-89.967
5b × 5s	52.467	58.428	54.407	55.756	6.764	-4.086	-89.967
4b × 5s	52.466	58.428	54.407	55.756	6.764	-4.086	-89.967
3b × 5s	52.466	58.428	54.406	55.756	6.764	-4.086	-89.967
			120 knots				
5b × 10s	45.035	81.096	48.581	75.612	1.658	-2.039	1.319
5b × 5s	44.465	80.895	48.594	75.492	1.657	-1.992	1.316
4b × 5s	44.466	80.895	48.595	75.493	1.656	-1.992	1.317
3b × 5s	44.465	80.895	48.598	75.493	1.657	-1.992	1.344

*b denotes blade and s denotes blade segment; thus, 5b × 10s denotes a five-blade—ten-blade-segment configuration.

TABLE III.- EFFECT OF BLADE-SEGMENT REDUCTION ON STATIC TRIM

[Integration interval of 1/240 second]

Rotor configuration*	x_c, percent	x_b, percent	x_a, percent	x_p, percent	θ, deg	ϕ, deg	α, deg
			Hover				
5b × 10s	53.047	58.420	54.458	55.901	6.765	-4.137	-89.967
5b × 5s	52.467	58.428	54.407	55.756	6.764	-4.086	-89.967
5b × 4s	52.086	58.436	54.362	55.622	6.767	-4.093	-89.967
5b × 3s	51.304	58.443	54.283	55.393	6.771	-4.073	-89.967
			120 knots				
5b × 10s	45.035	81.096	48.581	75.612	1.659	-2.039	1.319
5b × 5s	44.465	80.895	48.594	75.492	1.657	-1.992	1.316
5b × 4s	44.088	80.825	48.568	75.439	1.661	-1.998	1.320
5b × 3s	43.275	80.576	48.442	75.295	1.677	-1.939	1.338

*b denotes blade and s denotes blade segment; thus, 5b × 10s denotes a five-blade—ten-blade-segment configuration.

TABLE IV.- EFFECT OF COMBINATION BLADE AND BLADE-SEGMENT REDUCTION ON STATIC TRIM

[Integration interval of 1/240 second]

Rotor configuration*	x_c, percent	x_b, percent	x_a, percent	x_p, percent	θ, deg	ϕ, deg	α, deg
Hover							
5b × 10s	53.047	58.420	54.458	55.901	6.765	-4.137	-89.967
5b × 5s	52.467	58.428	54.407	55.756	6.764	-4.086	-89.967
3b × 3s	51.304	58.443	54.283	55.392	6.771	-4.073	-89.967
120 knots							
5b × 10s	45.035	81.096	48.581	75.612	1.659	-2.039	1.319
5b × 5s	44.465	80.895	48.594	75.492	1.657	-1.992	1.316
3b × 3s	43.276	80.576	48.438	75.295	1.677	-1.939	1.311

*b denotes blade and s denotes blade segment; thus, 5b × 10s denotes a five-blade—ten-blade-segment configuration.

TABLE V.- EFFECT OF INCREASING INTEGRATION INTERVAL

FOR TWO ROTOR CONFIGURATIONS

Rotor configuration*	Integration interval, sec	x_c, percent	x_b, percent	x_a, percent	x_p, percent	θ, deg	ϕ, deg	α, deg
			Hover					
5b × 10s	1/240	53.047	58.420	54.458	55.901	6.765	-4.137	-89.967
5b × 5s	1/240	52.467	58.428	54.407	55.756	6.764	-4.086	-89.967
5b × 5s	1/30	52.650	58.475	54.462	55.765	6.801	-4.587	-89.967
5b × 5s	1/20	52.739	58.539	54.500	55.797	6.787	-4.622	-89.967
3b × 3s	1/240	51.304	58.443	54.283	55.392	6.771	-4.073	-89.967
3b × 3s	1/30	51.417	58.481	54.364	55.356	6.789	-4.582	-89.967
3b × 3s	1/20	51.547	58.563	54.368	55.419	6.795	-4.586	-89.967
			120 knots					
5b × 10s	1/240	45.035	81.096	48.581	75.612	1.659	-2.039	1.319
5b × 5s	1/240	44.465	80.895	48.594	75.492	1.657	-1.992	1.316
5b × 5s	1/30	42.276	79.661	49.117	76.037	1.853	-2.163	1.528
5b × 5s	1/20	28.305	70.212	49.144	80.964	2.817	-.746	2.646
3b × 3s	1/240	43.276	80.576	48.438	75.295	1.677	-1.939	1.311
3b × 3s	1/30	41.023	79.344	48.993	76.102	1.855	-2.078	1.501
3b × 3s	1/20	35.761	76.347	45.576	78.605	2.279	-2.007	2.067

*b denotes blade and s denotes blade segment; thus, 5b × 10s denotes a five-blade—ten-blade-segment configuration.

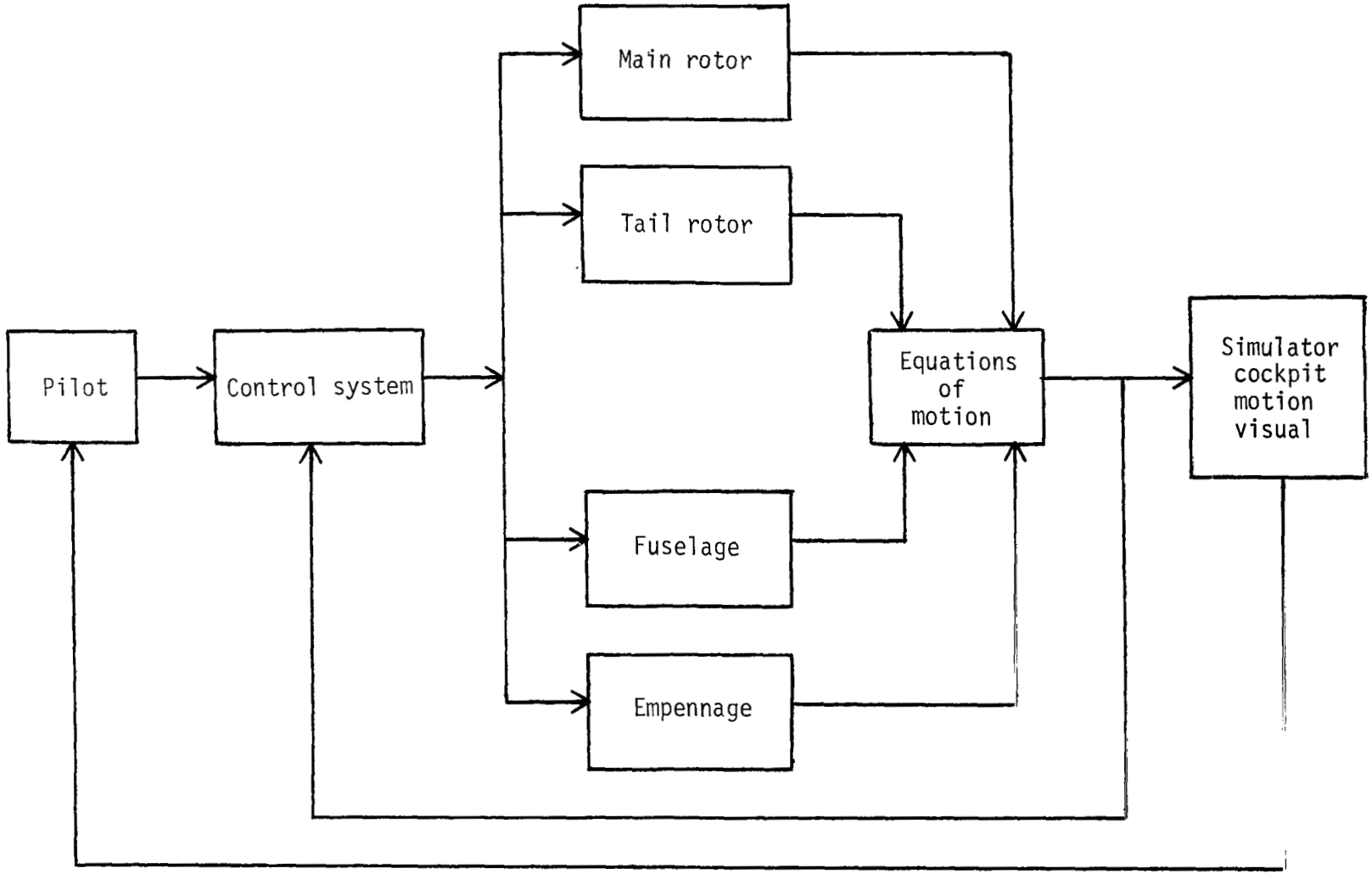

Figure 1.- Simplified block diagram of mathematical model.

*Human factors such as visual flicker, motion base stepping, instrument flicker, etc. which are noticeable to pilot.

**Mathematical convergence and divergence.

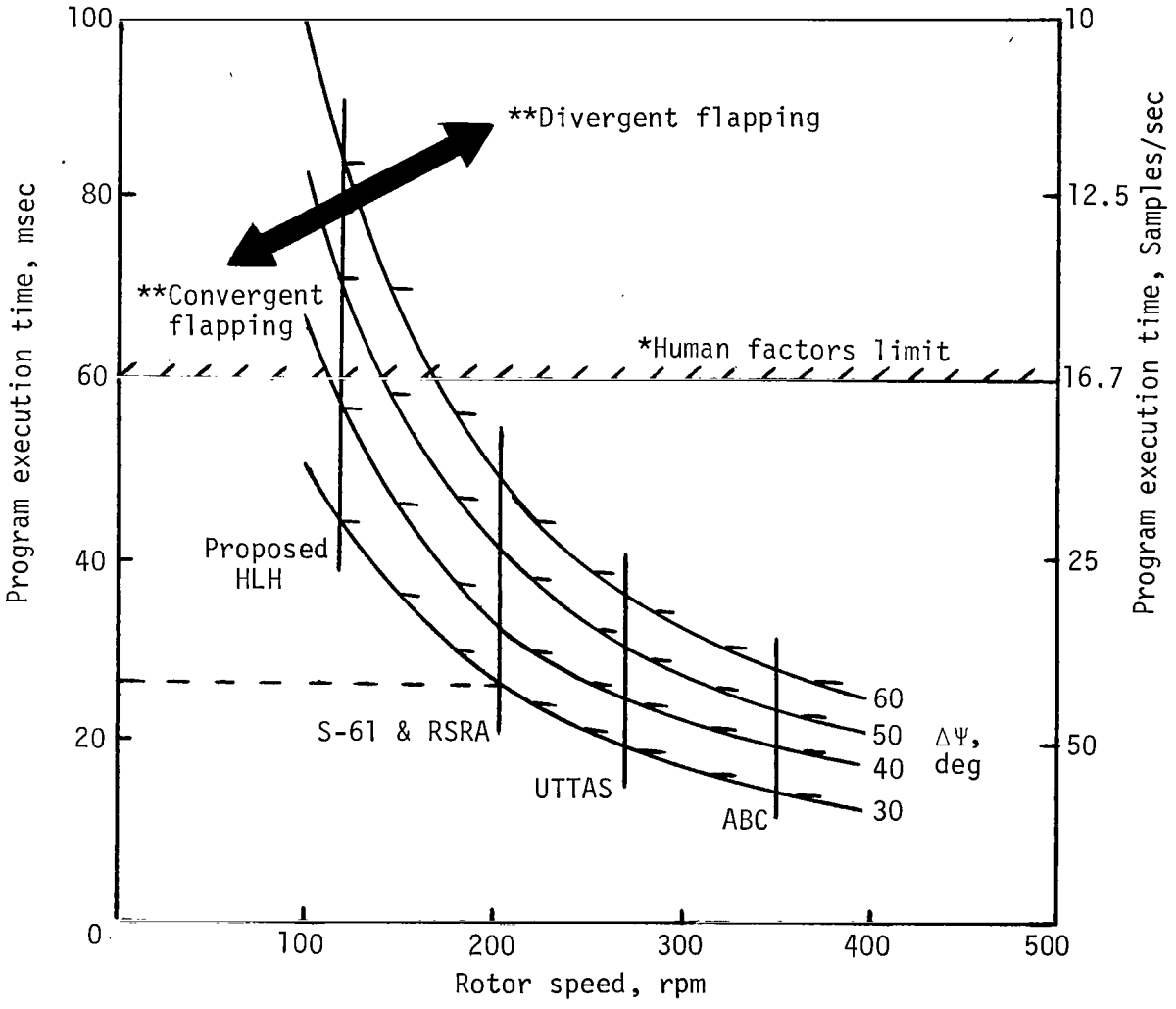

Figure 2.- Effect of rotor speed and azimuthal update on allowable program execution time for flapping convergence.

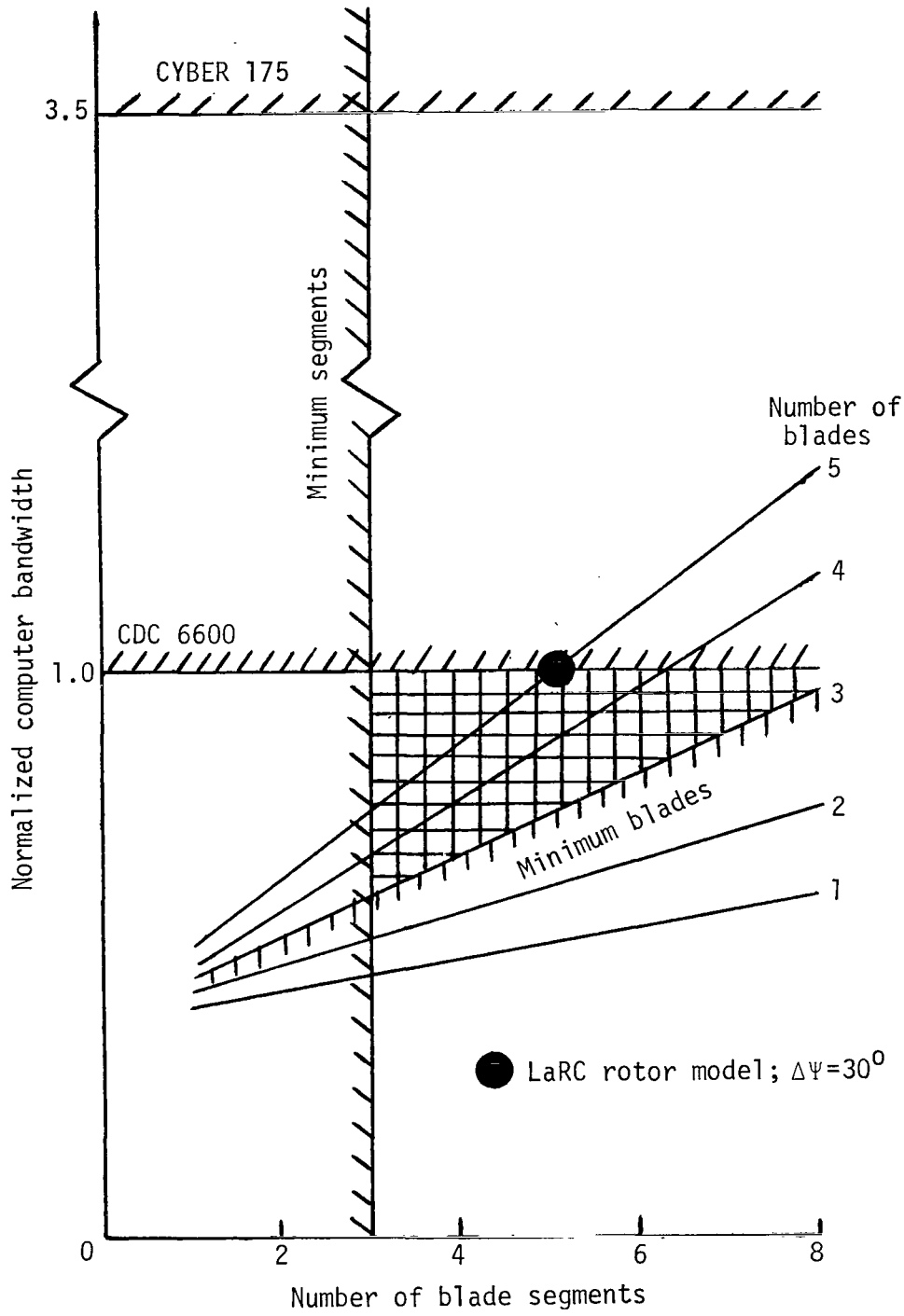

Figure 3.- Comparison of program execution time for a CDC 6600 computer with a CDC CYBER 175 computer for a five-blade, 200-rpm rotor model.

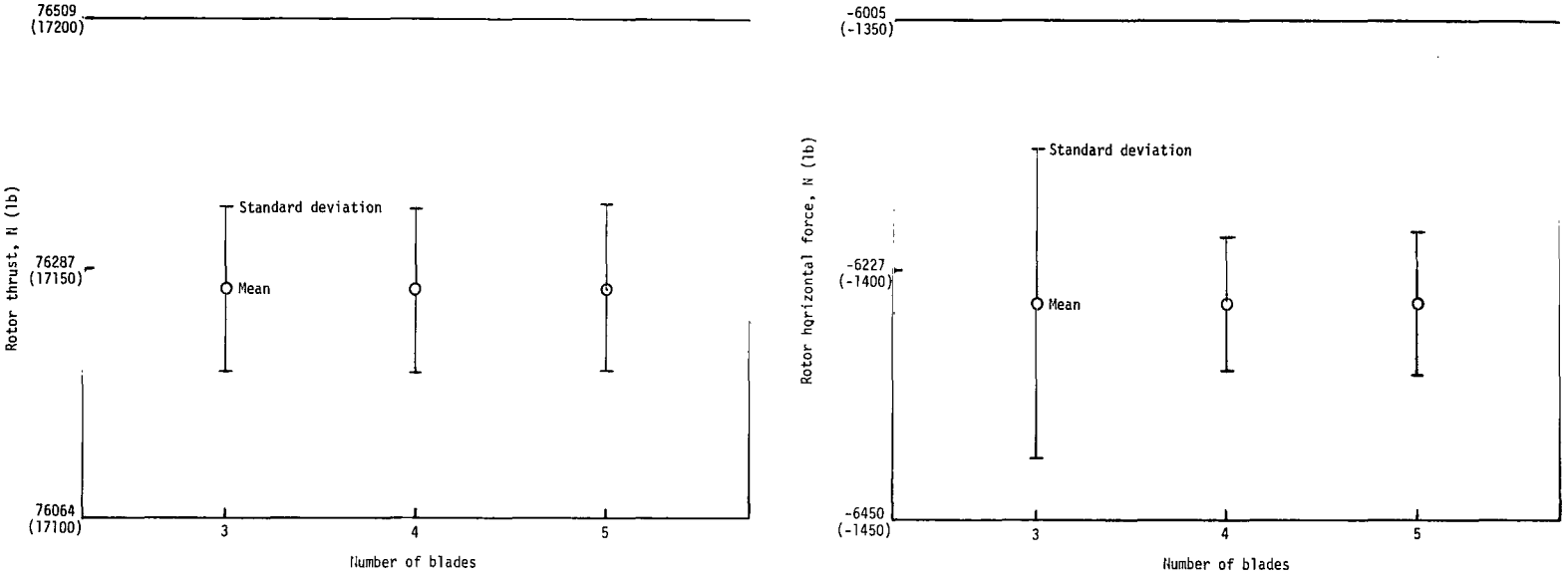

Figure 4.- Effect of blade reduction on total rotor forces and moments at hover. Integration interval, 1/240 second; five blade segments.

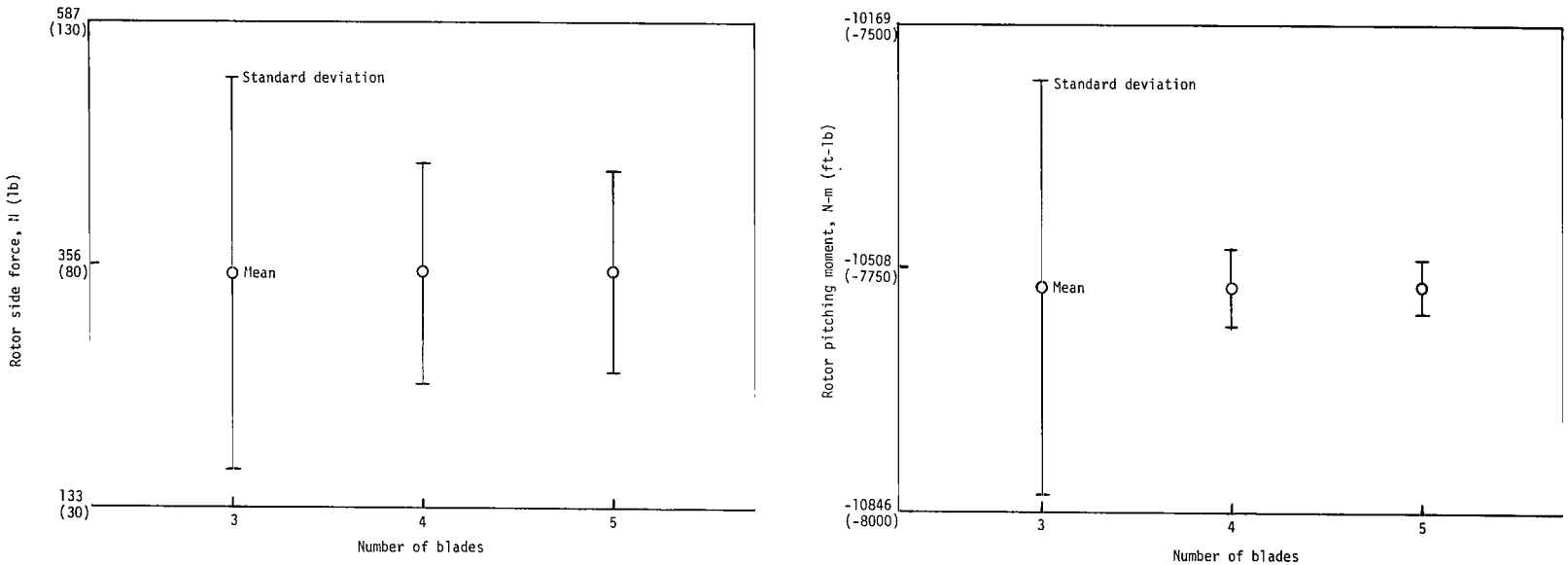

Figure 4.- Continued.

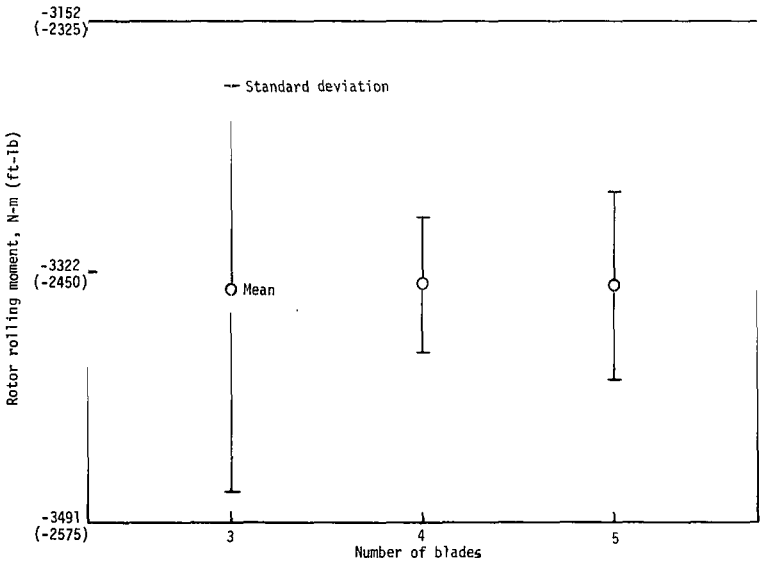

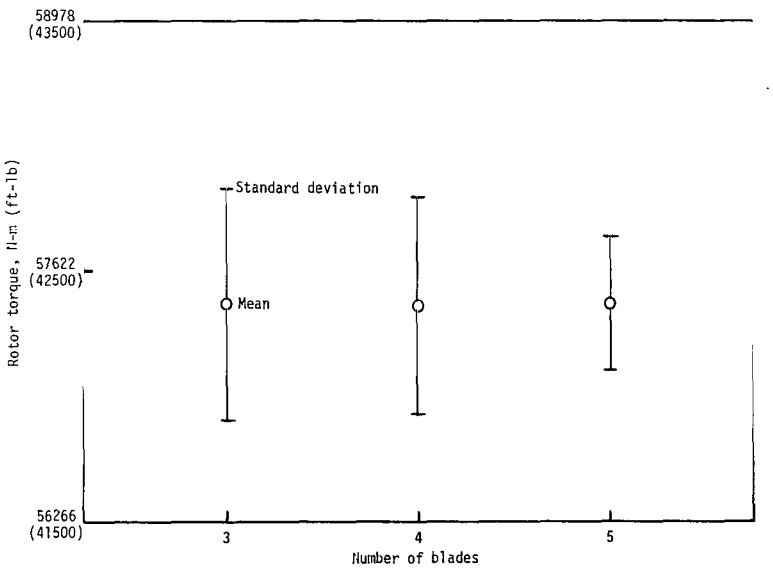

Figure 4.- Concluded.

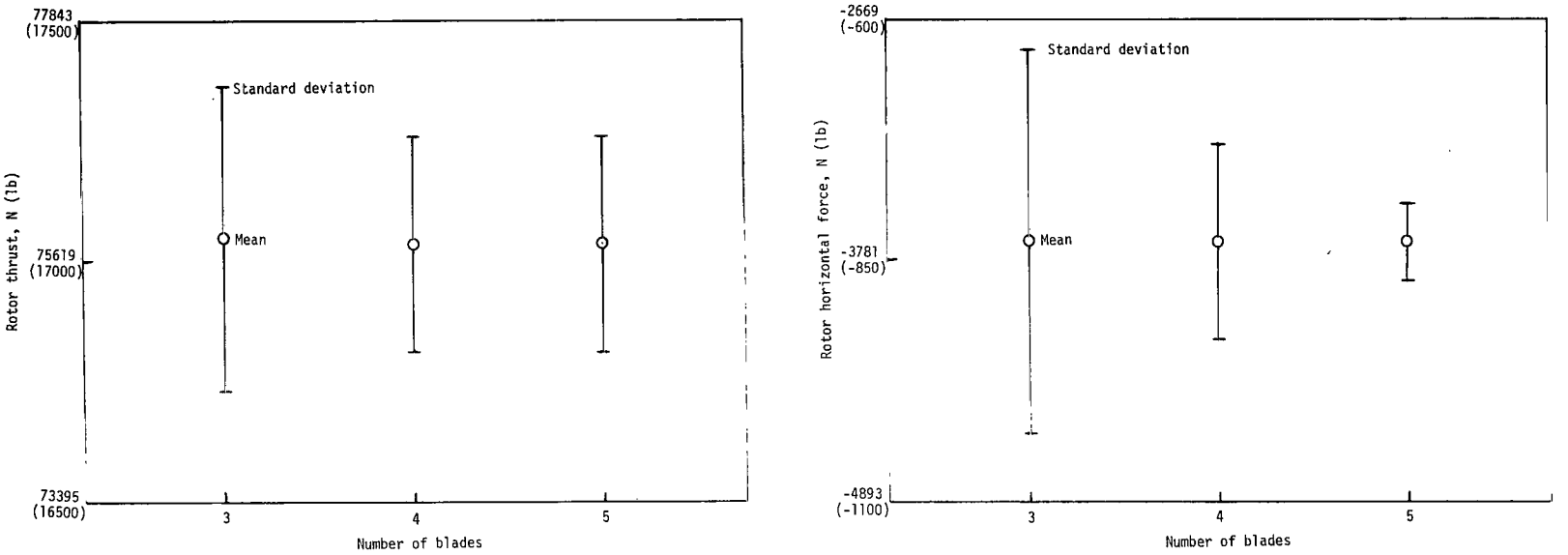

Figure 5.- Effect of blade reduction on total rotor forces and moments at 120 knots. Integration interval, 1/240 second; five blade segments.

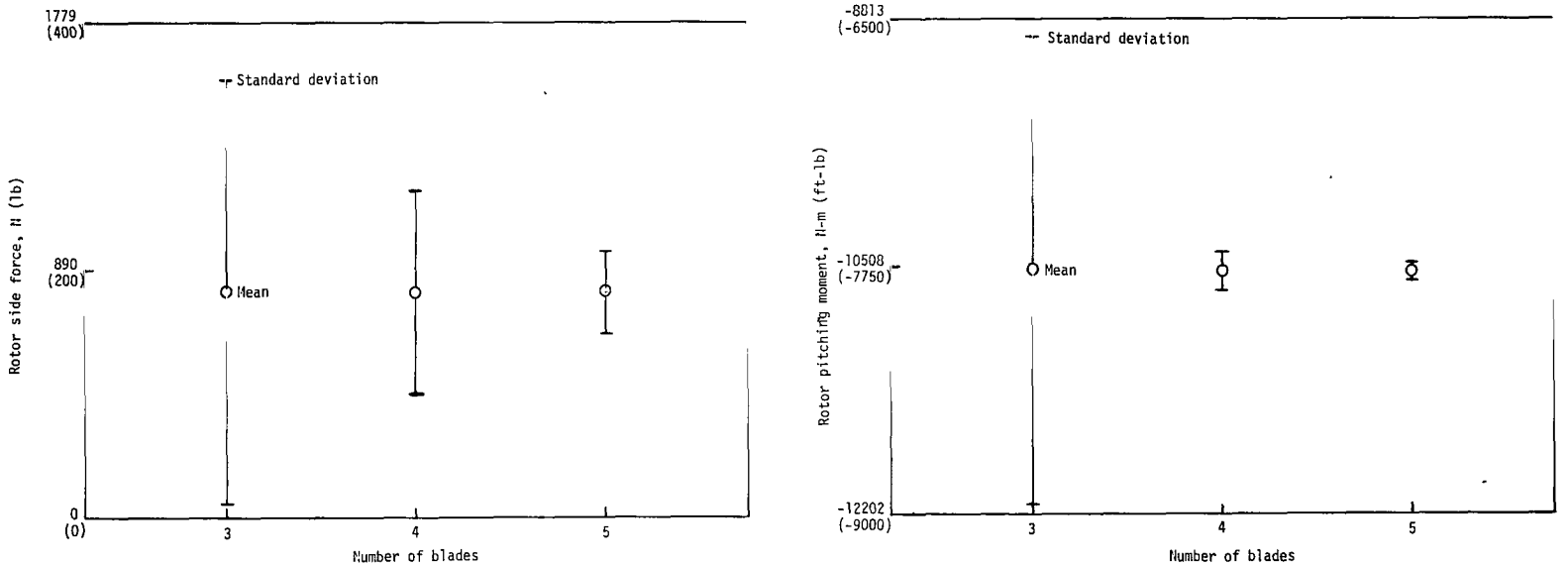

Figure 5.- Continued.

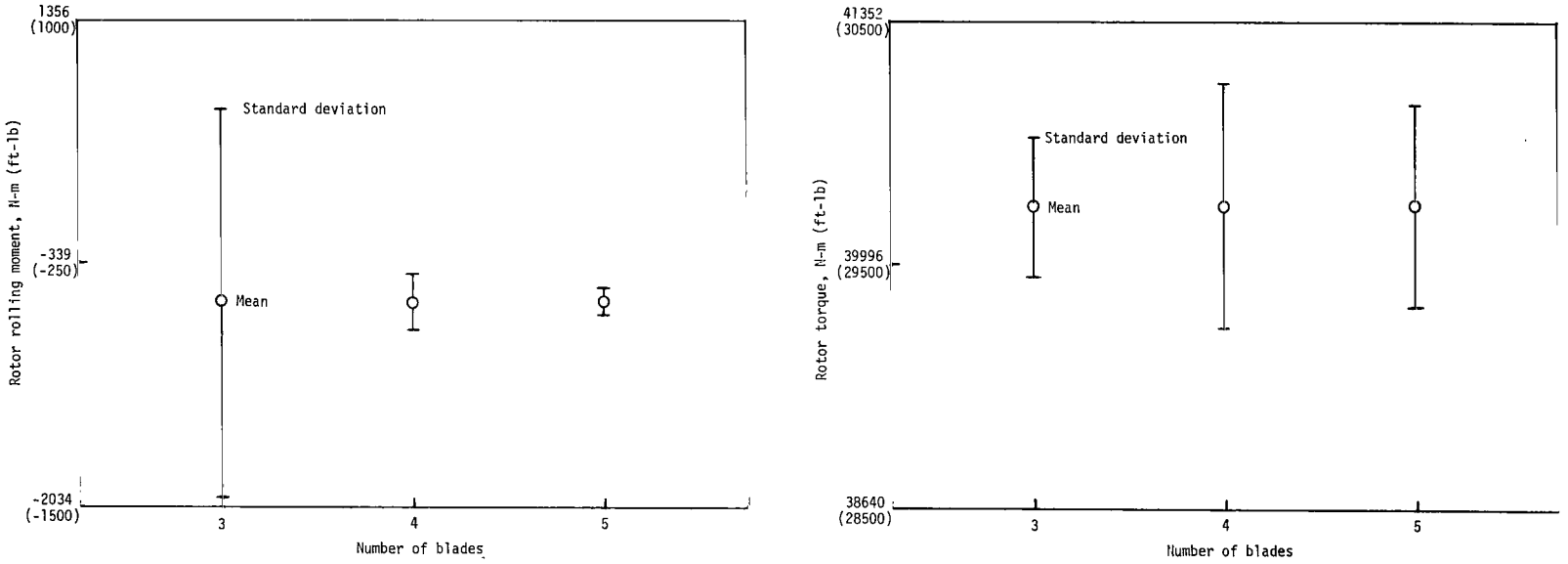

Figure 5.- Concluded.

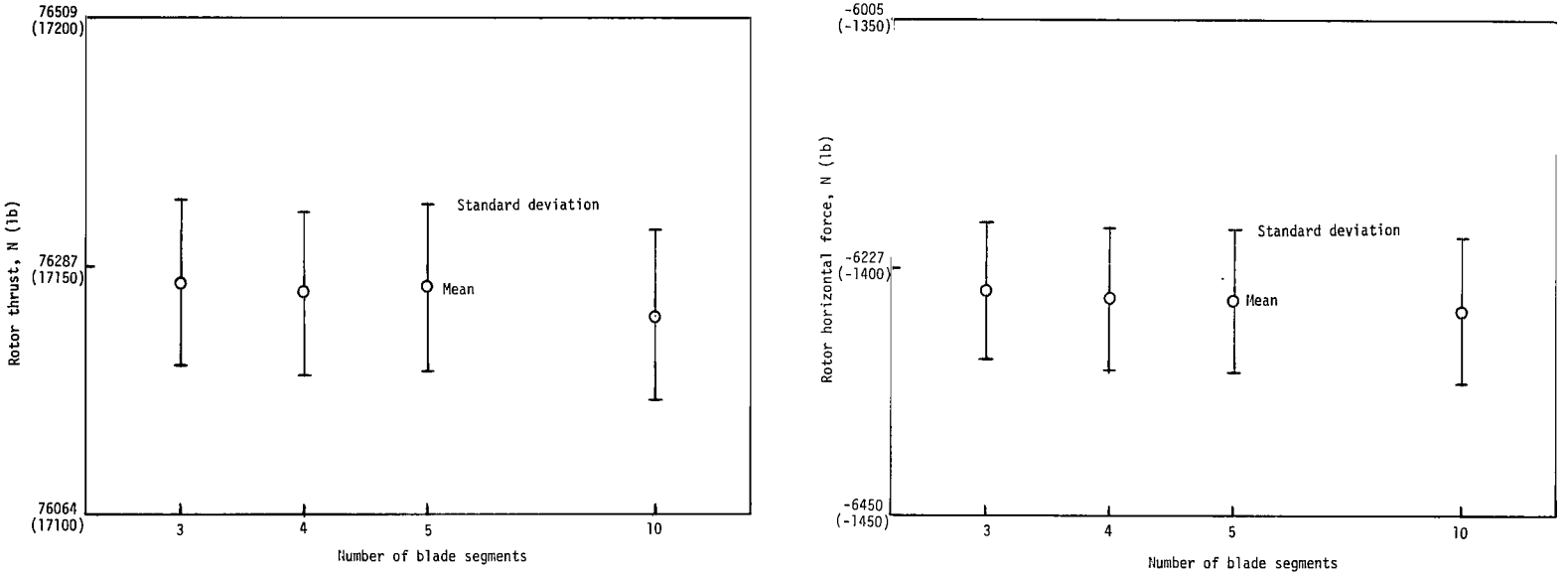

Figure 6.- Effect of blade segment reduction on total rotor forces and moments at hover. Integration interval, 1/240 second; five blades.

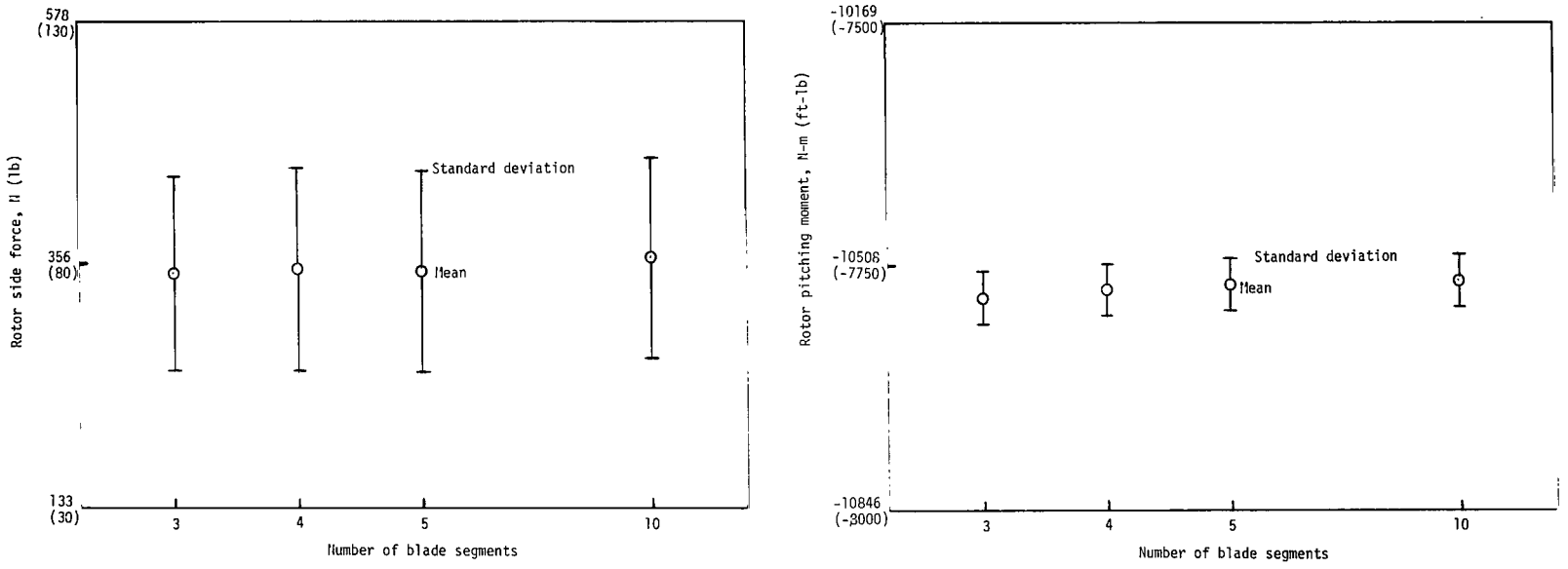

Figure 6.- Continued.

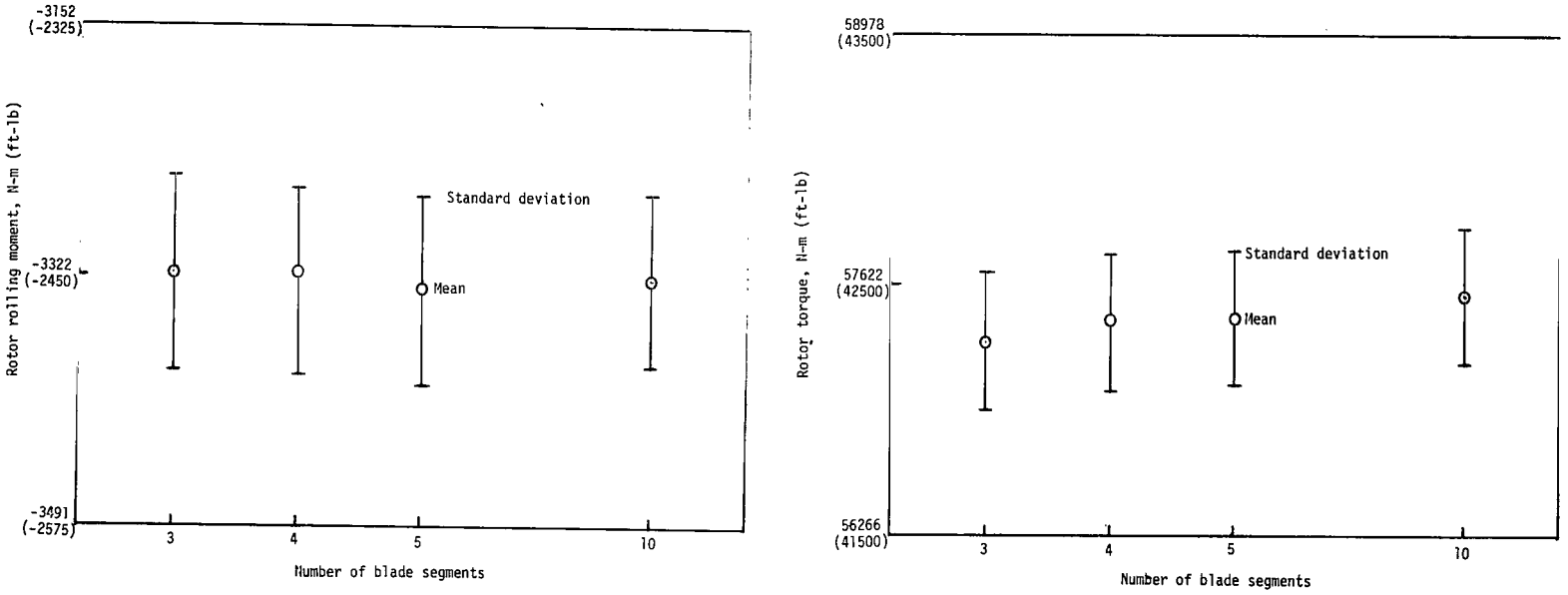

Figure 6.- Concluded.

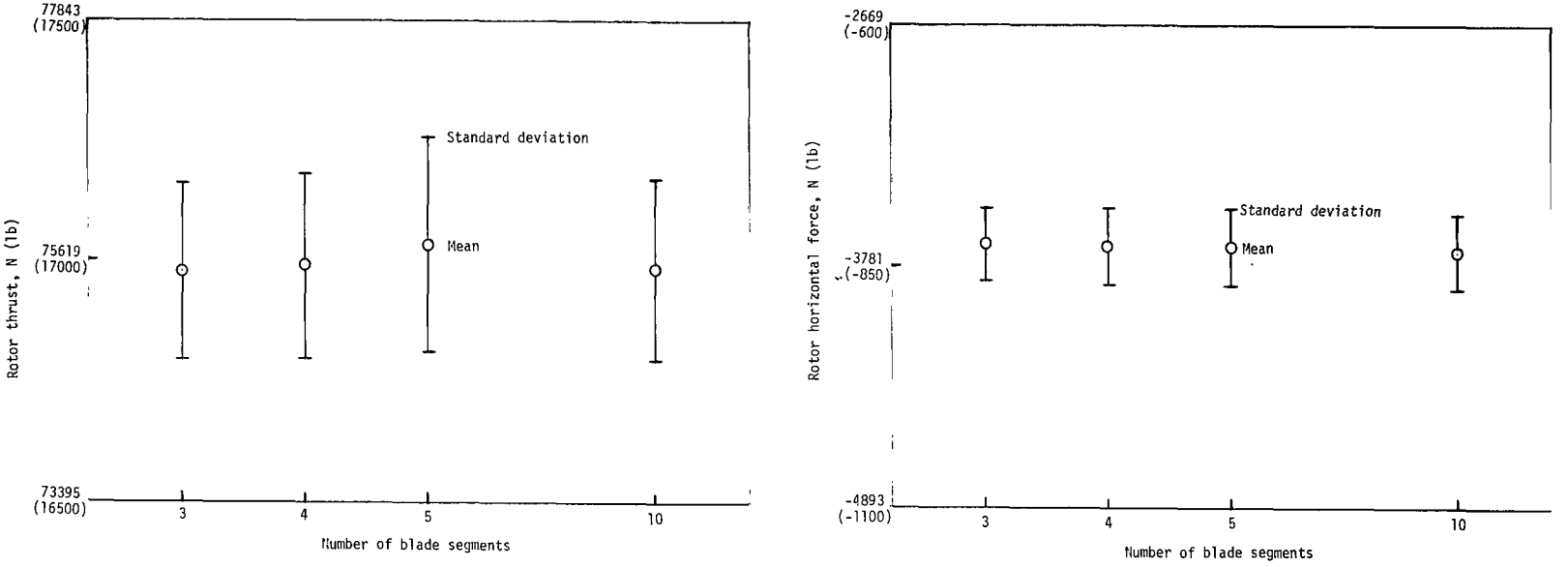

Figure 7.- Effect of blade segment reduction on total rotor forces and moments at 120 knots. Integration interval, 1/240 second; five blades.

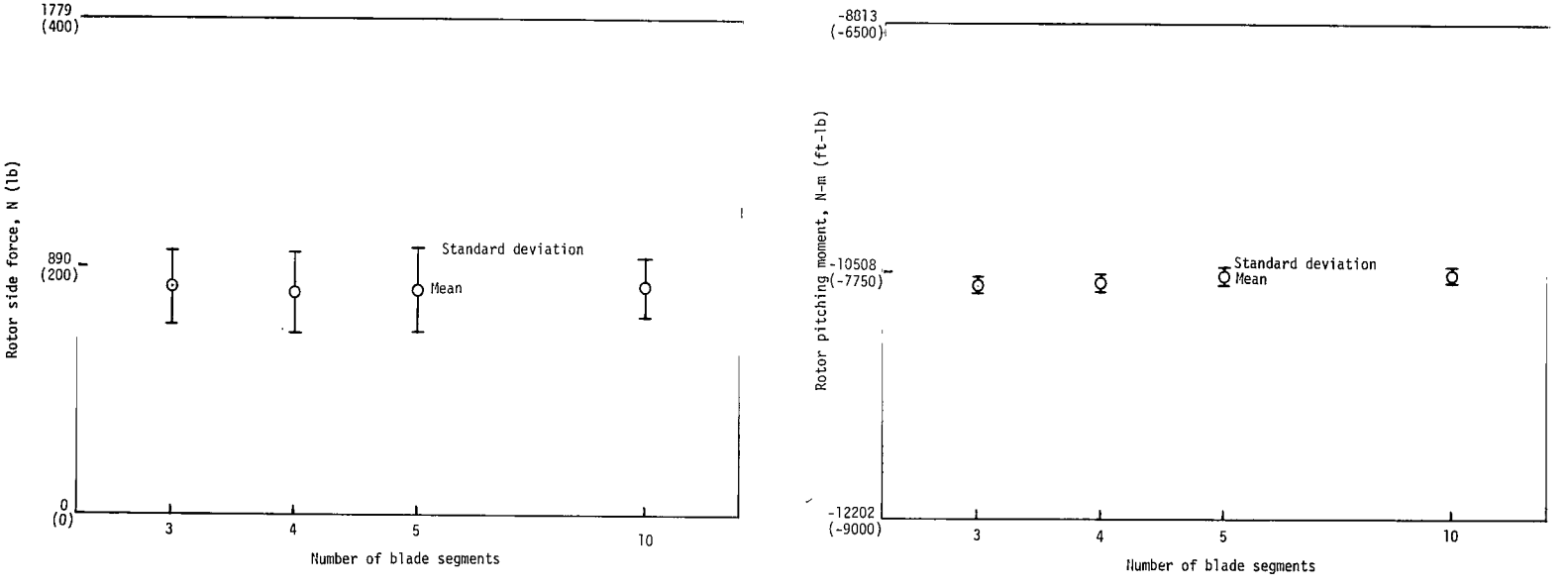

Figure 7.- Continued.

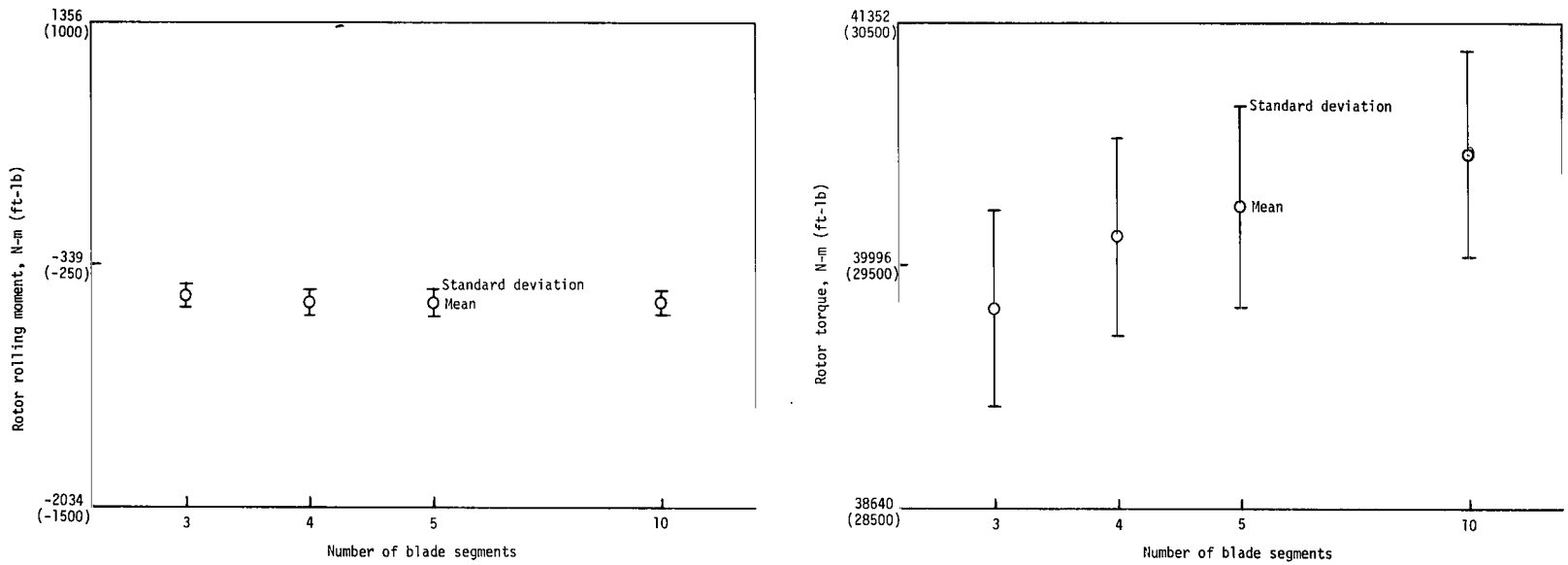

Figure 7.- Concluded.

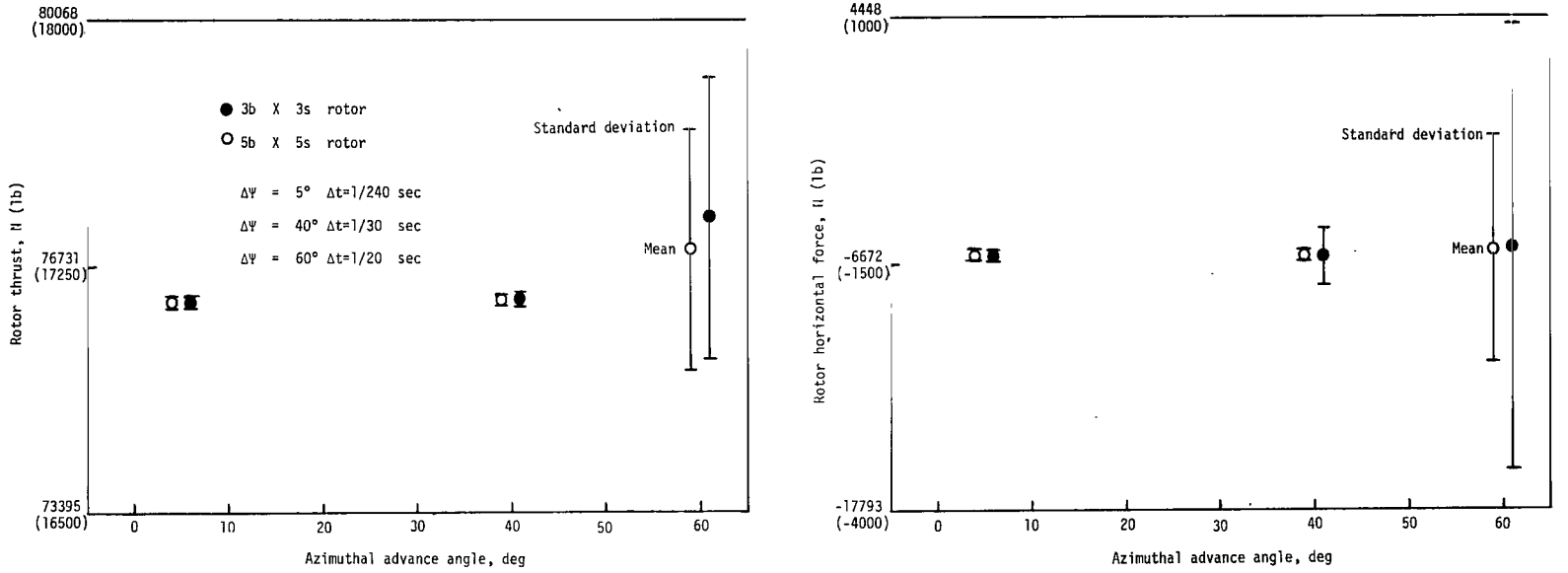

Figure 8.- Effect of increasing integration interval on total rotor forces and moments at hover.

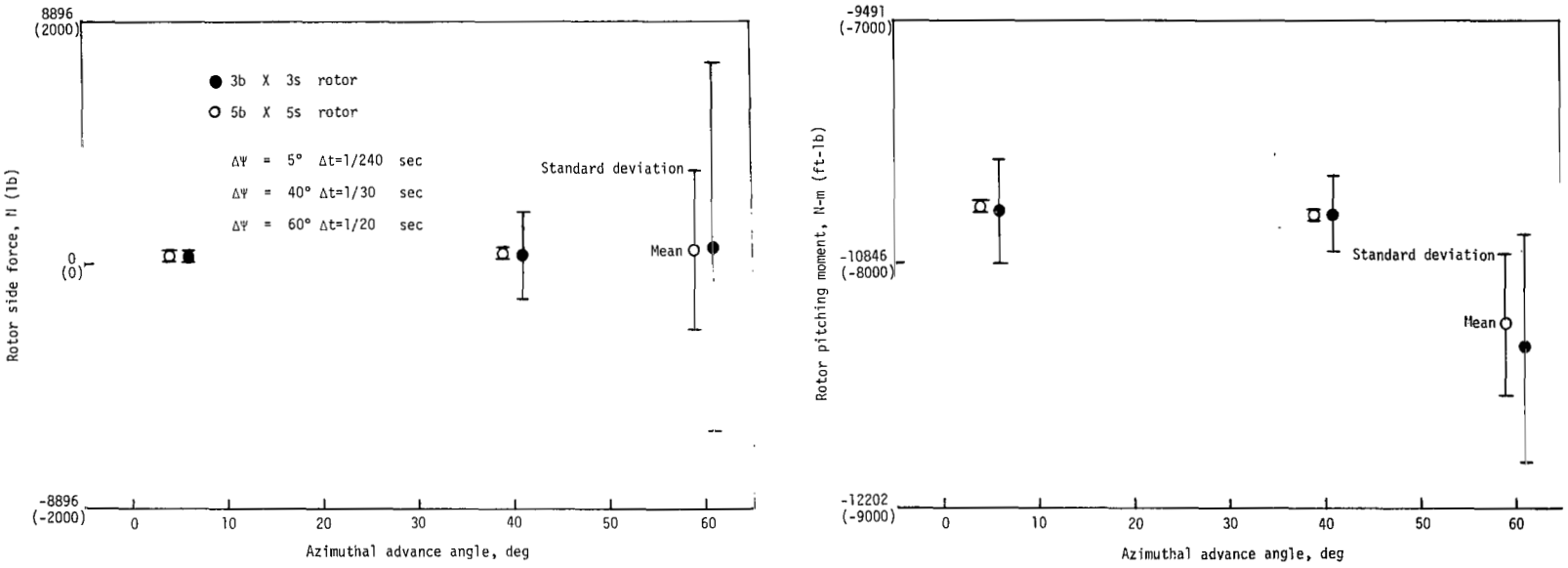

Figure 8.- Continued.

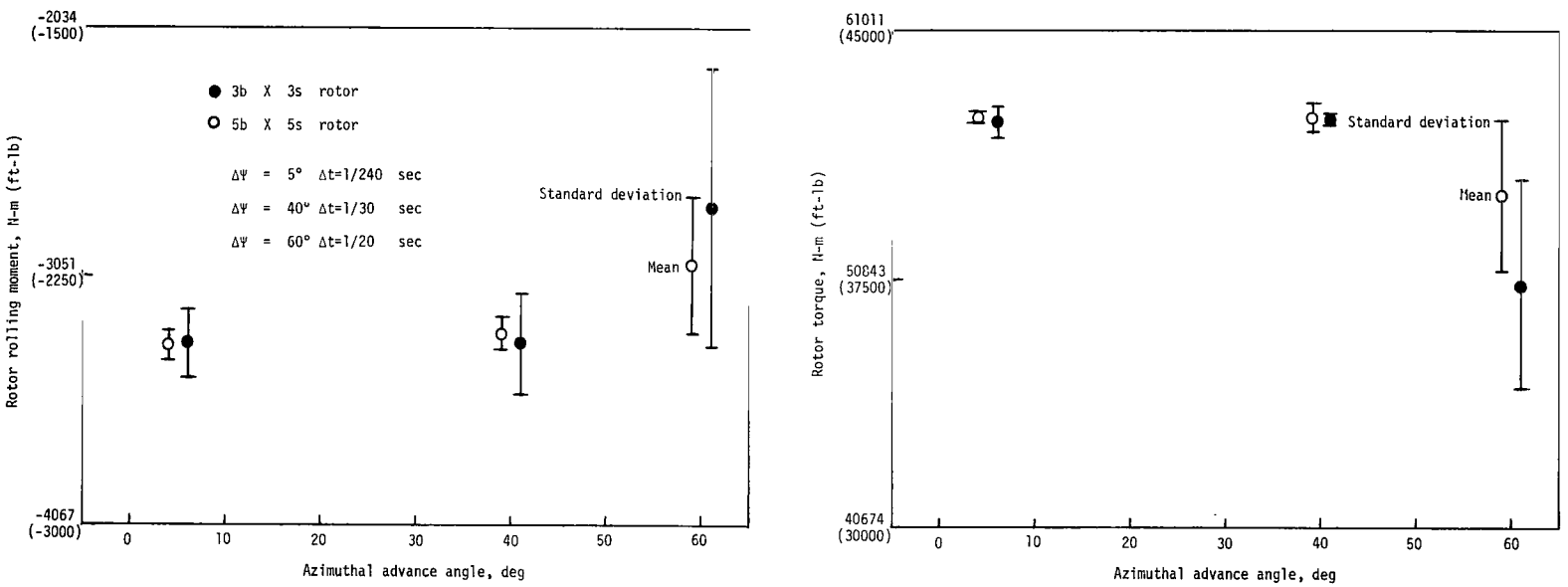

Figure 8.- Concluded.

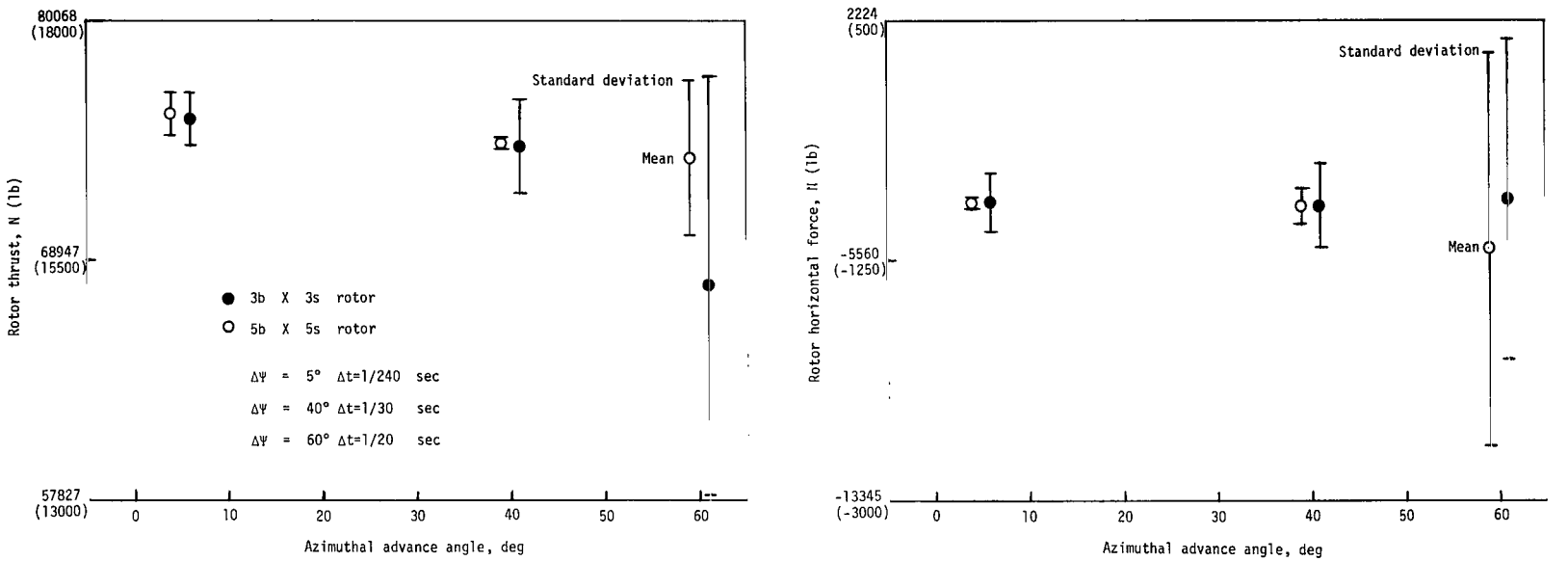

Figure 9.- Effect of increasing integration interval on total rotor forces and moments at 120 knots.

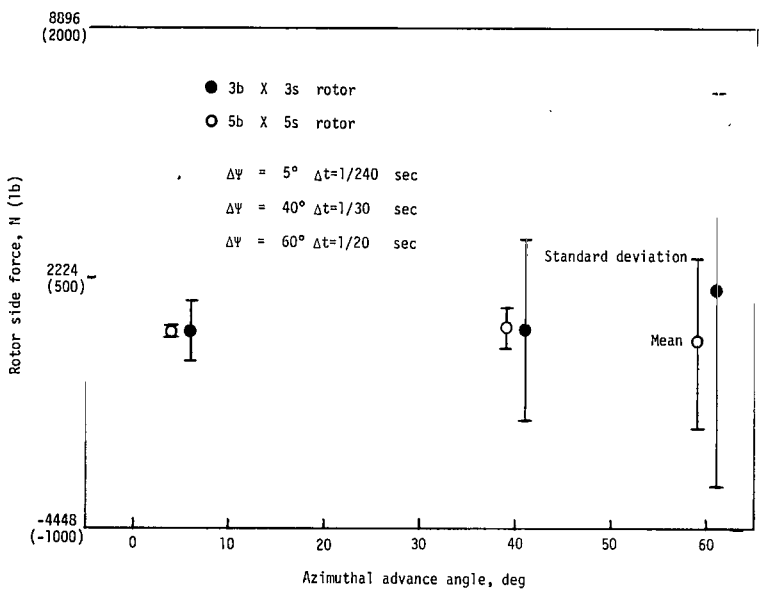

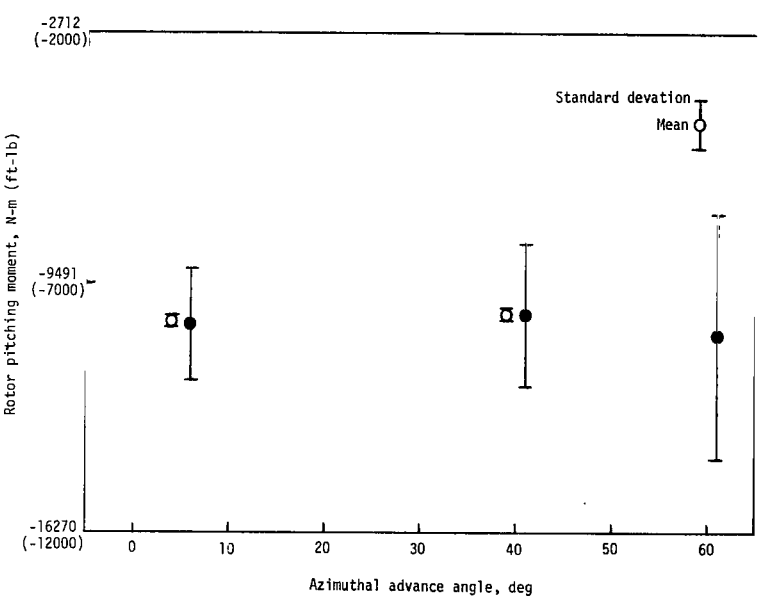

Figure 9.- Continued.

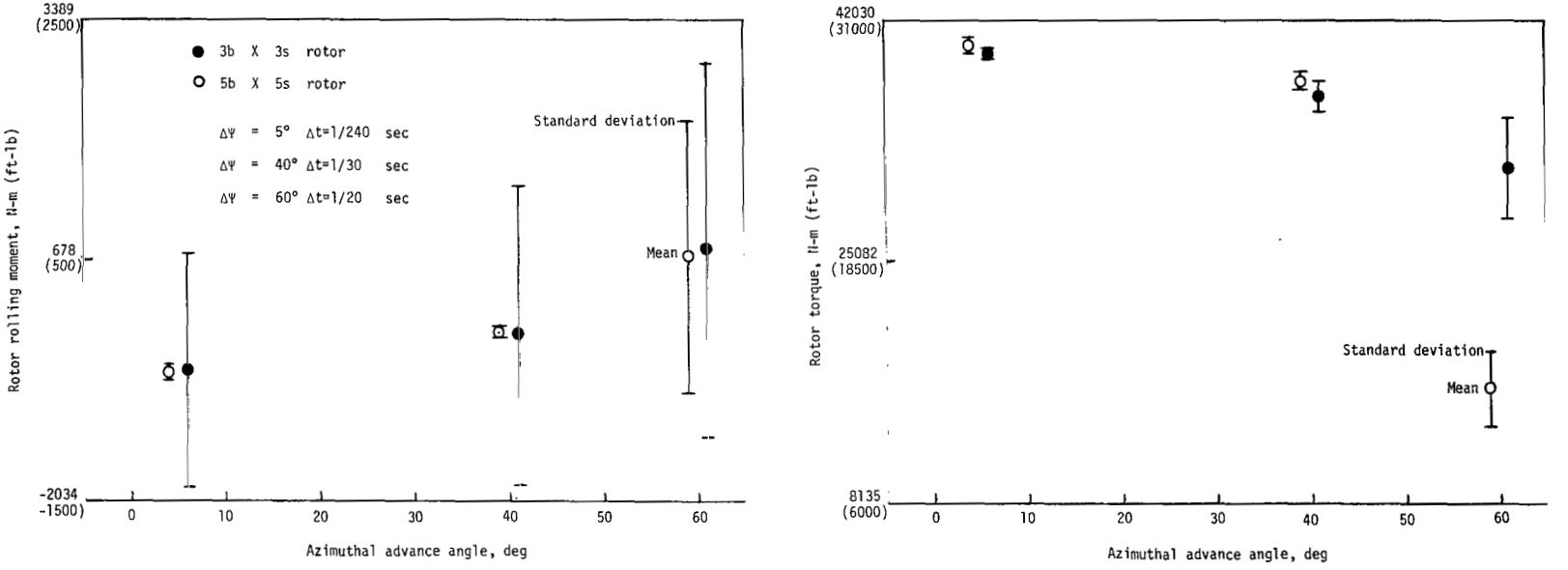

Figure 9.- Concluded.

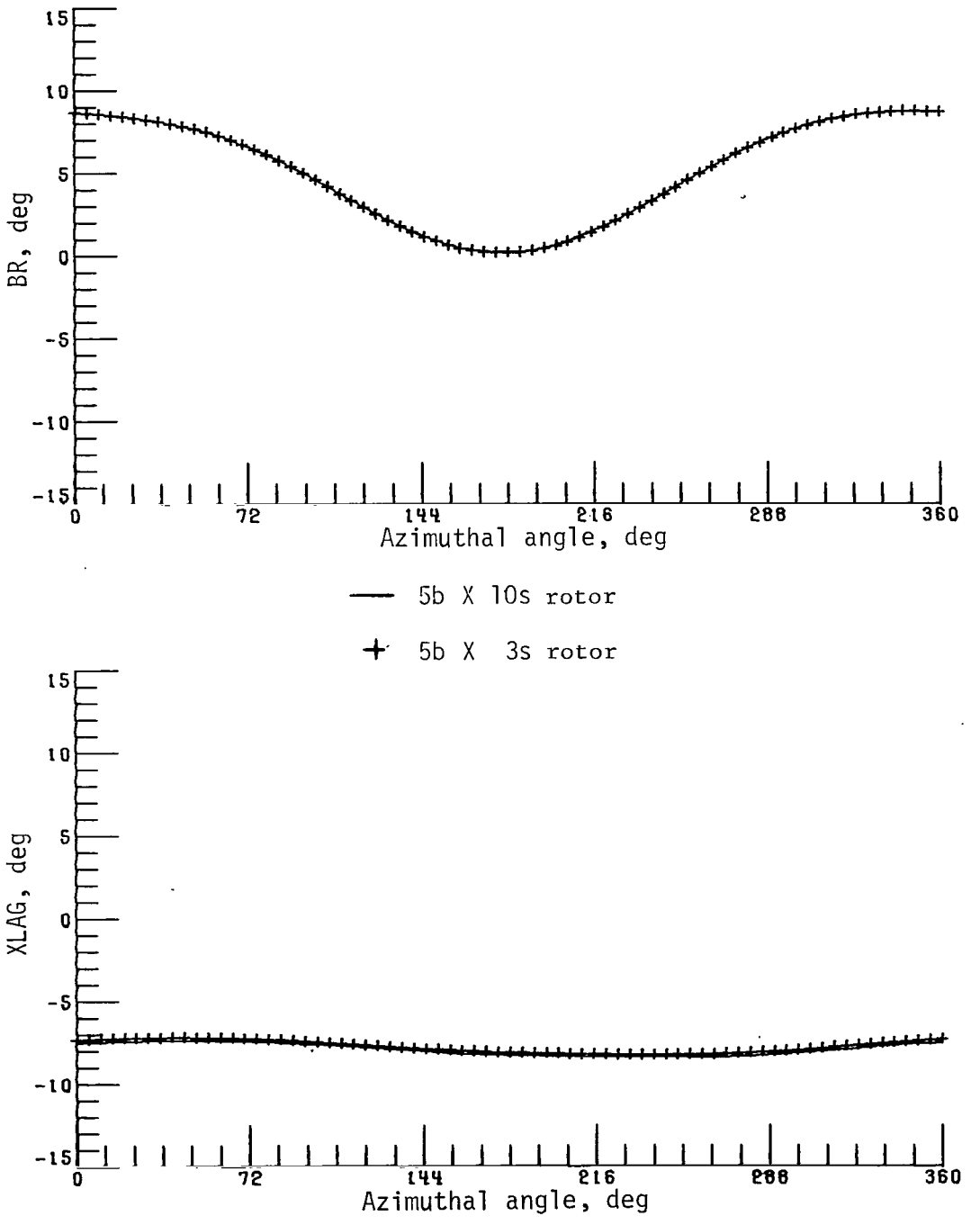

Figure 10.- Effect of blade-segment reduction on one blade revolution data at 120 knots. Integration interval, 1/240 second.

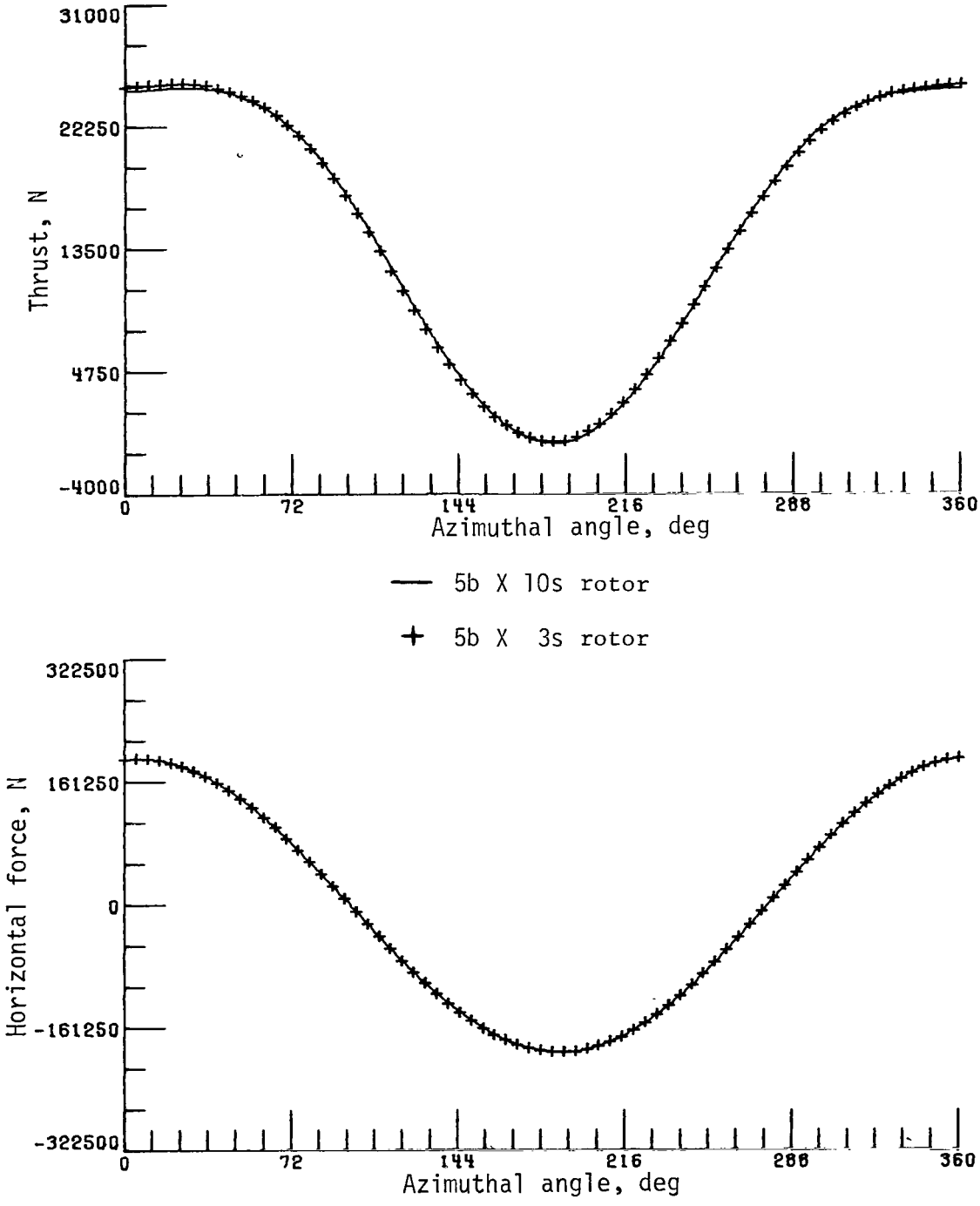

Figure 10.- Continued.

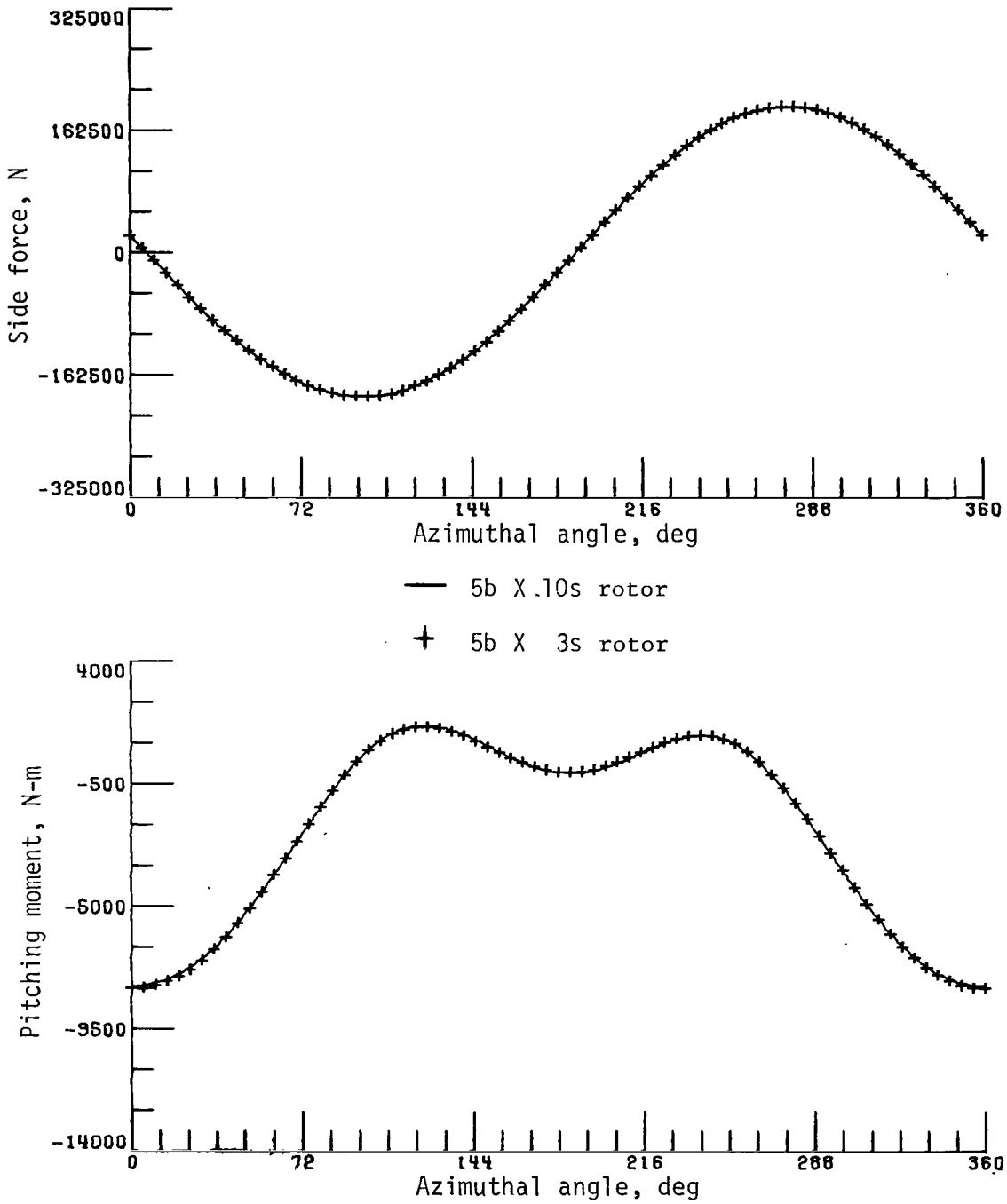

Figure 10.- Continued.

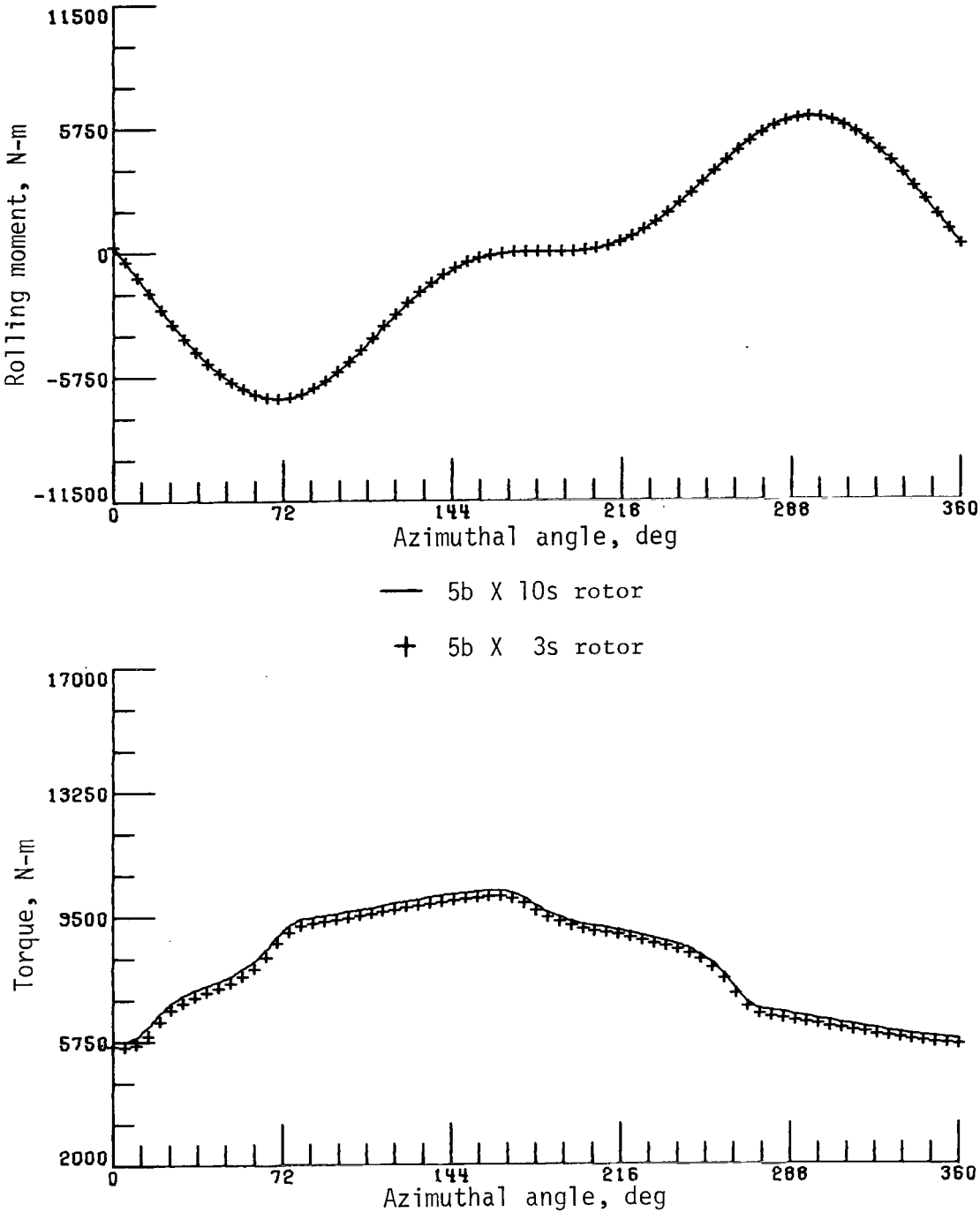

Figure 10.- Concluded.

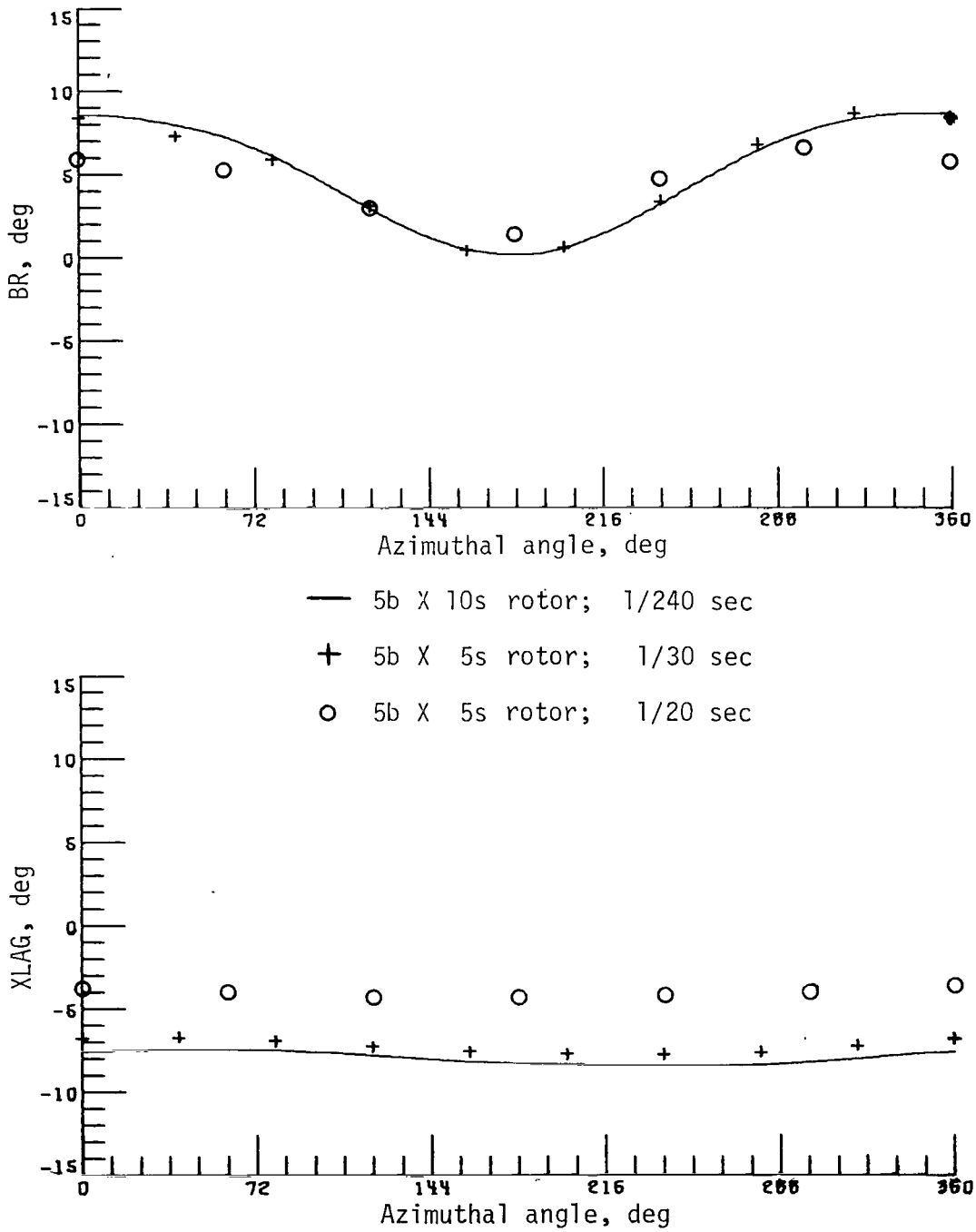

Figure 11.- Effect of increasing integration interval to 1/30 second and 1/20 second on one blade revolution data at 120 knots.

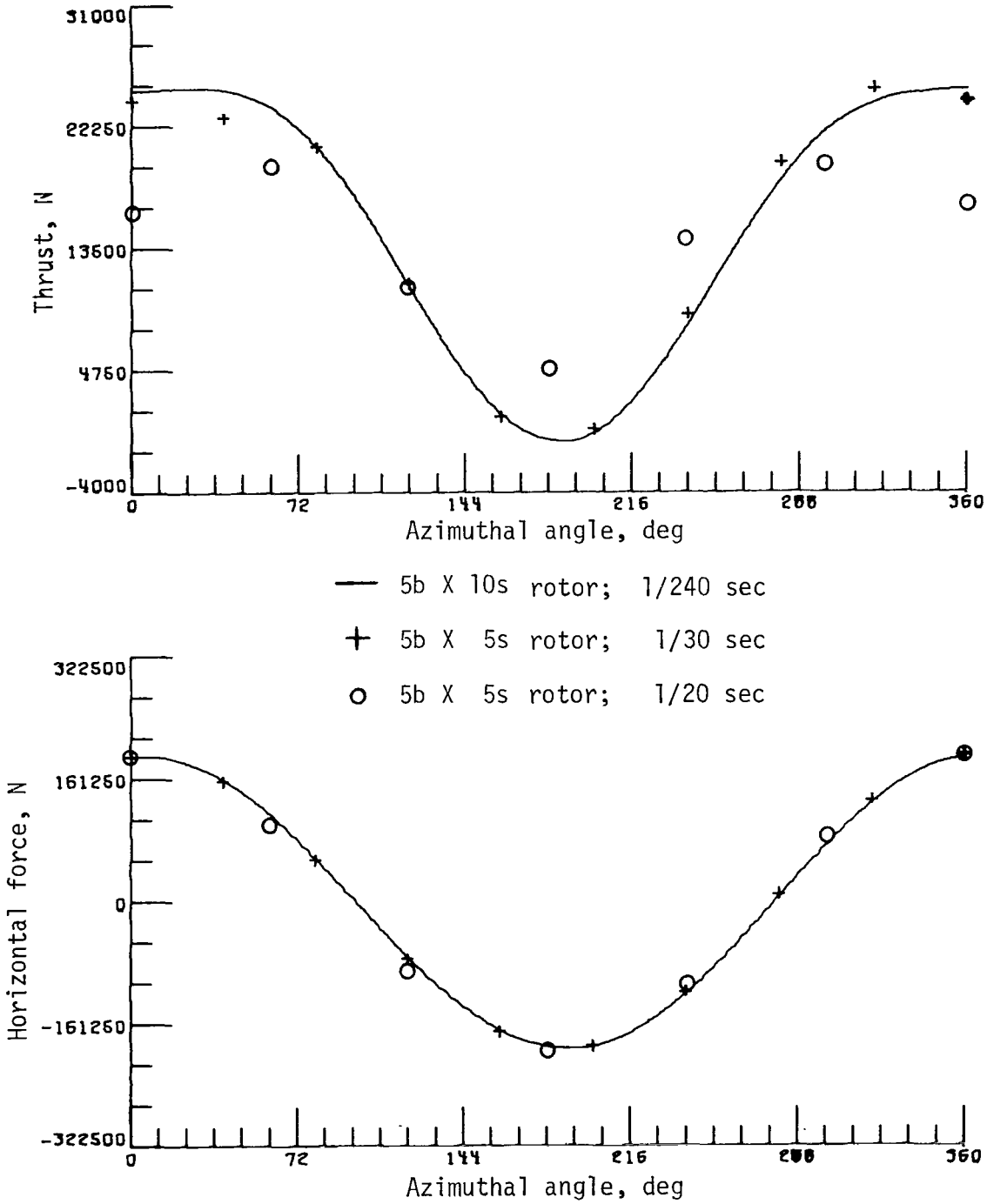

Figure 11.- Continued.

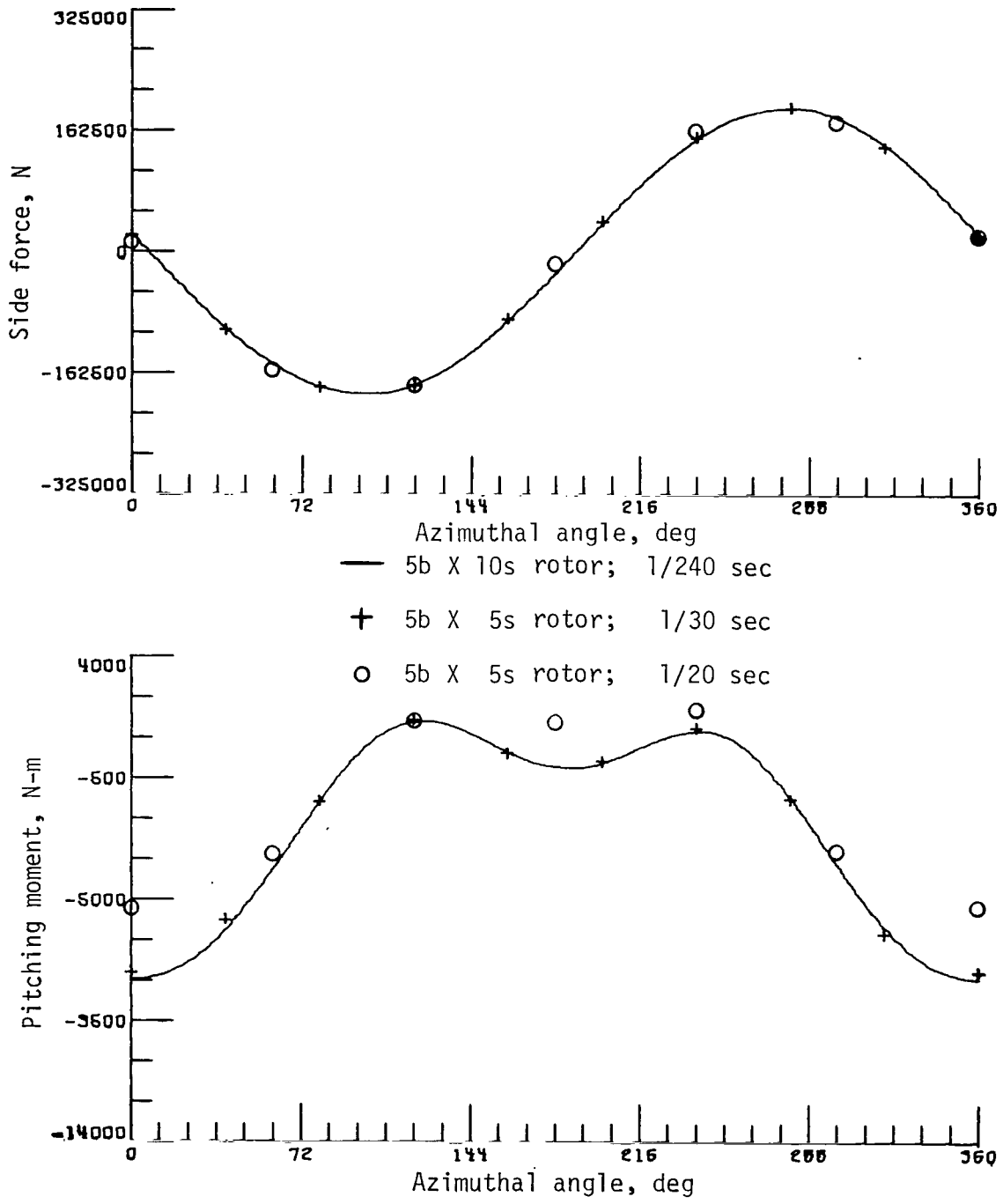

Figure 11.- Continued.

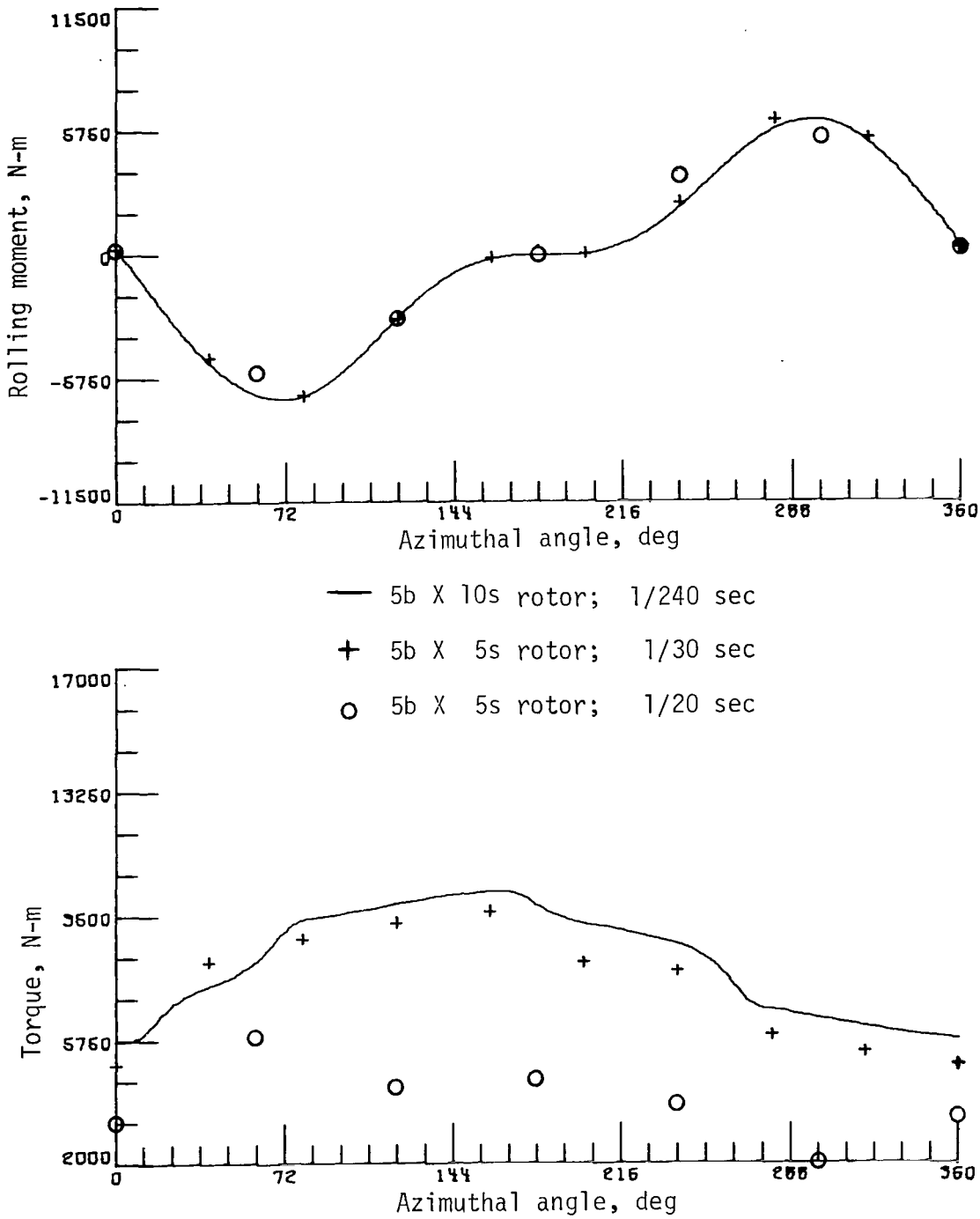

Figure 11.- Concluded.

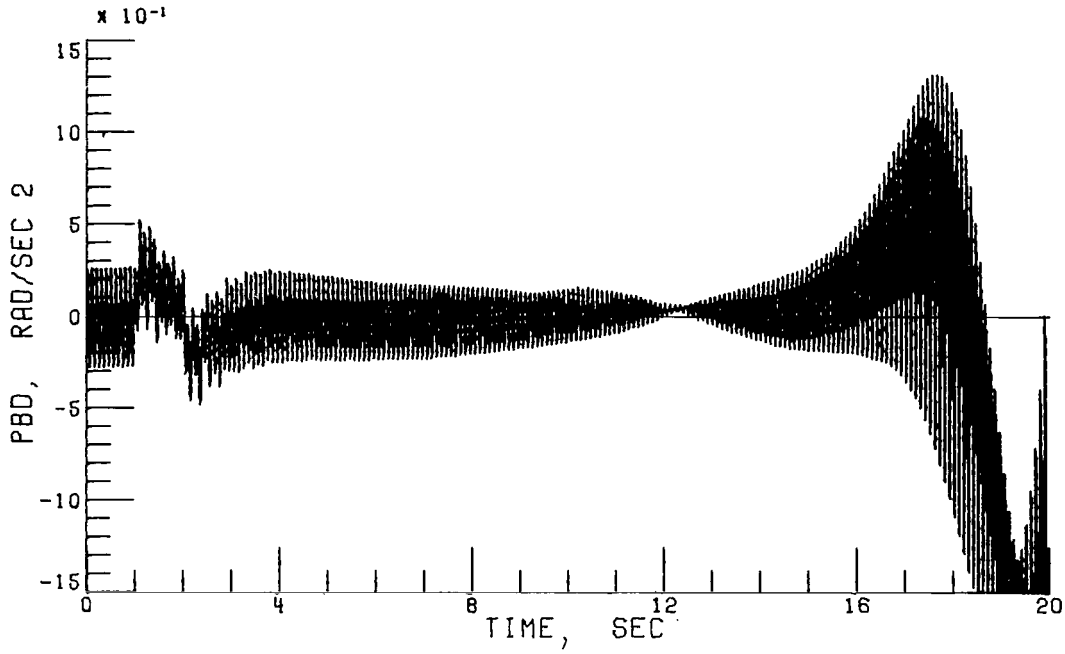

(a) 3b × 5s rotor.

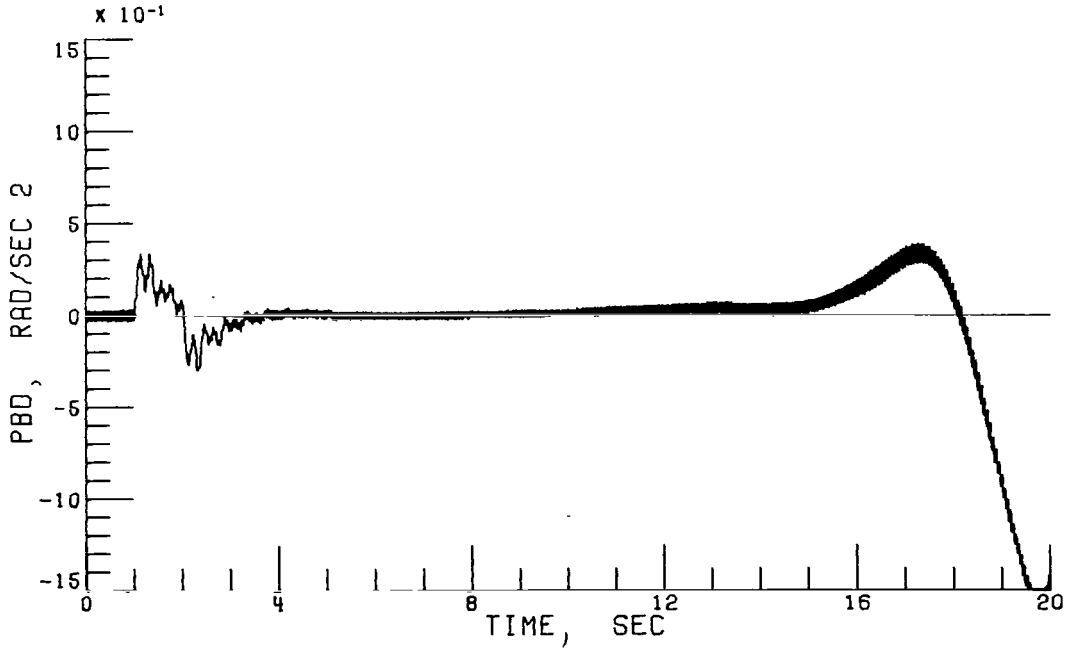

(b) 5b × 10s rotor.

Figure 12.- Effect of blade reduction on vehicle dynamic response at 120 knots. Integration interval, 1/240 second.

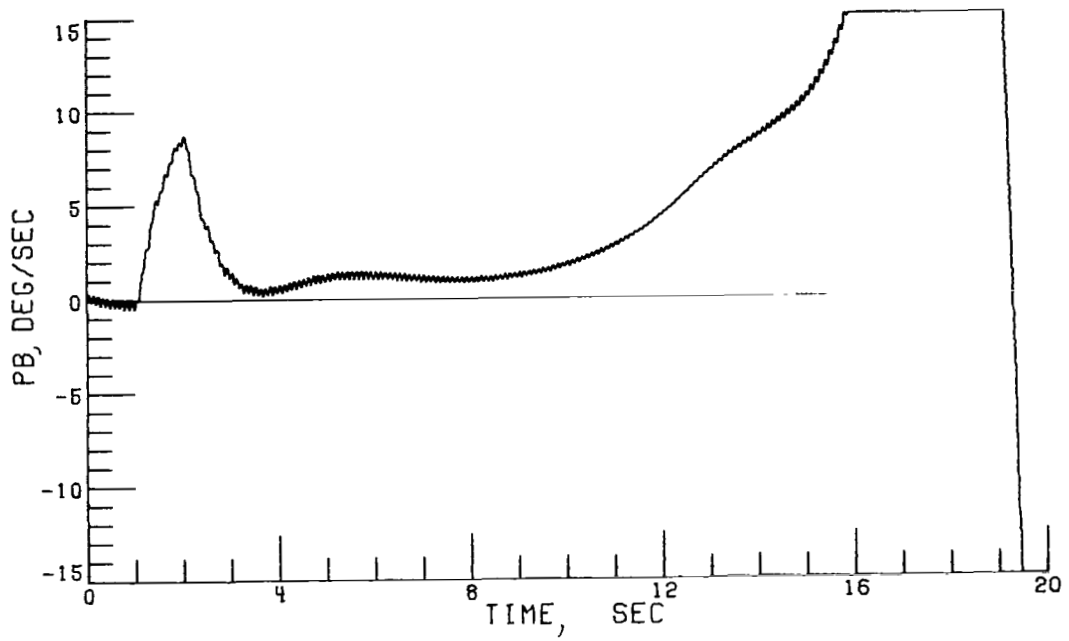

(c) 3b × 5s rotor.

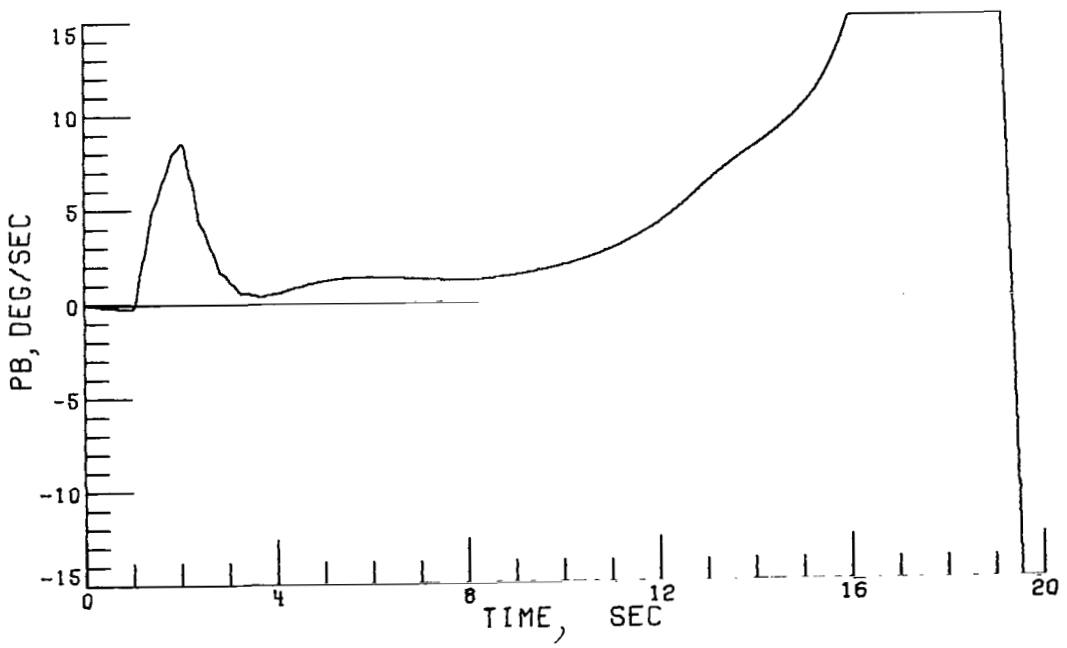

(d) 5b × 10s rotor.

Figure 12.- Continued.

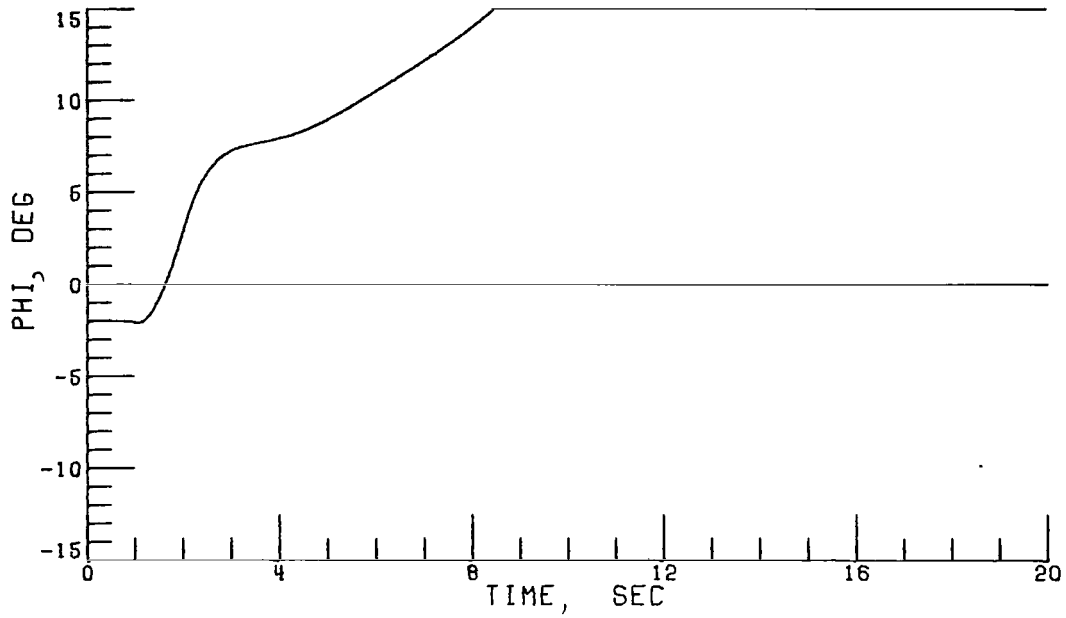

(e) 3b x 5s rotor.

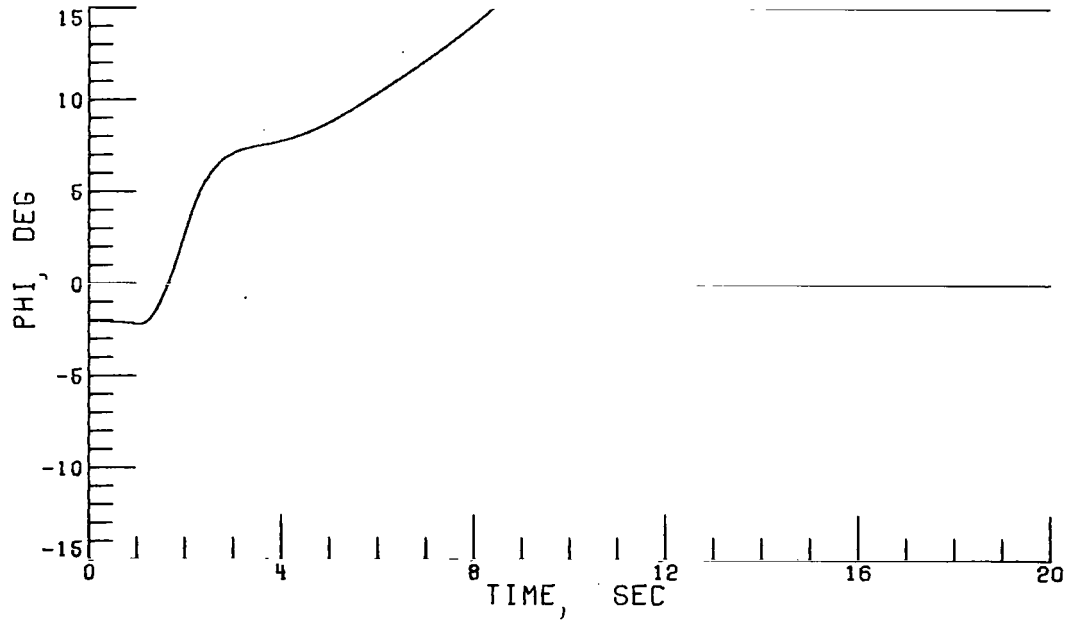

(f) 5b x 10s rotor.

Figure 12.- Continued.

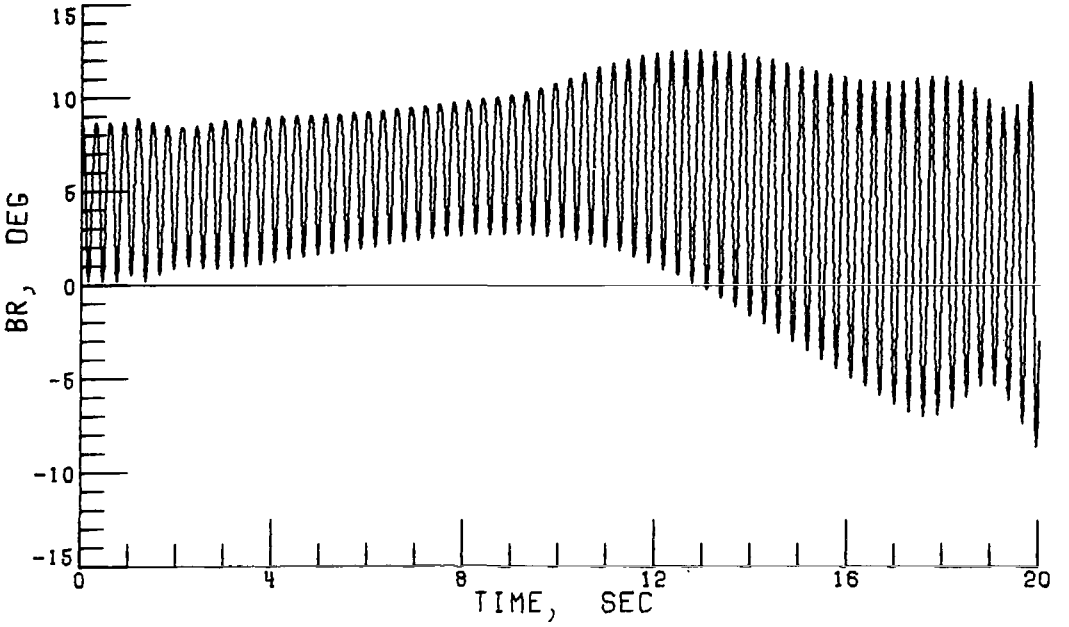

(g) 3b × 5s rotor.

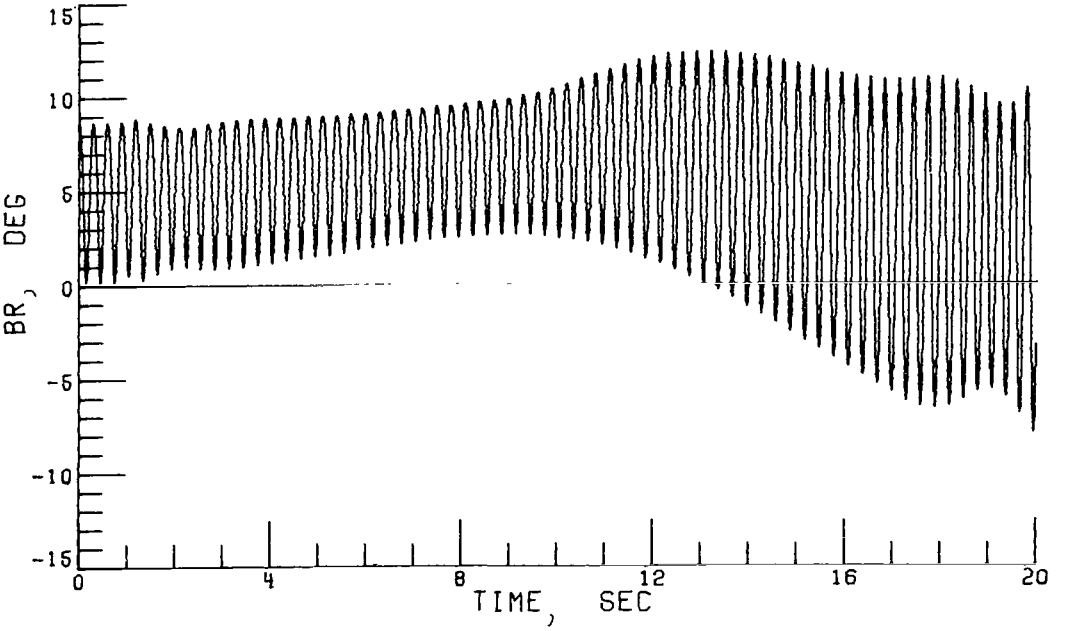

(h) 5b × 10s rotor.

Figure 12.- Concluded.

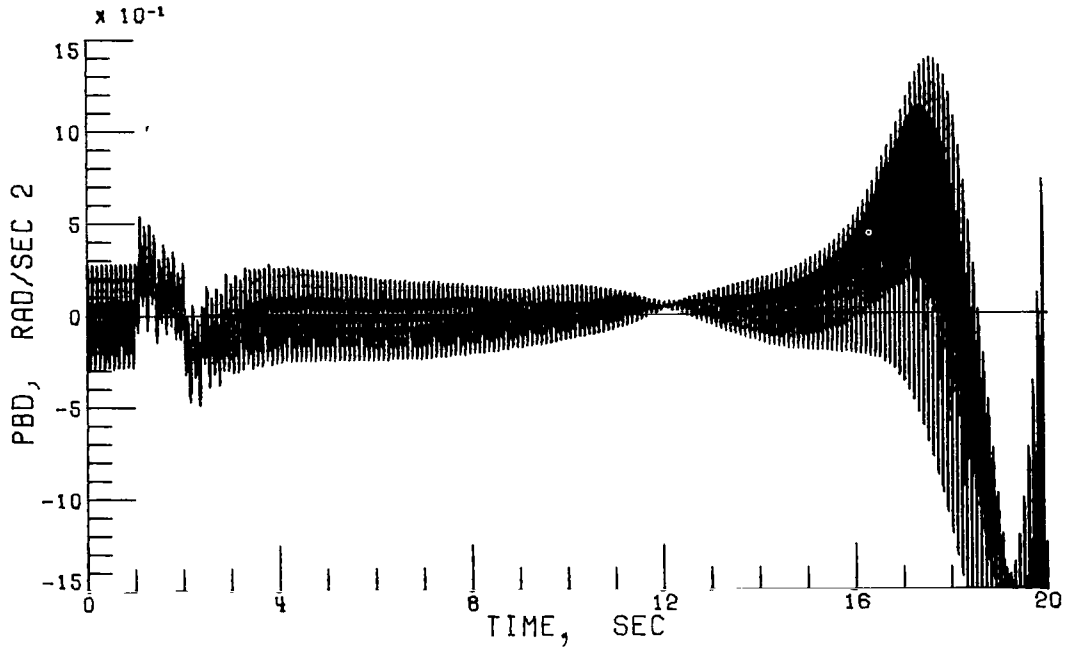

(a) 3b × 3s rotor.

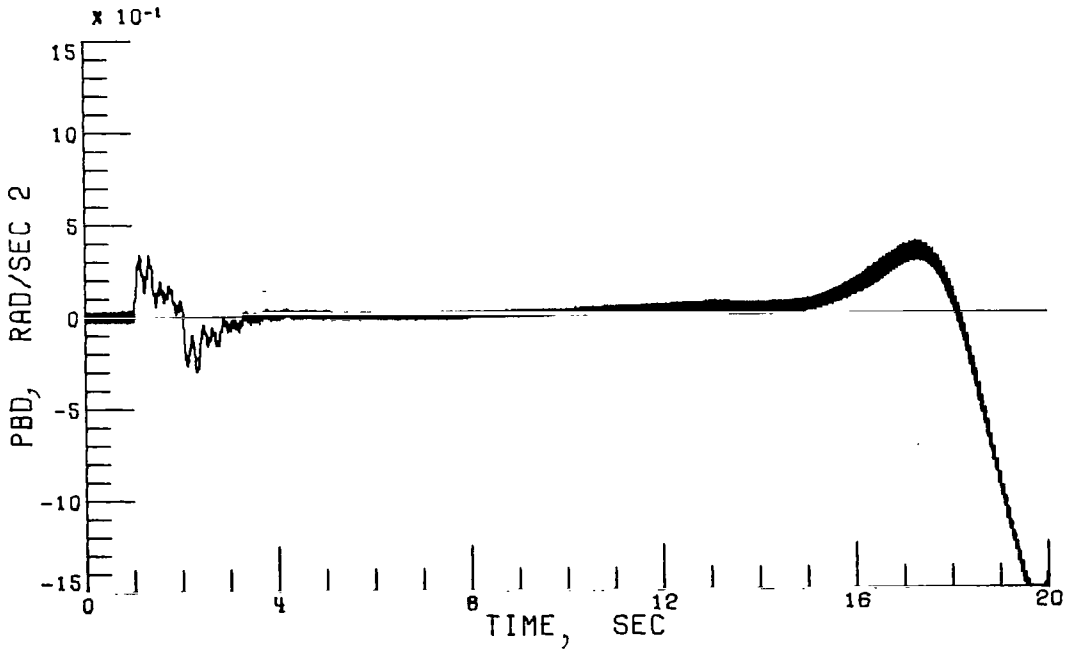

(b) 5b × 10s rotor.

Figure 13.- Effect of combination blade and blade-segment reduction on vehicle dynamic response at 120 knots. Integration interval, 1/240 second.

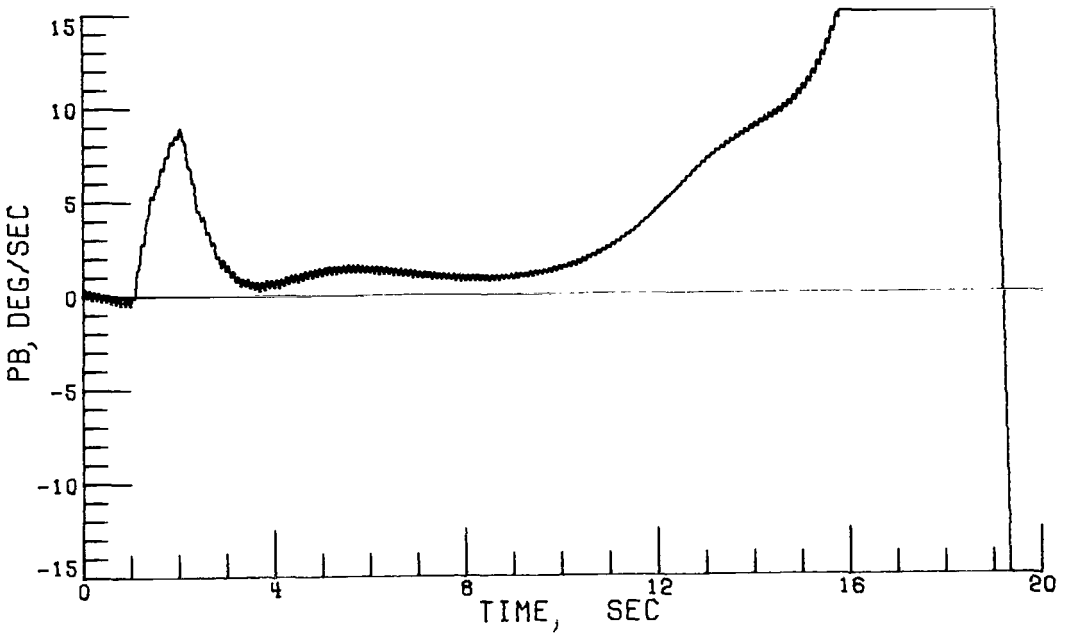

(c) 3b x 3s rotor.

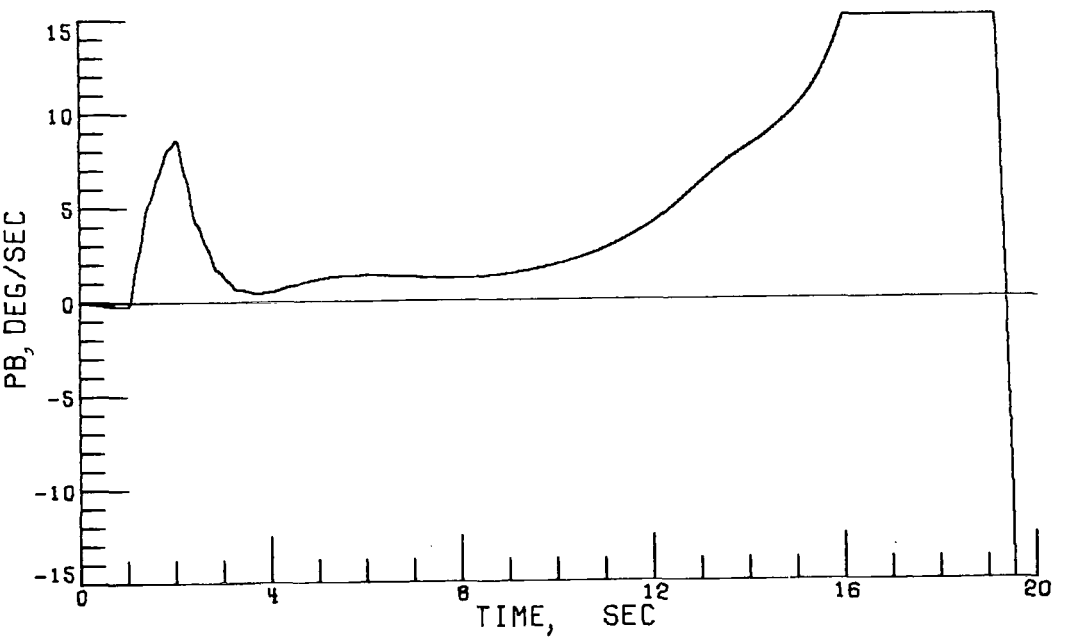

(d) 5b x 10s rotor.

Figure 13.- Continued.

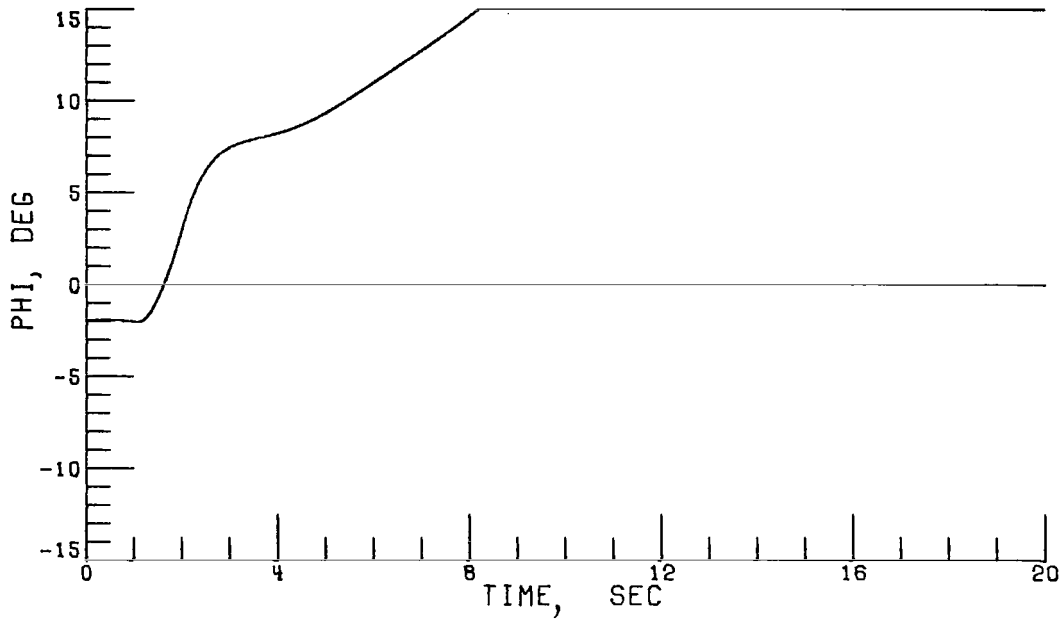

(e) 3b × 3s rotor.

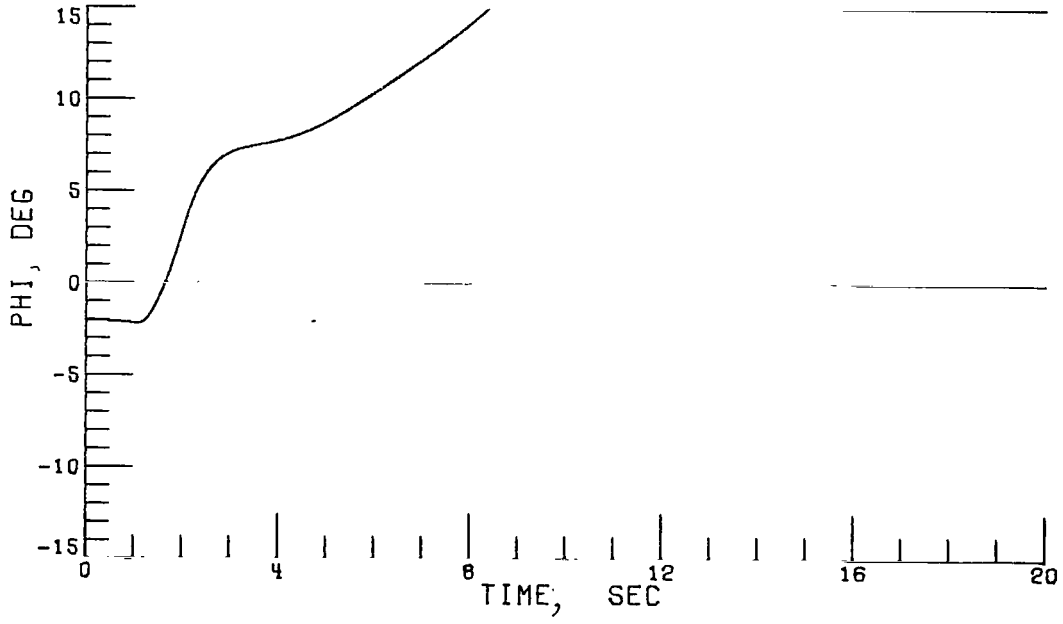

(f) 5b × 10s rotor.

Figure 13.- Continued.

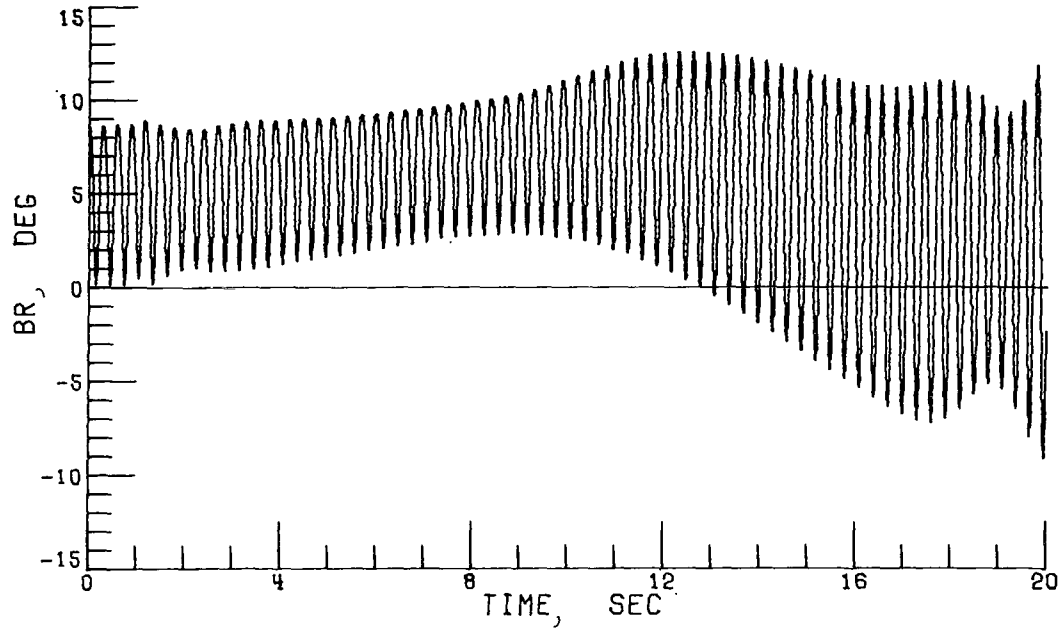

(g) 3b x 3s rotor.

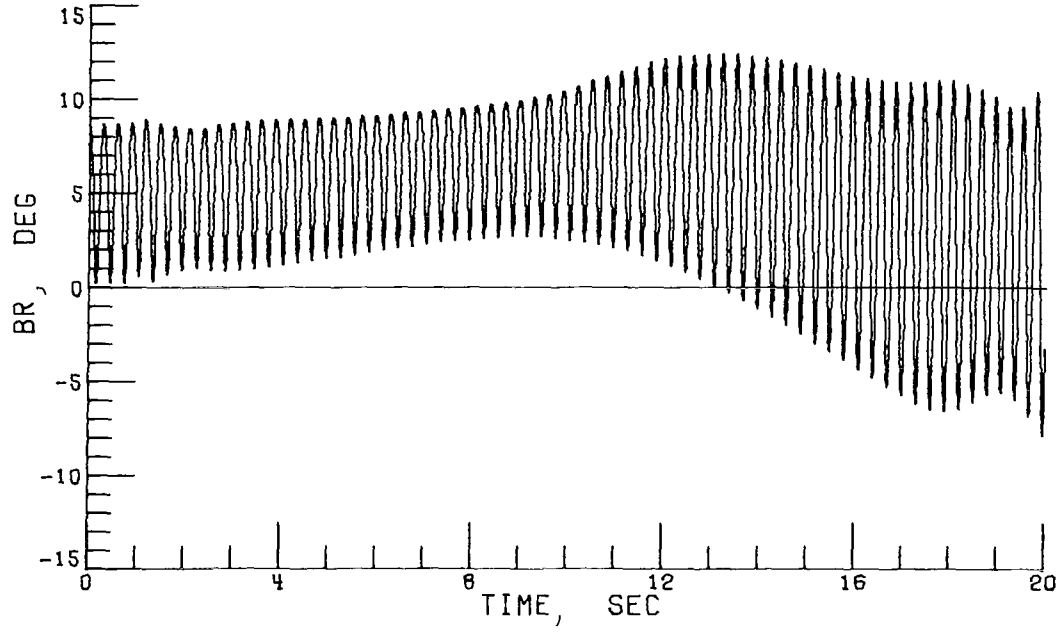

(h) 5b x 10s rotor.

Figure 13.- Concluded.

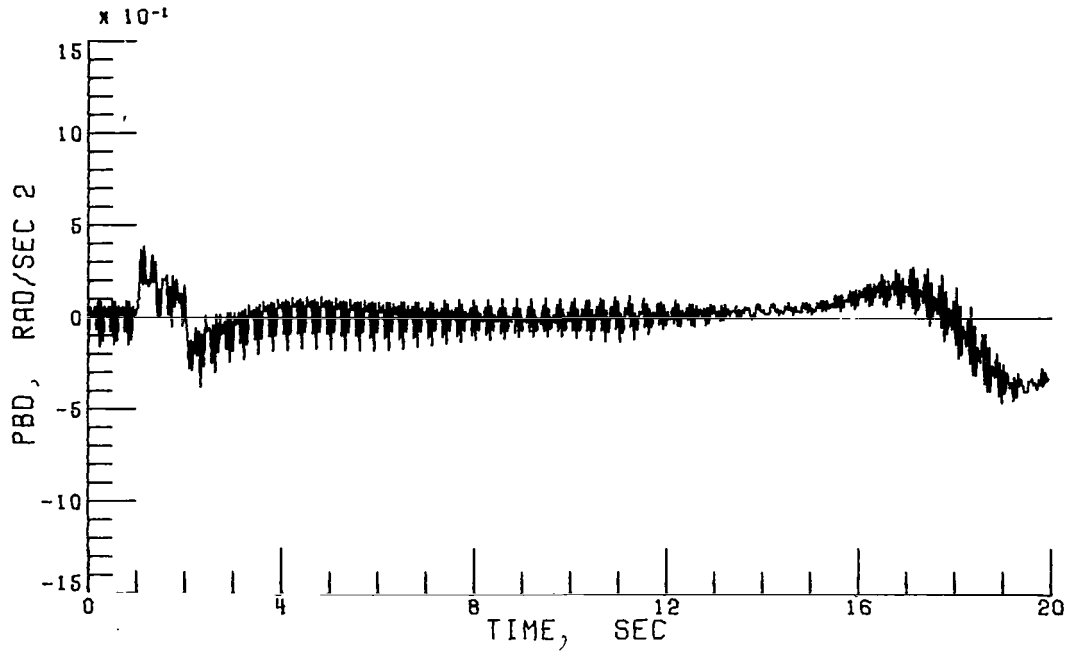

(a) 5b × 5s rotor; 1/30 second.

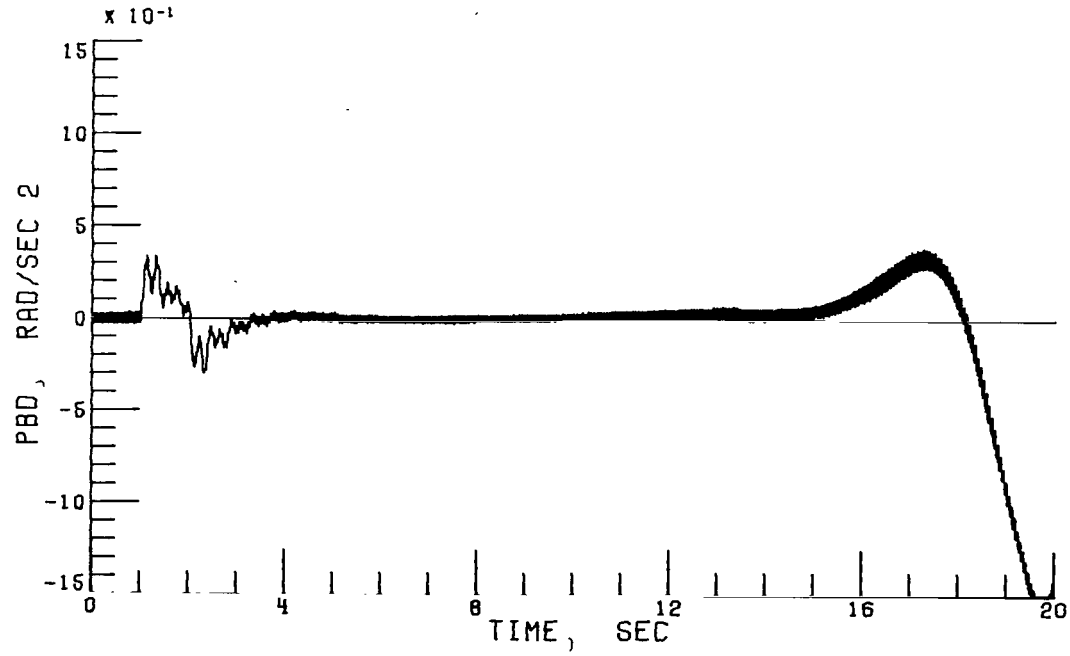

(b) 5b × 10s rotor; 1/240 second.

Figure 14.- Effect of increasing integration interval to 1/30 second on vehicle dynamic response at 120 knots for a five-blade—five-blade-segment rotor compared with the five-blade—ten-blade-segment baseline rotor with an integration interval of 1/240 second.

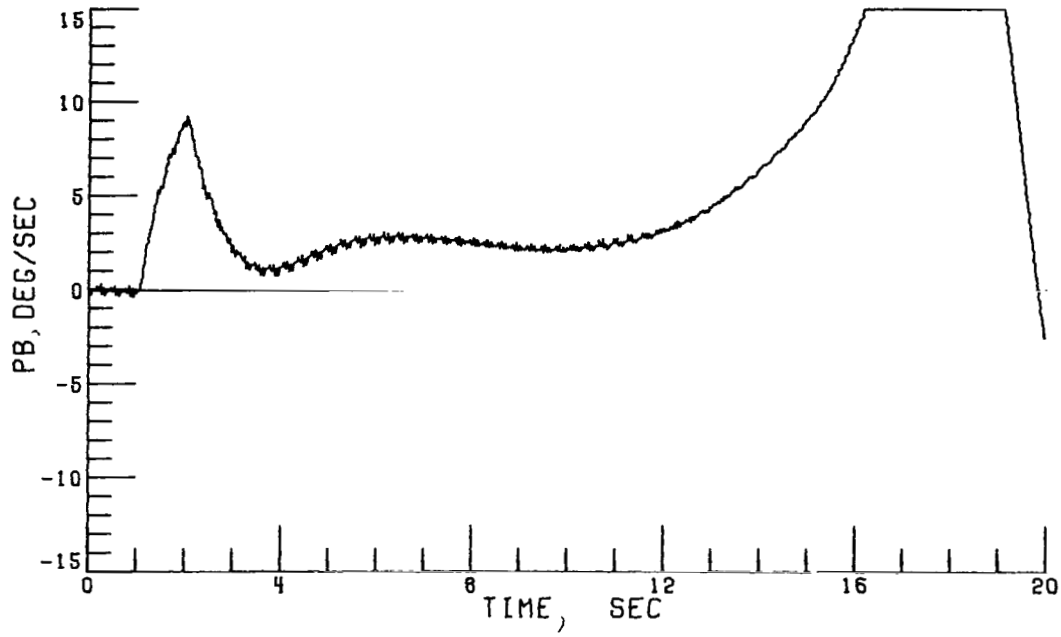

(c) 5b x 5s rotor; 1/30 second.

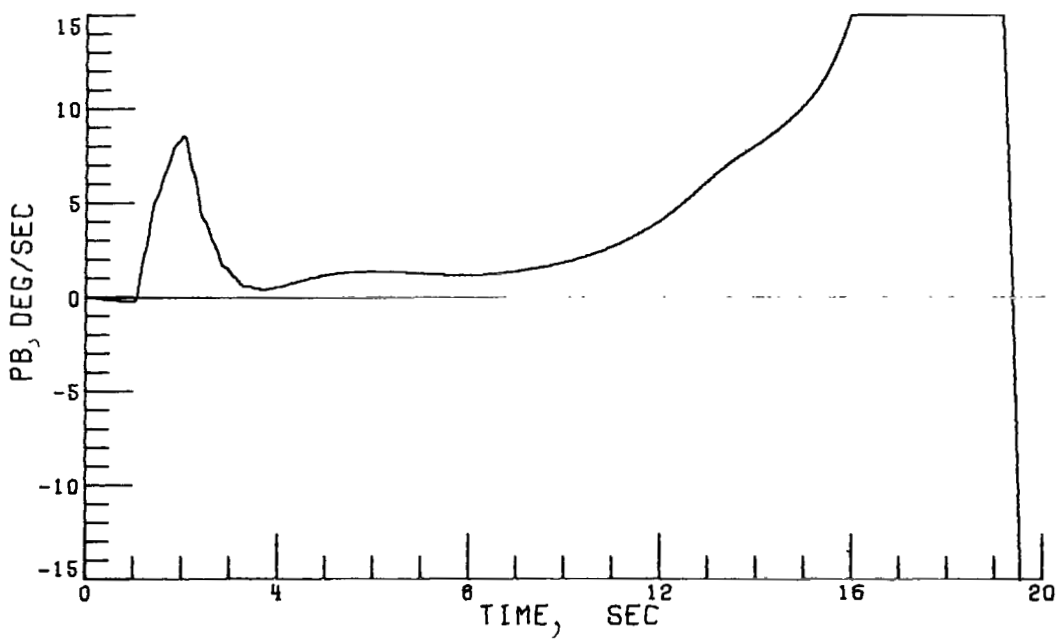

(d) 5b x 10s rotor; 1/240 second.

Figure 14.- Continued.

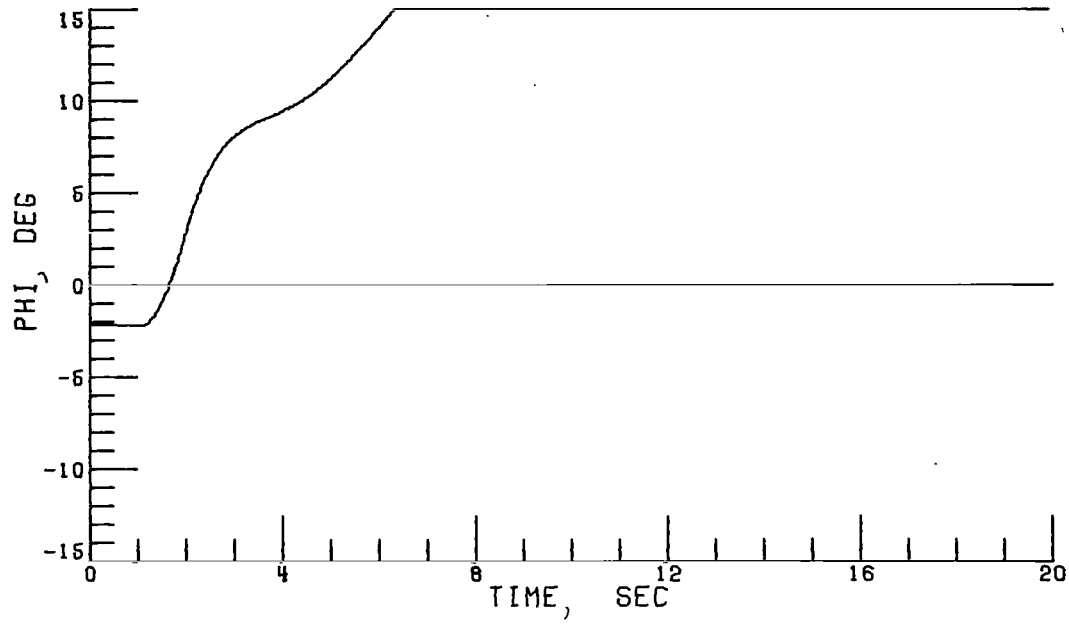

(e) 5b × 5s rotor; 1/30 second.

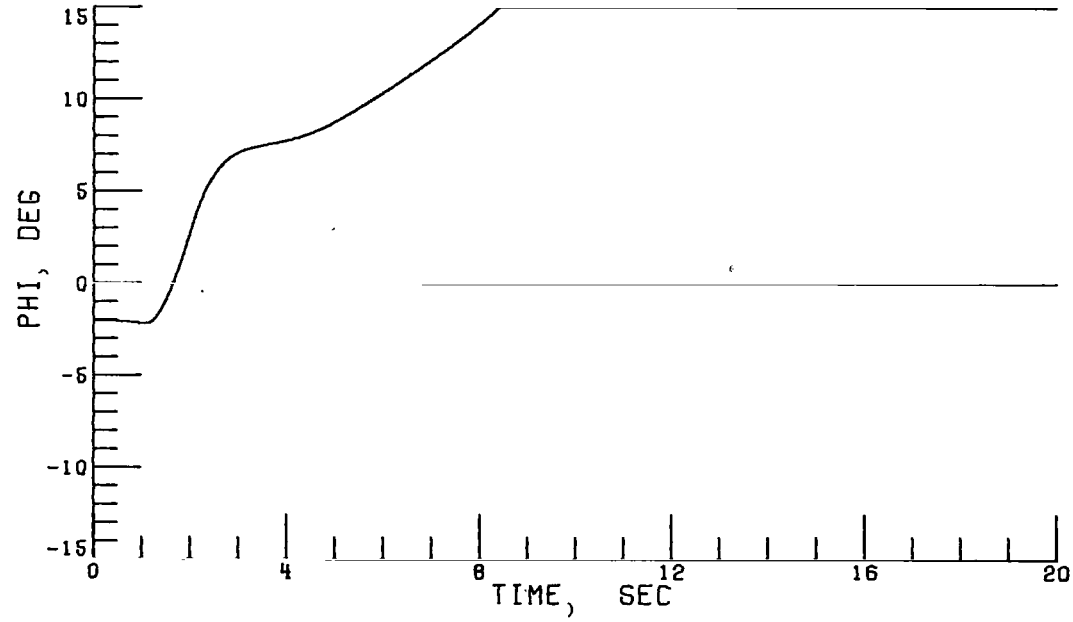

(f) 5b × 10s rotor; 1/240 second.

Figure 14.- Continued.

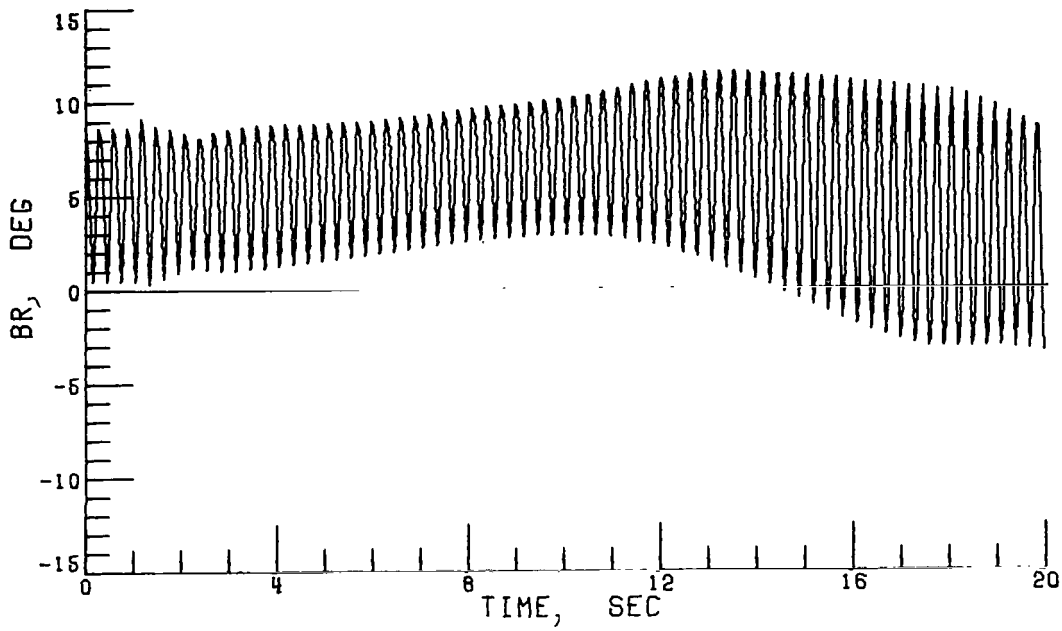

(g) 5b × 5s rotor; 1/30 second.

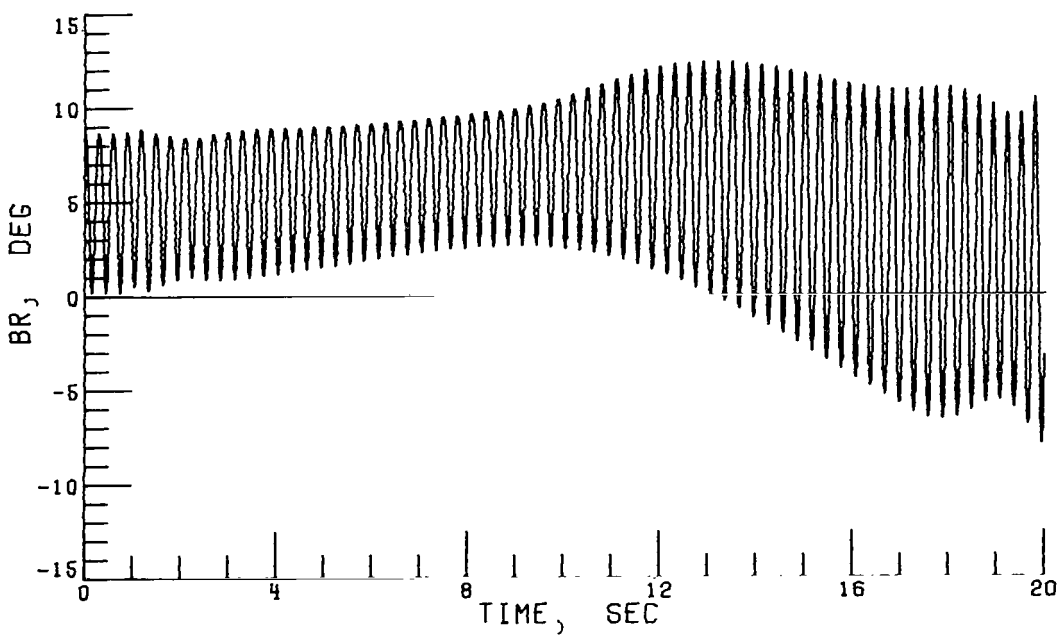

(h) 5b × 10s rotor; 1/240 second.

Figure 14.- Concluded.

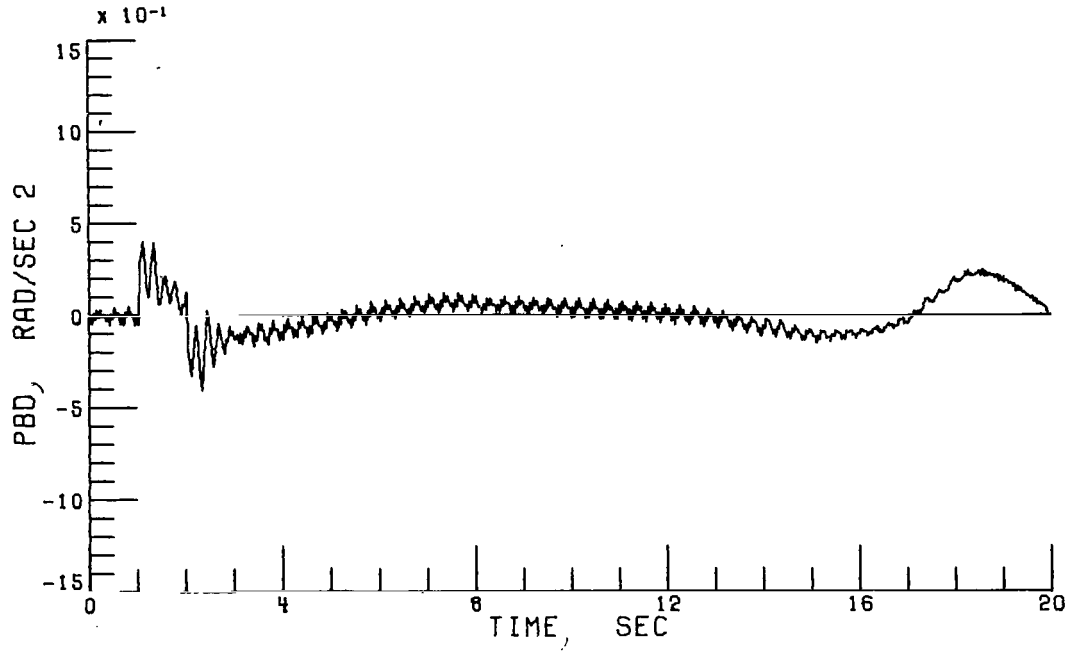

(a) 5b × 5s rotor; 1/30 second.

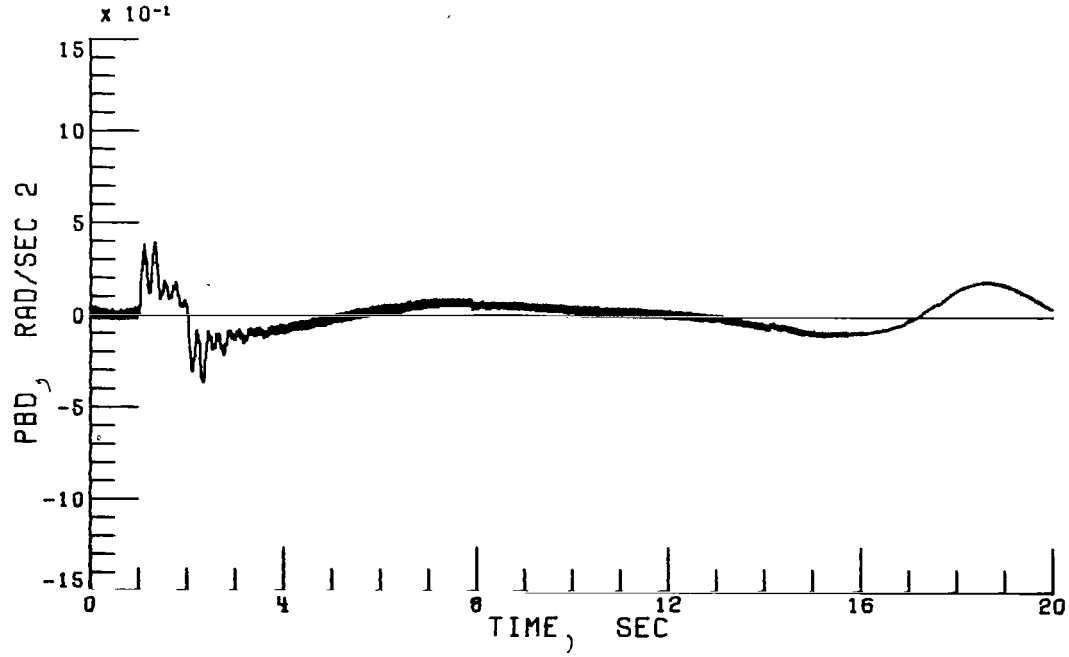

(b) 5b × 10s rotor; 1/240 second.

Figure 15.- Effect of increasing integration interval to 1/30 second on vehicle dynamic response at hover for a five-blade—five-blade-segment rotor compared with the five-blade—ten-blade-segment baseline rotor with an integration interval of 1/240 second.

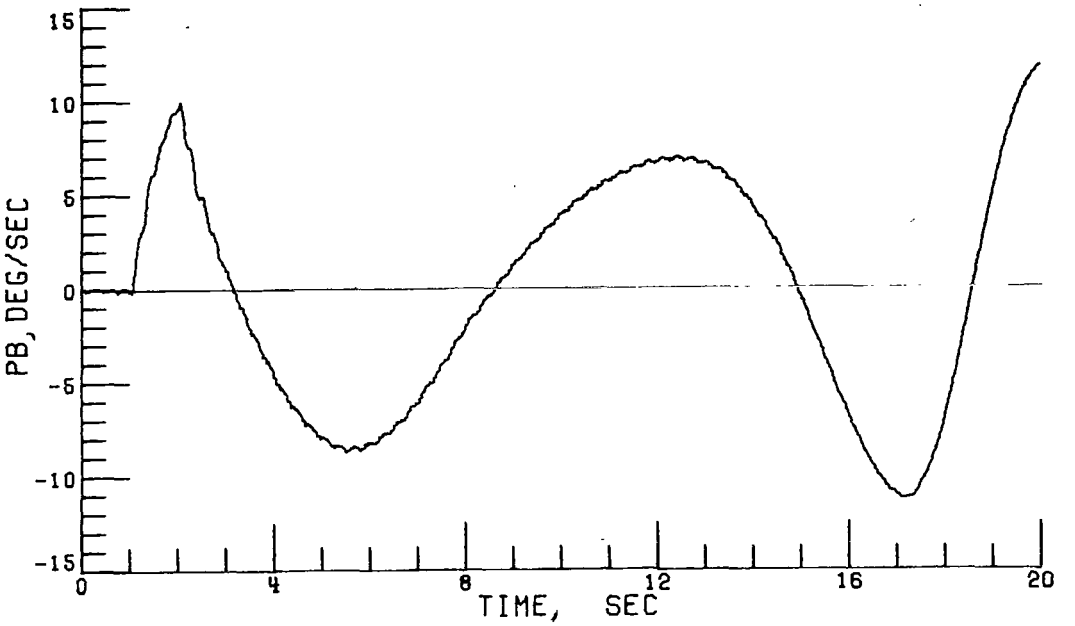

(c) 5b × 5s rotor; 1/30 second.

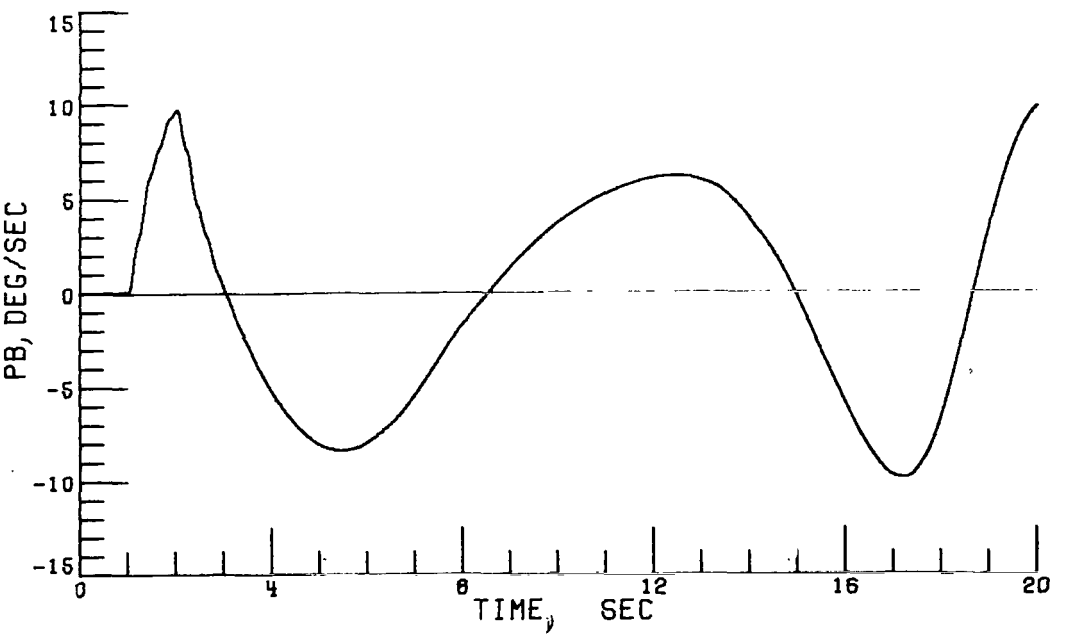

(d) 5b × 10s rotor; 1/240 second.

Figure 15.- Continued.

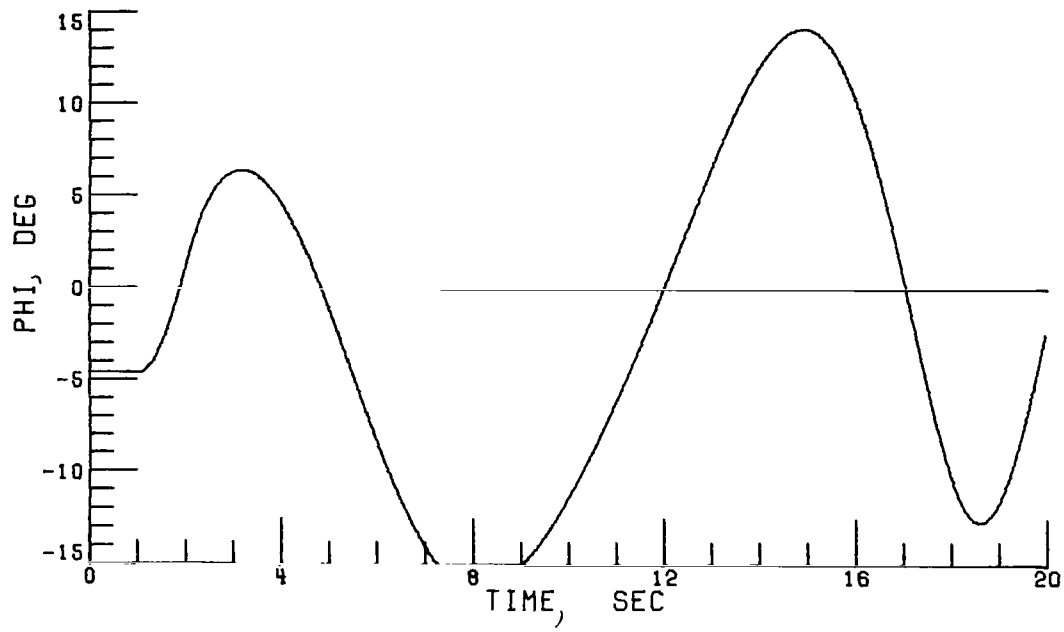

(e) 5b x 5s rotor; 1/30 second.

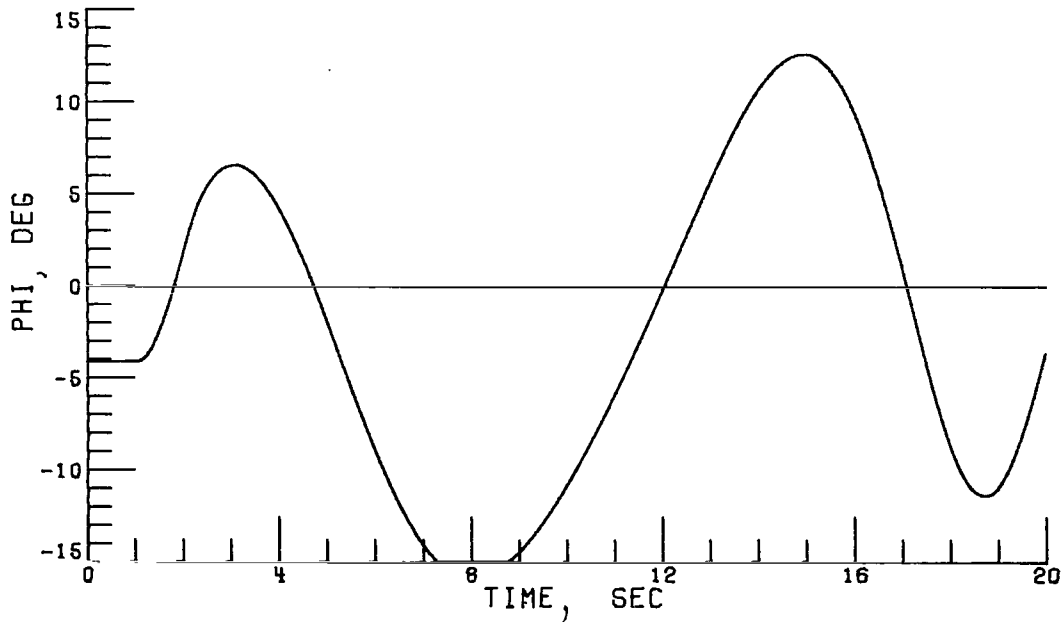

(f) 5b x 10s rotor; 1/240 second.

Figure 15.- Continued.

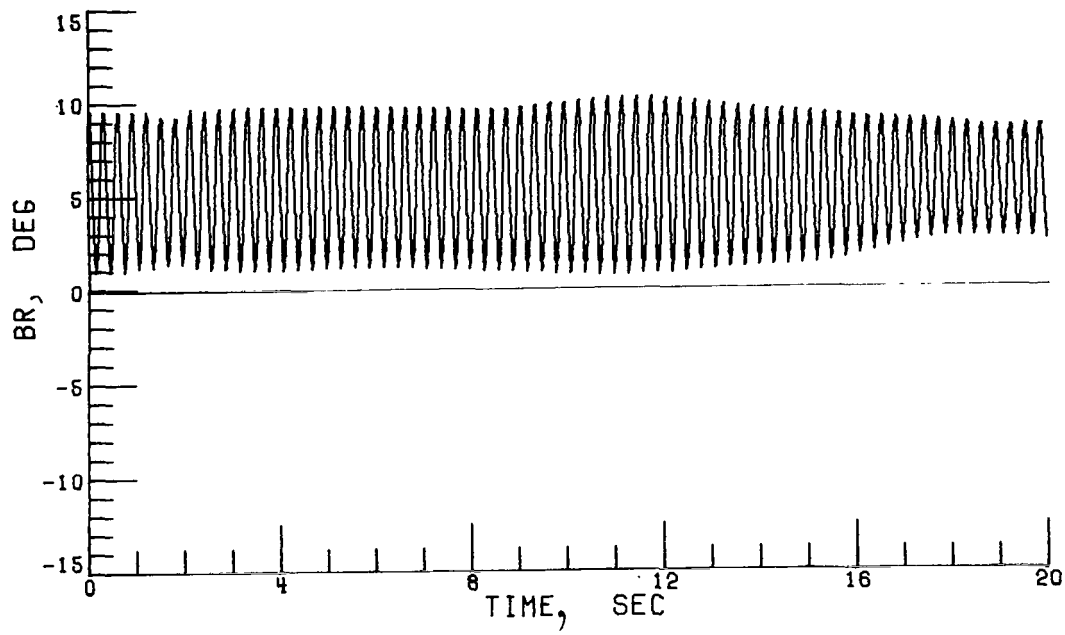

(g) 5b x 5s rotor; 1/30 second.

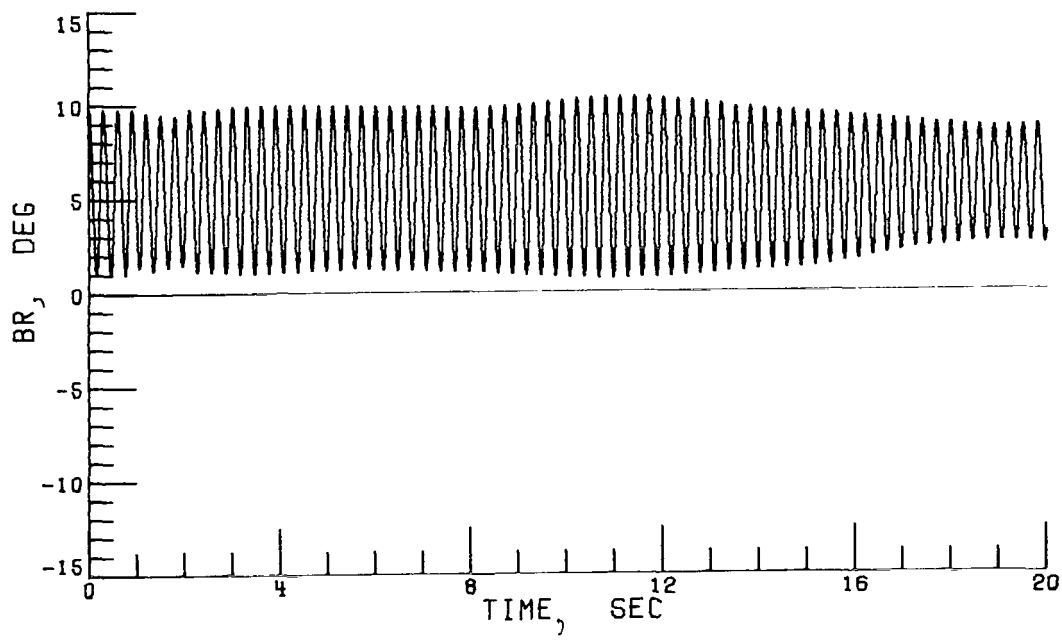

(h) 5b x 10s rotor; 1/240 second.

Figure 15.- Concluded.

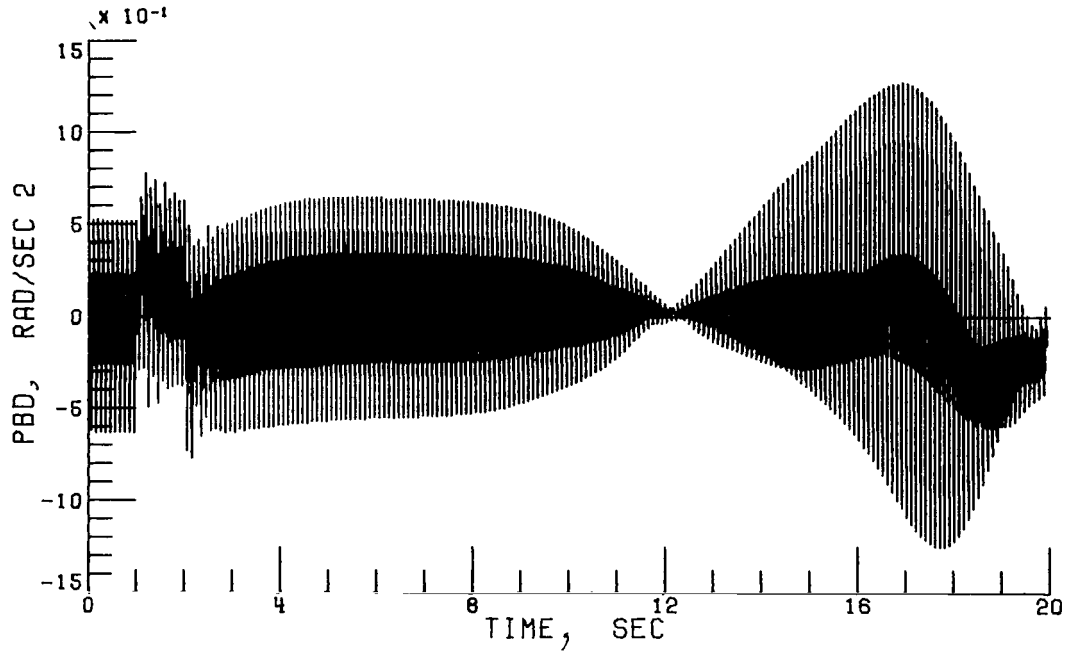

(a) 3b x 3s rotor; 1/30 second.

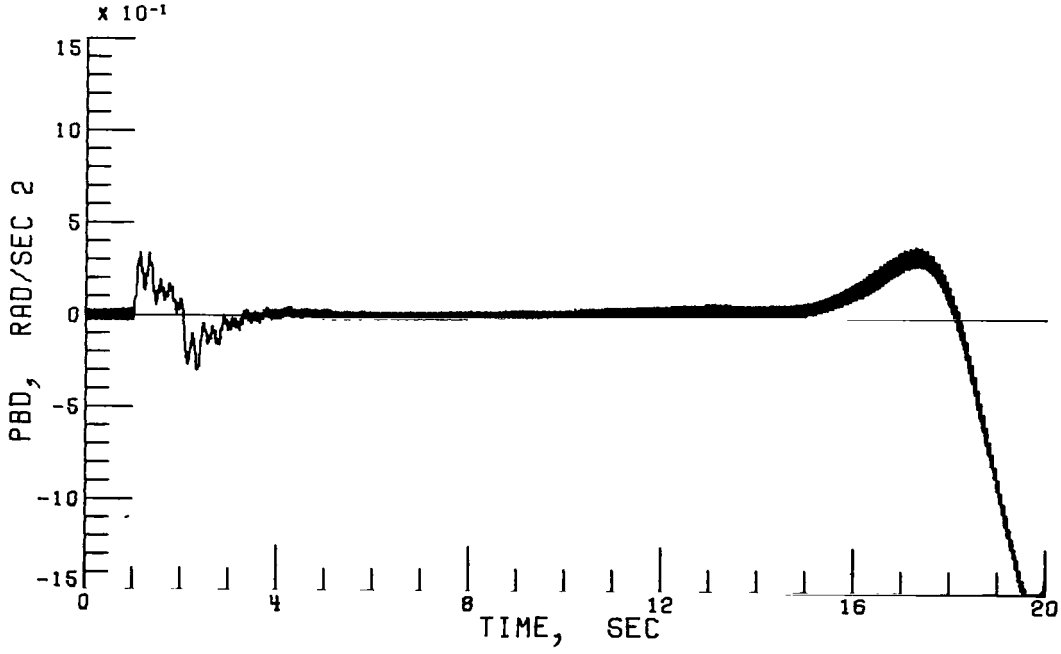

(b) 5b × 10s rotor; 1/240 second.

Figure 16.- Effect of increasing integration interval to 1/30 second on vehicle dynamic response at 120 knots for a three-blade—three-blade-segment rotor compared with the five-blade—ten-blade-segment baseline rotor with an integration interval of 1/240 second.

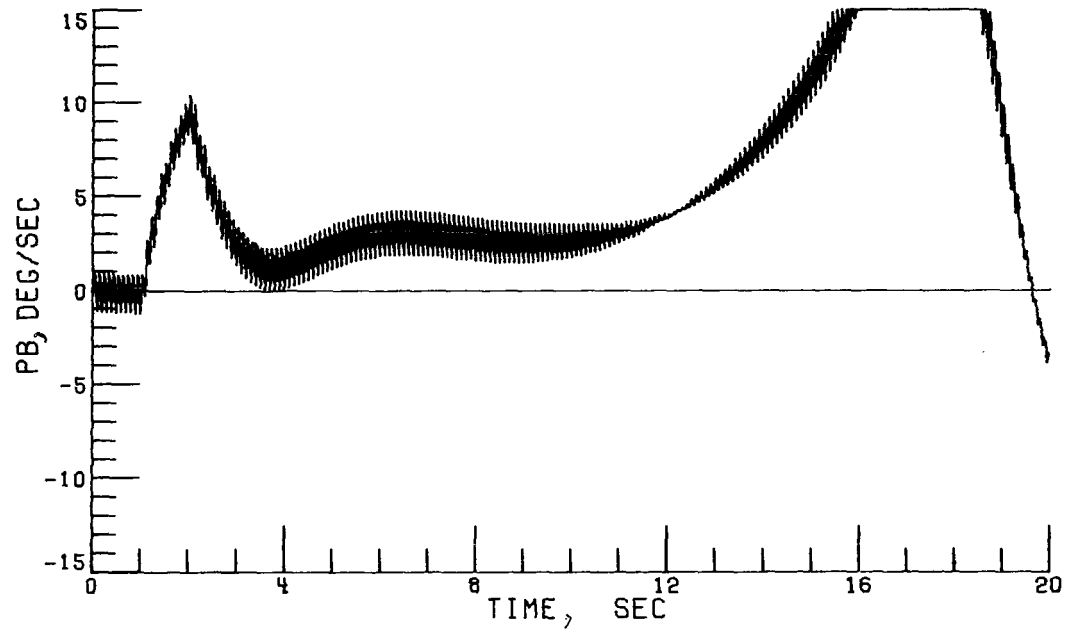

(c) 3b × 3s rotor; 1/30 second.

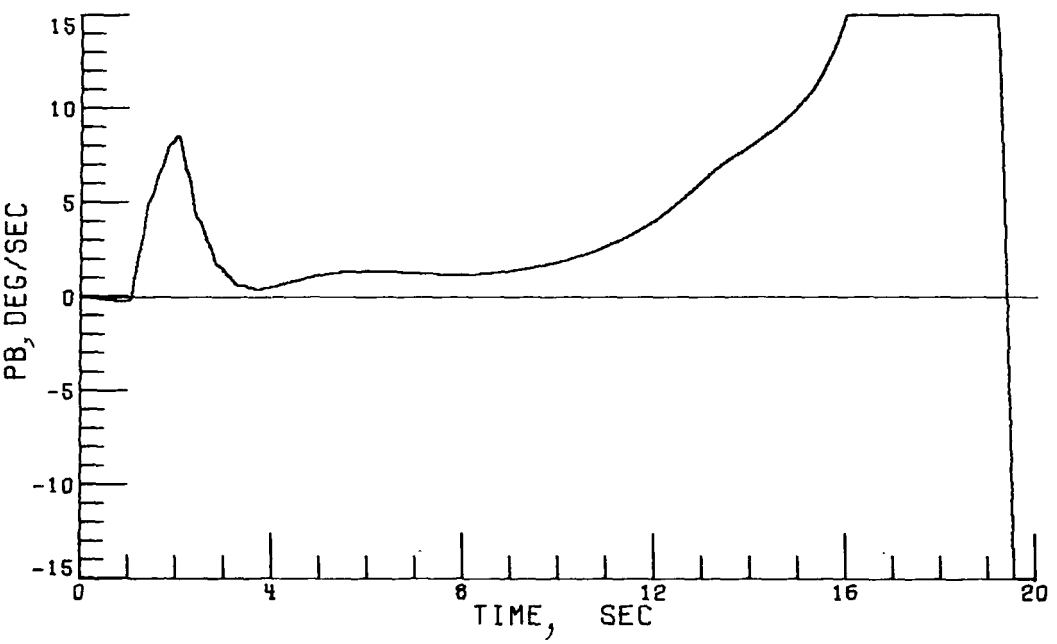

(d) 5b × 10s rotor; 1/240 second.

Figure 16.- Continued.

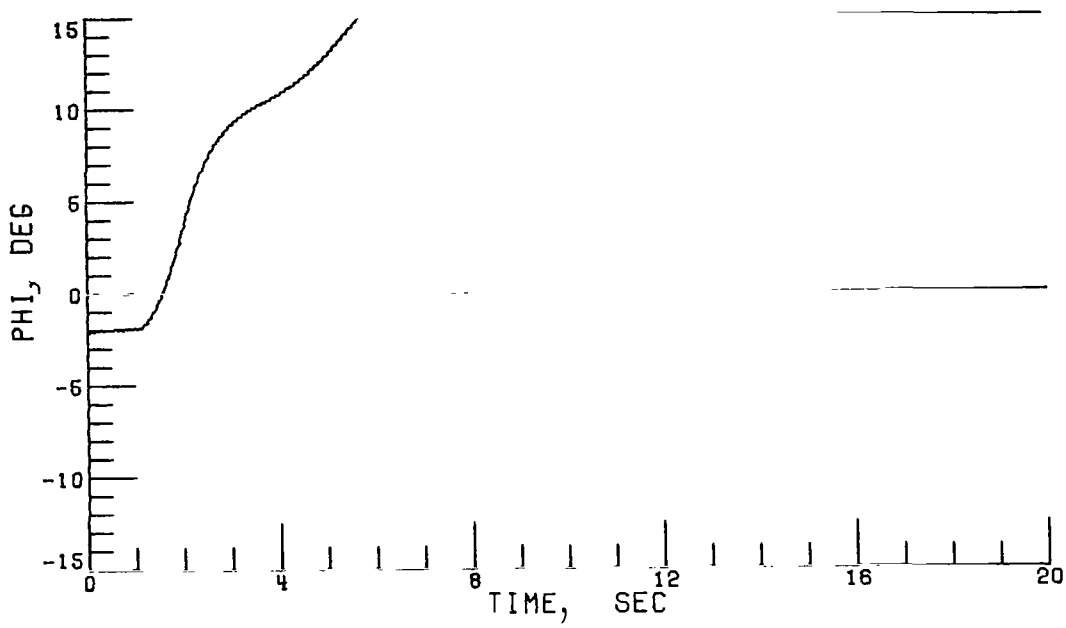

(e) 3b x 3s rotor; 1/30 second.

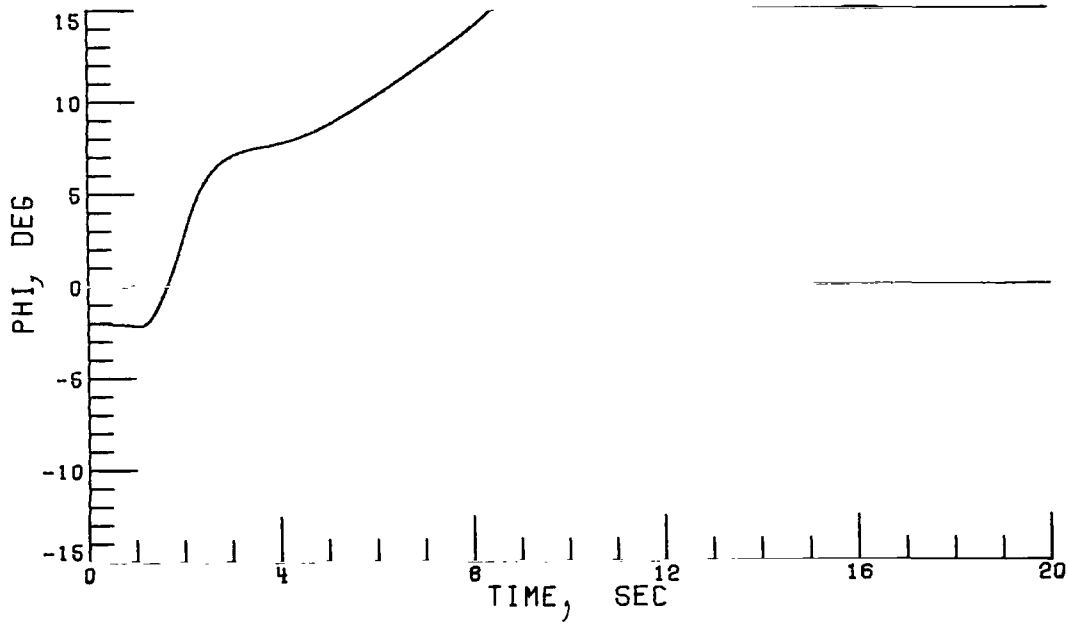

(f) 5b x 10s rotor; 1/240 second.

Figure 16.- Continued.

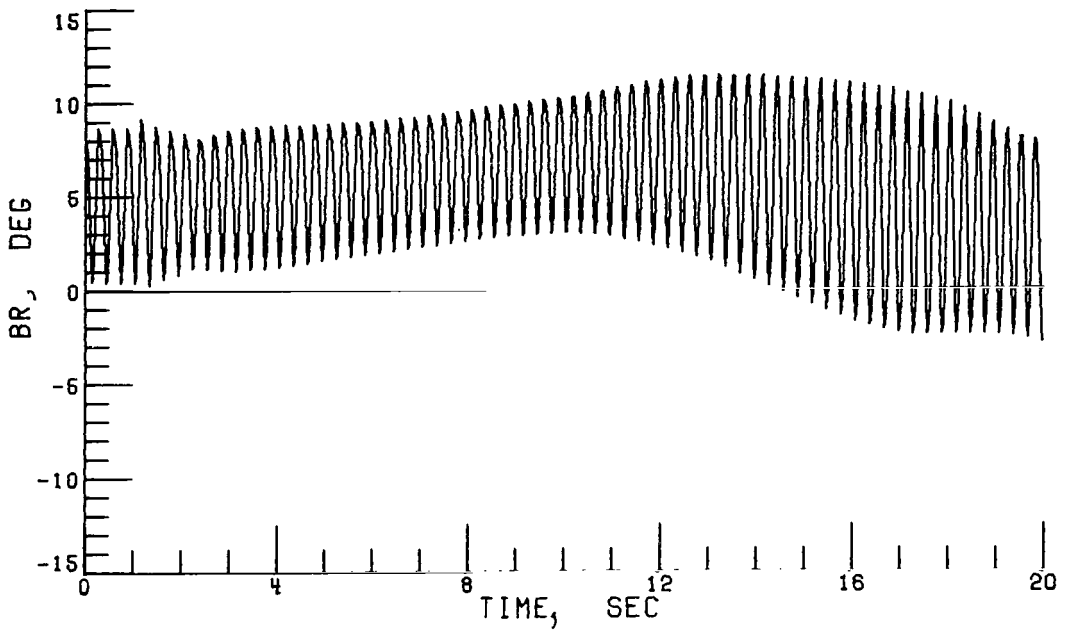

(g) 3b × 3s rotor; 1/30 second.

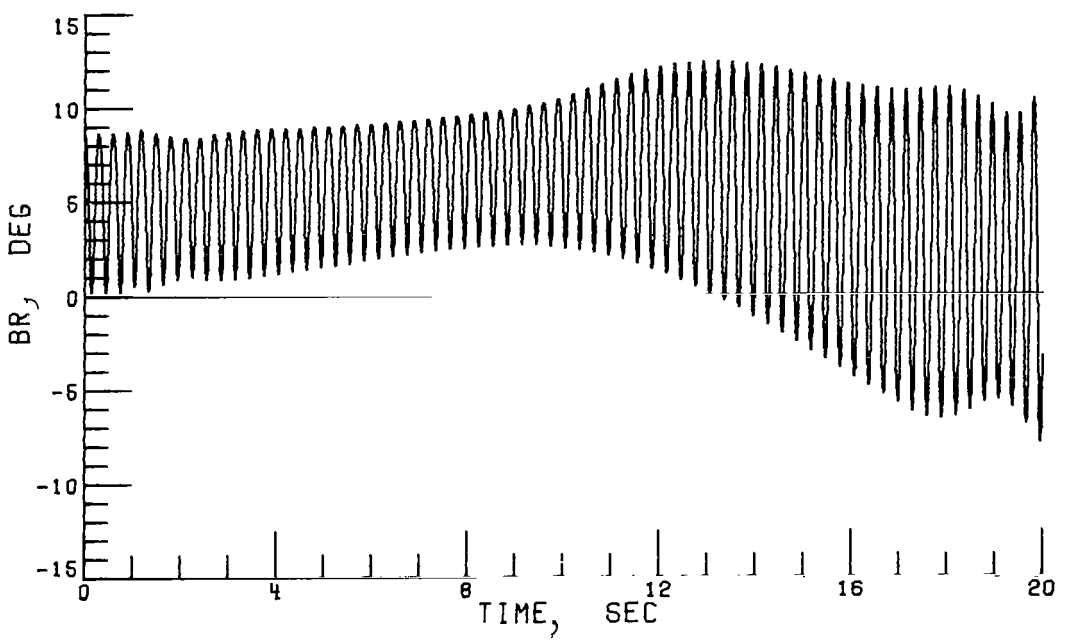

(h) 5b × 10s rotor; 1/240 second.

Figure 16.- Concluded.

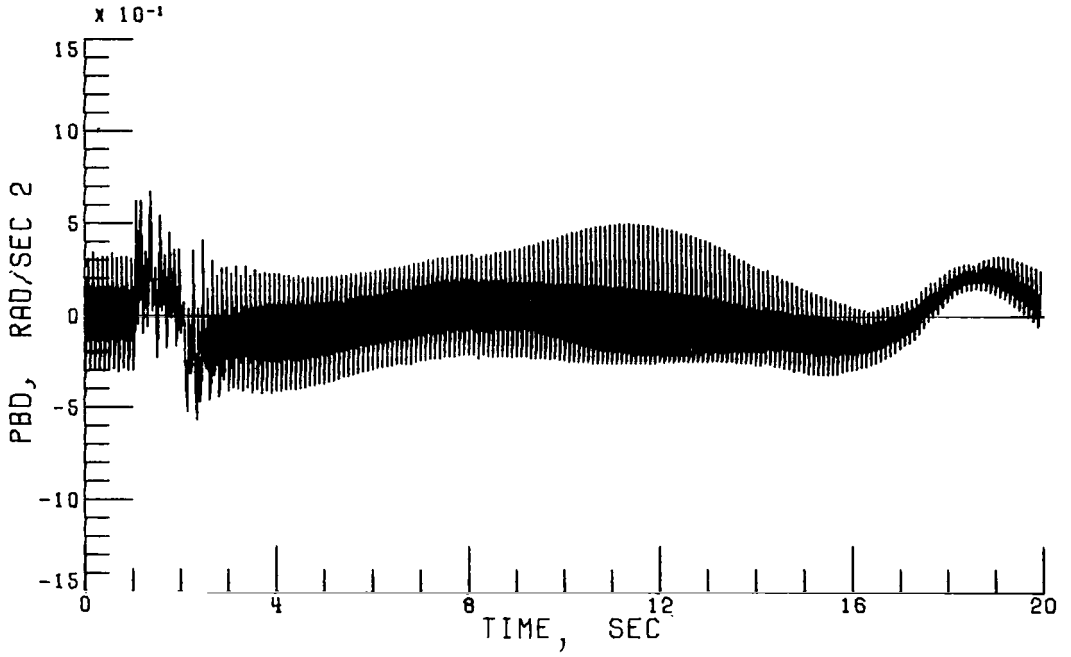

(a) 3b x 3s rotor; 1/30 second.

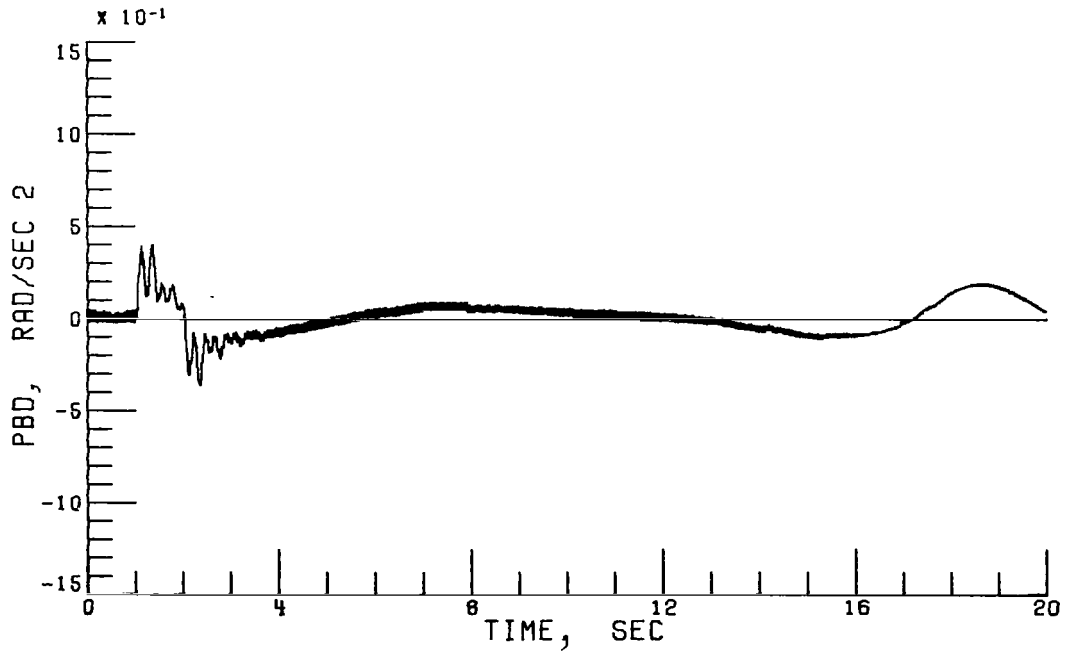

(b) 5b x 10s rotor; 1/240 second.

Figure 17.- Effect of increasing integration interval to 1/30 second on vehicle dynamic response at hover for a three-blade—three-blade-segment rotor compared with the five-blade—ten-blade-segment baseline rotor with an integration interval of 1/240 second.

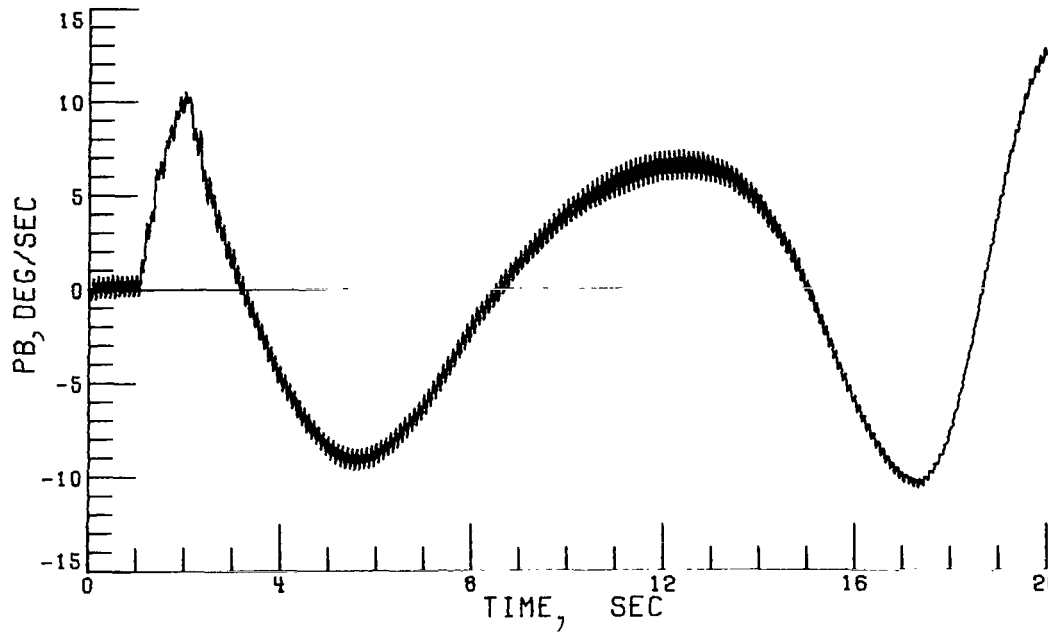

(c) 3b x 3s rotor; 1/30 second.

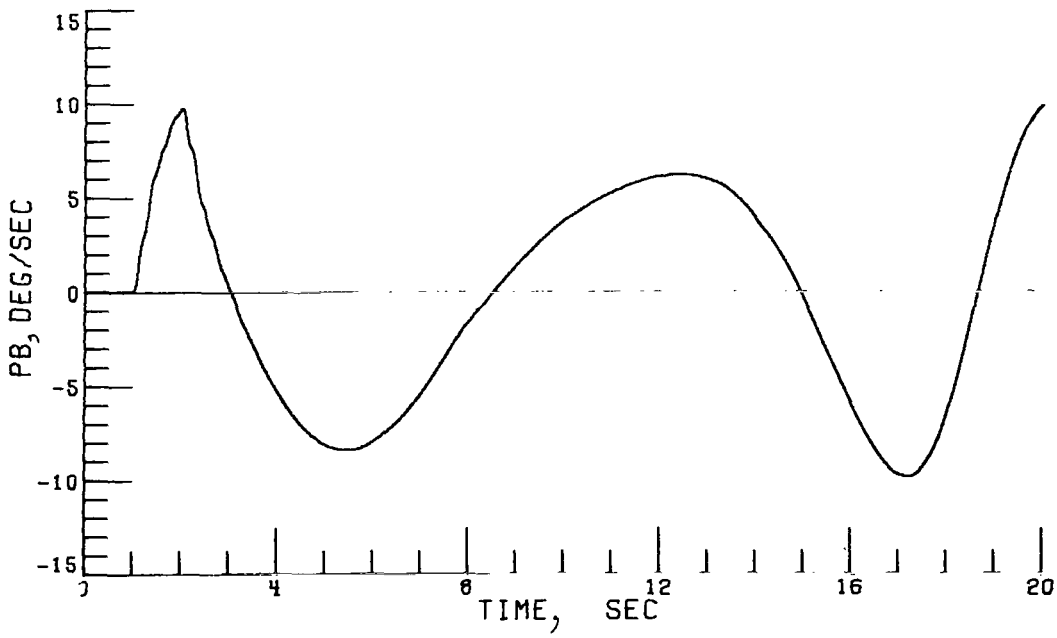

(d) 5b x 10s rotor; 1/240 second.

Figure 17.- Continued.

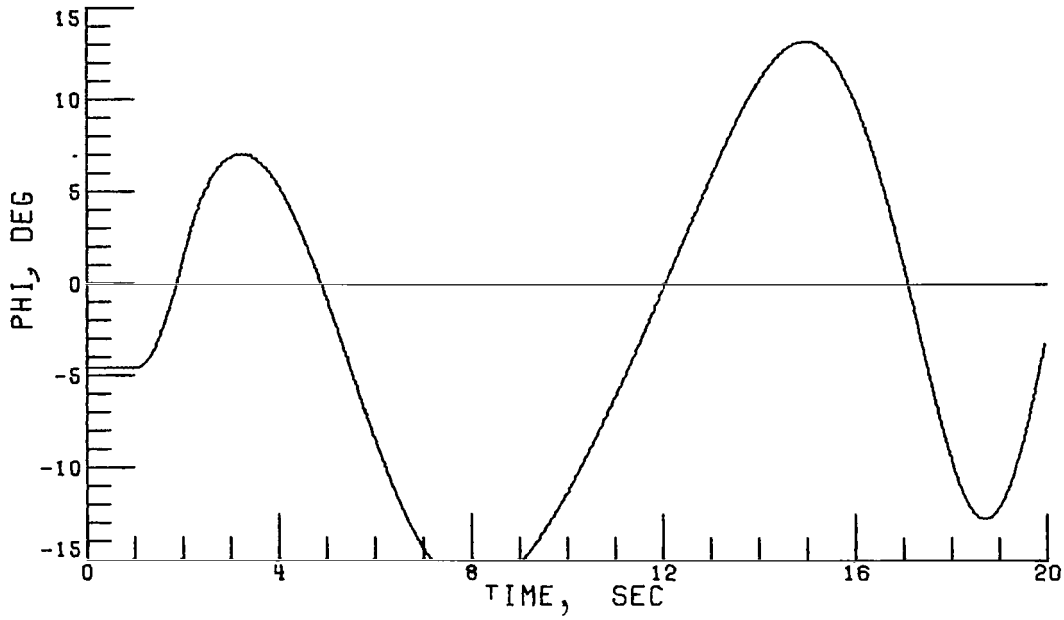

(e) 3b × 3s rotor; 1/30 second.

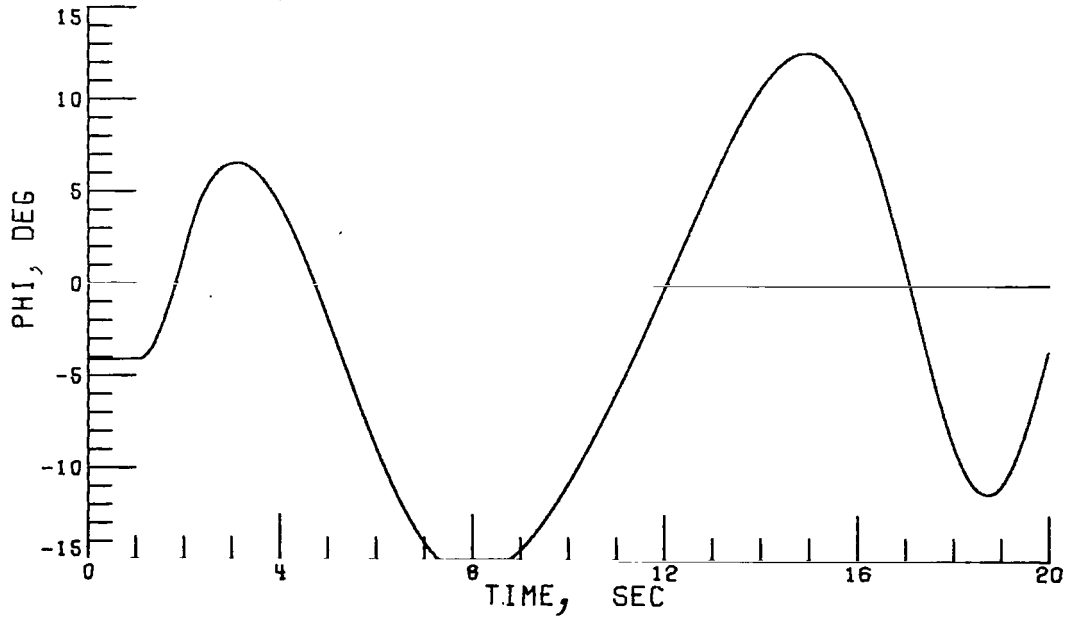

(f) 5b × 10s rotor; 1/240 second.

Figure 17.- Continued.

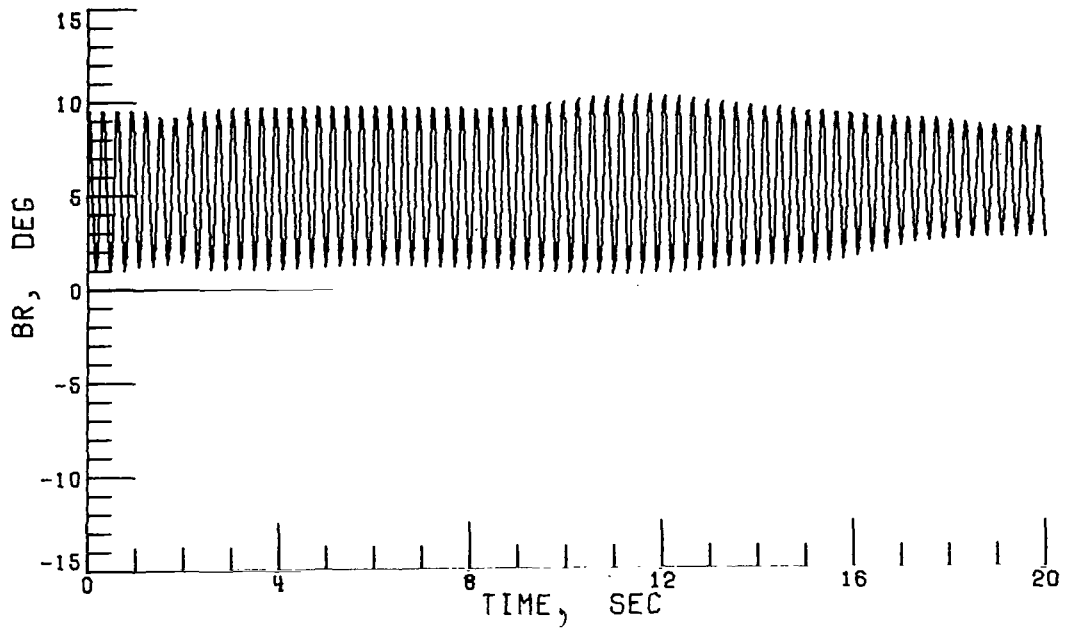

(g) 3b × 3s rotor; 1/30 second.

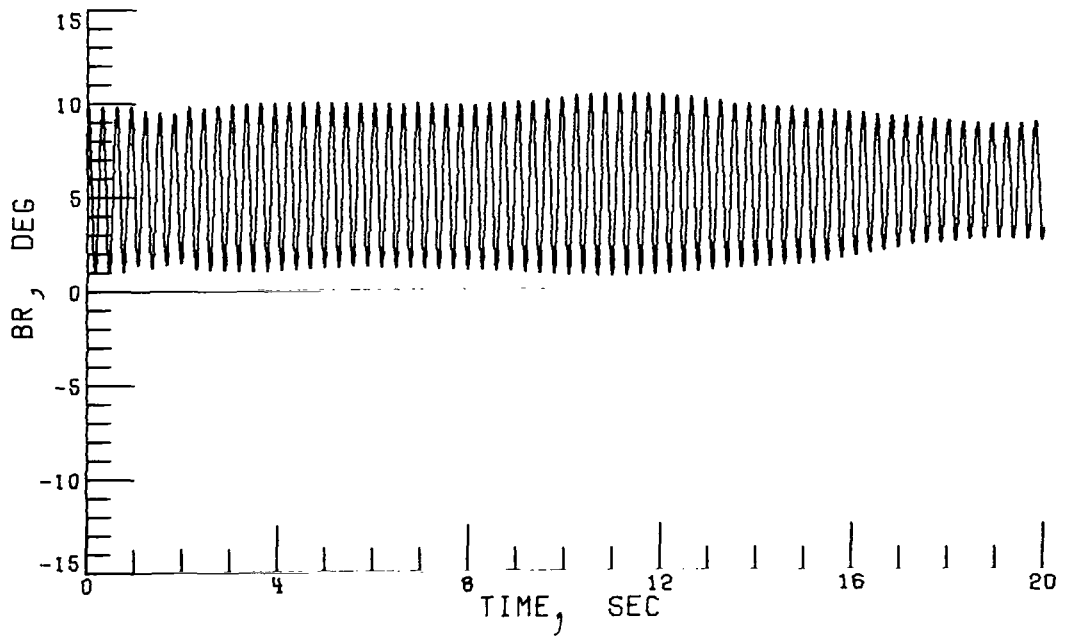

(h) 5b × 10s rotor; 1/240 second.

Figure 17.- Concluded.

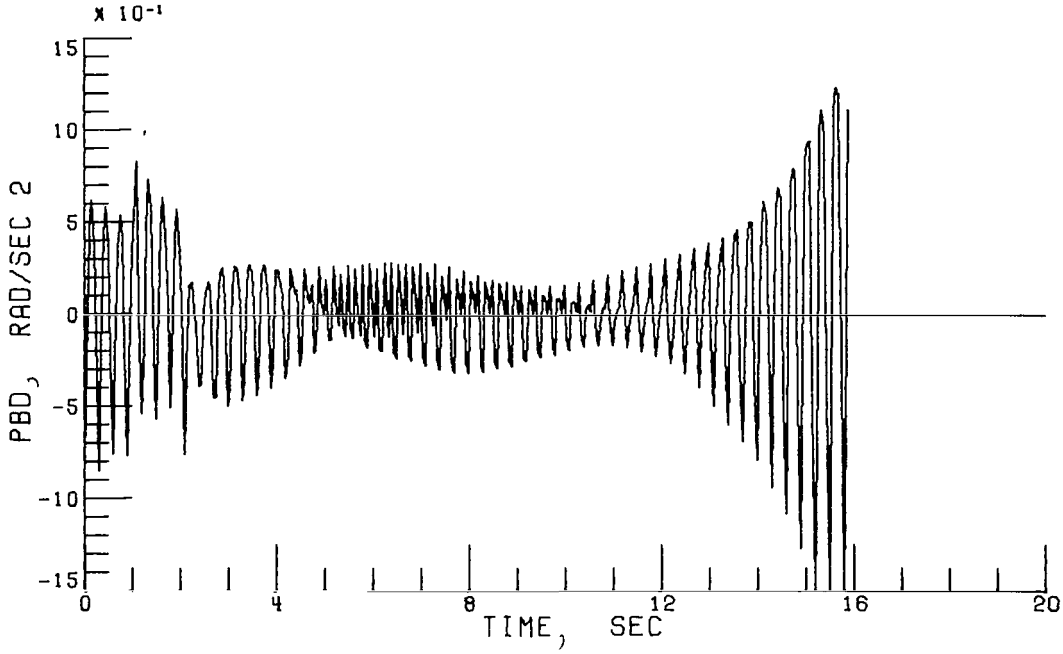

(a) 5b × 5s rotor; 1/20 second.

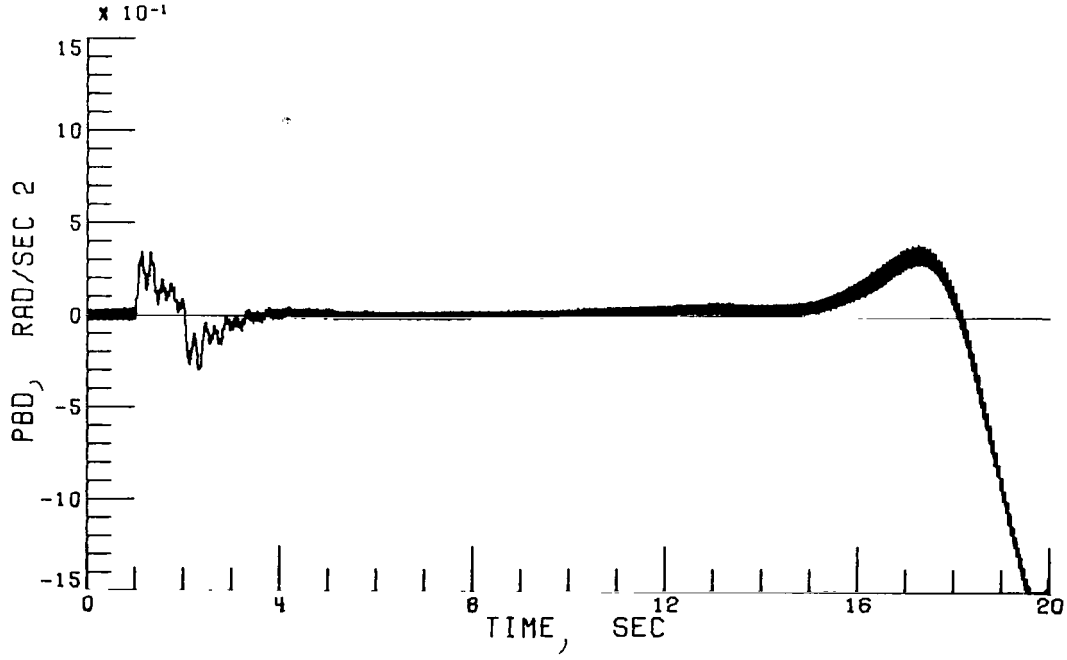

(b) 5b × 10s rotor; 1/240 second.

Figure 18.- Effect of increasing integration interval to 1/20 second on vehicle dynamic response of 120 knots for a five-blade—five-blade-segment rotor compared with the five-blade—ten-blade-segment baseline rotor with an integration interval of 1/240 second.

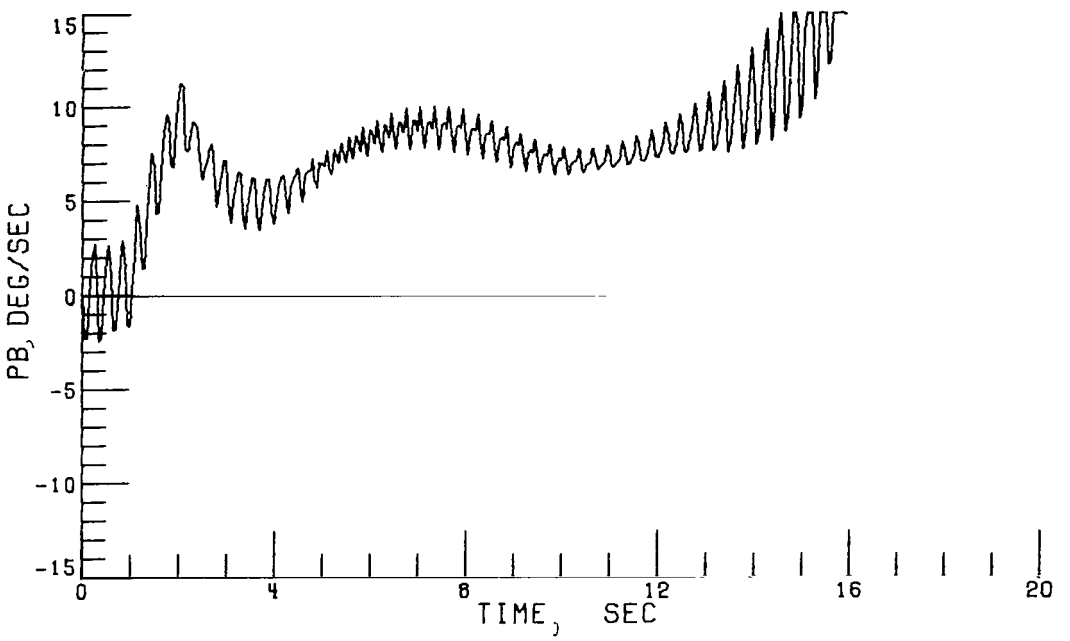

(c) 5b x 5s rotor; 1/20 second.

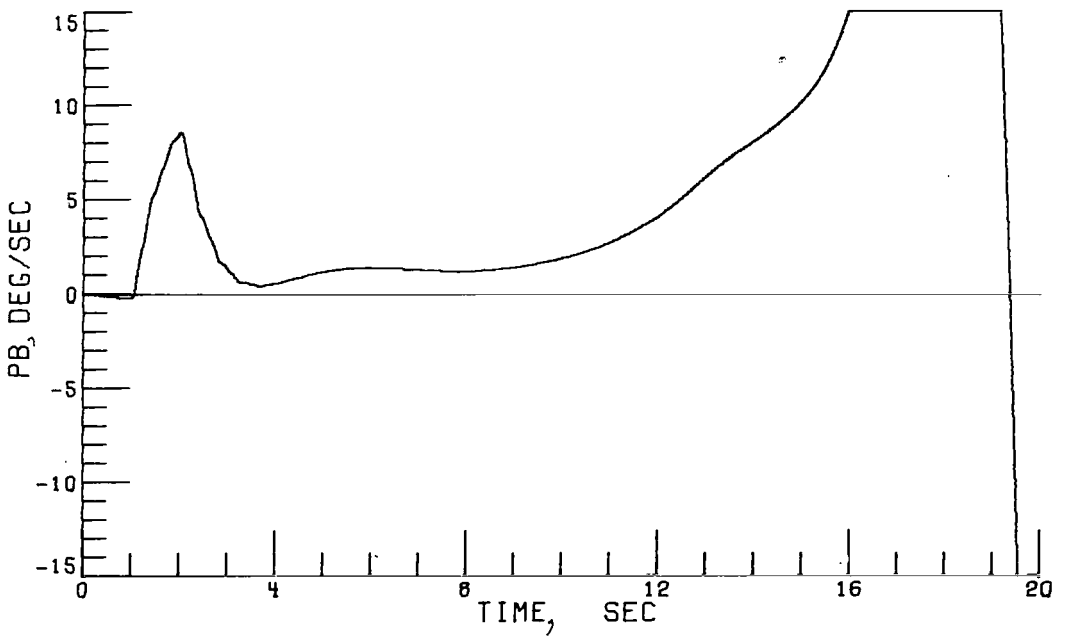

(d) 5b x 10s rotor; 1/240 second.

Figure 18.- Continued.

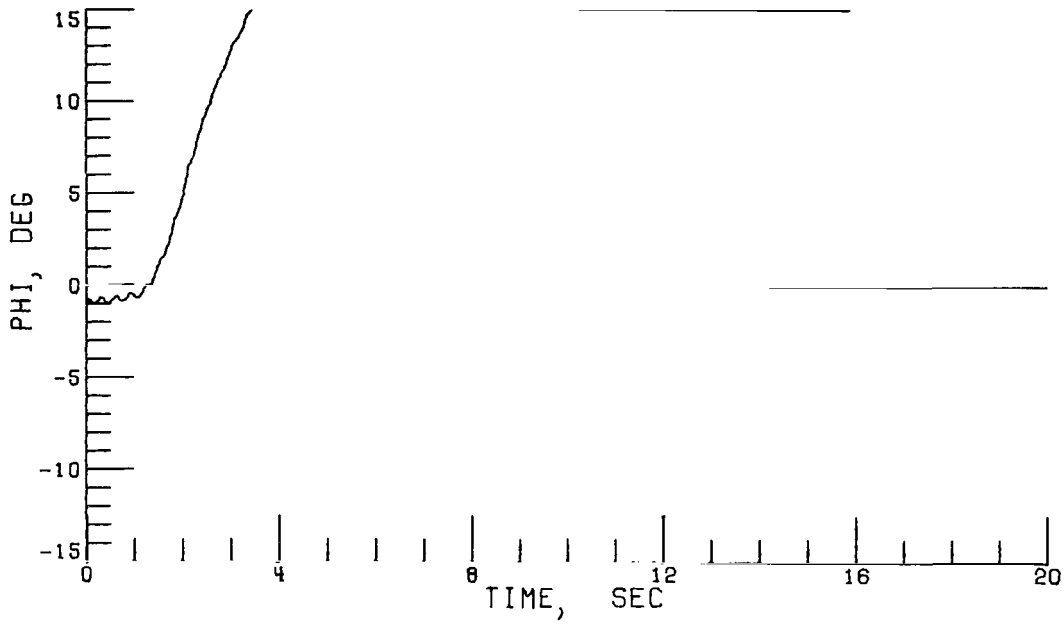

(e) 5b x 5s rotor; 1/20 second.

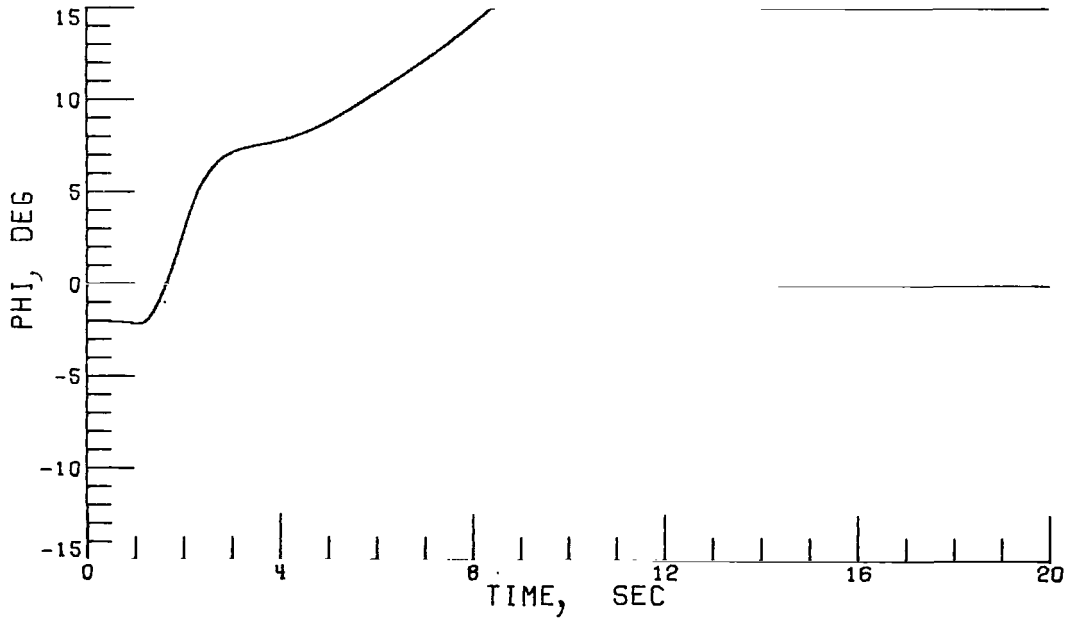

(f) 5b x 10s rotor; 1/240 second.

Figure 18.- Continued.

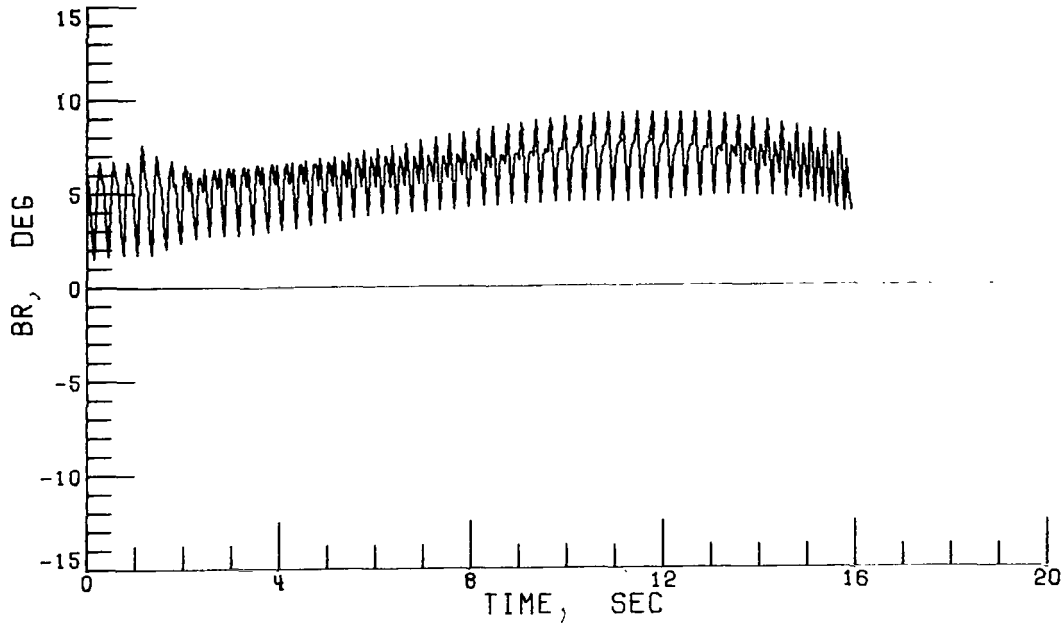

(g) 5b x 5s rotor; 1/20 second.

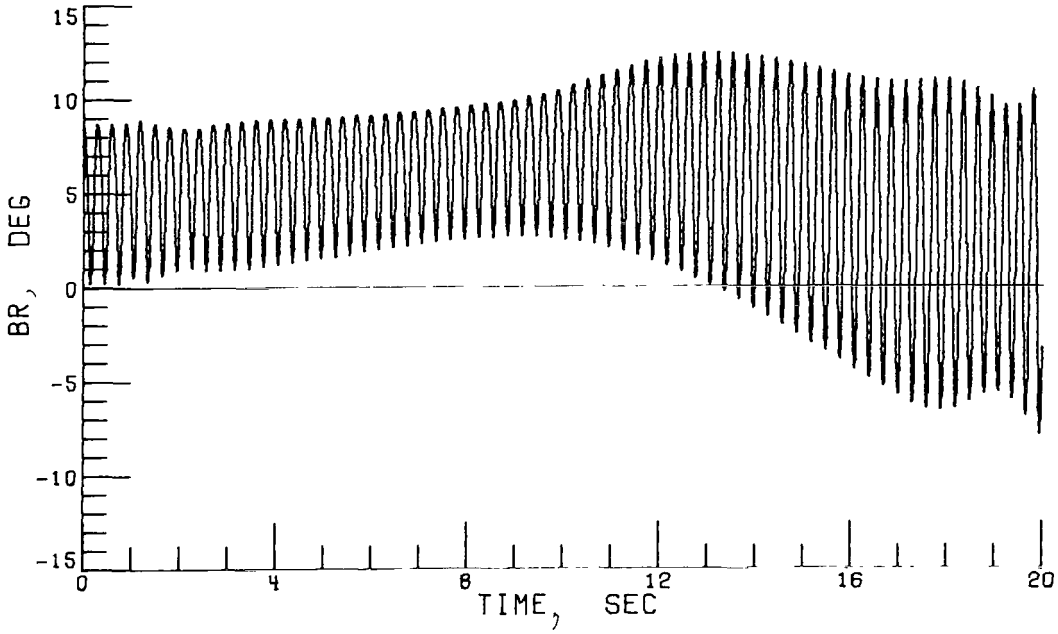

(h) 5b x 10s rotor; 1/240 second.

Figure 18.- Concluded.

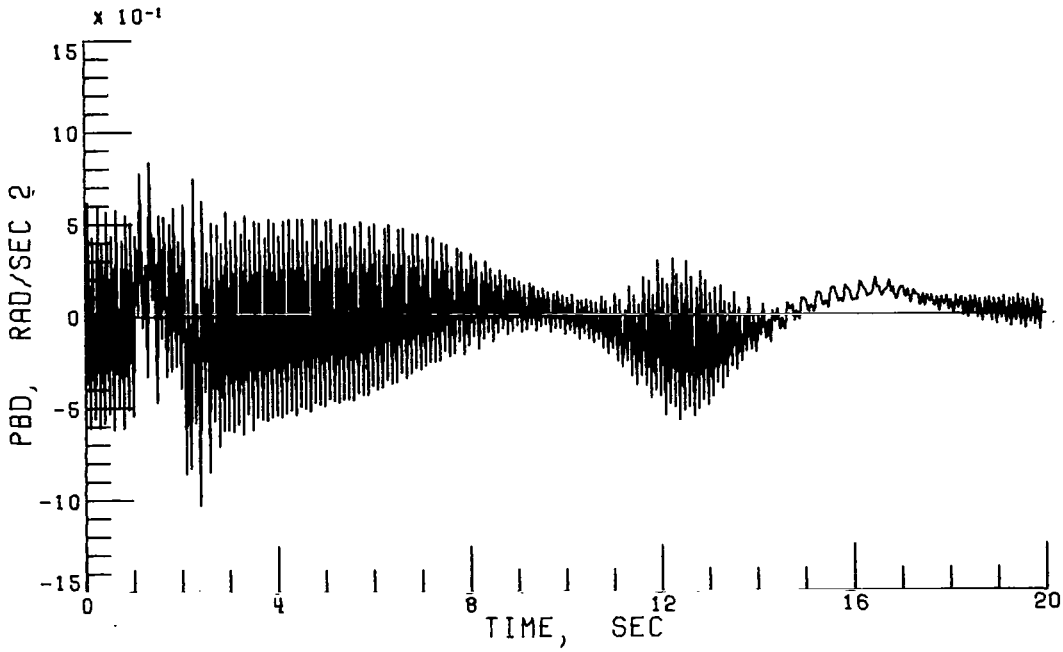

(a) 5b × 5s rotor; 1/20 second.

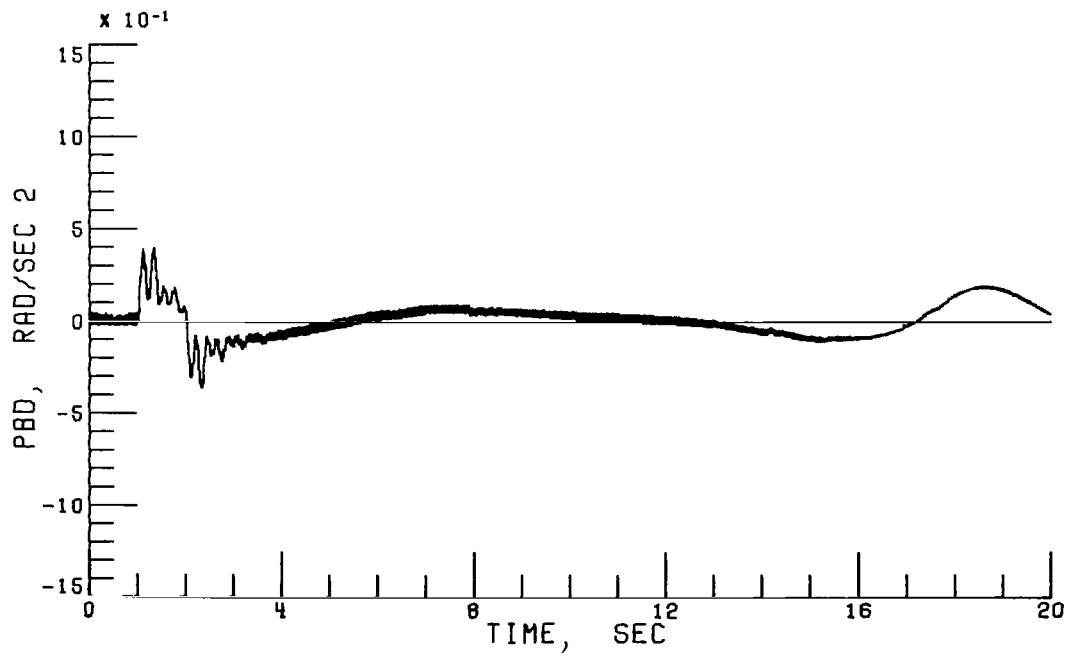

(b) 5b × 10s rotor; 1/240 second.

Figure 19.- Effect of increasing integration interval to 1/20 second on vehicle dynamic response at hover for a five-blade—five-blade-segment rotor compared with the five-blade—ten-blade-segment baseline rotor with an integration interval of 1/240 second.

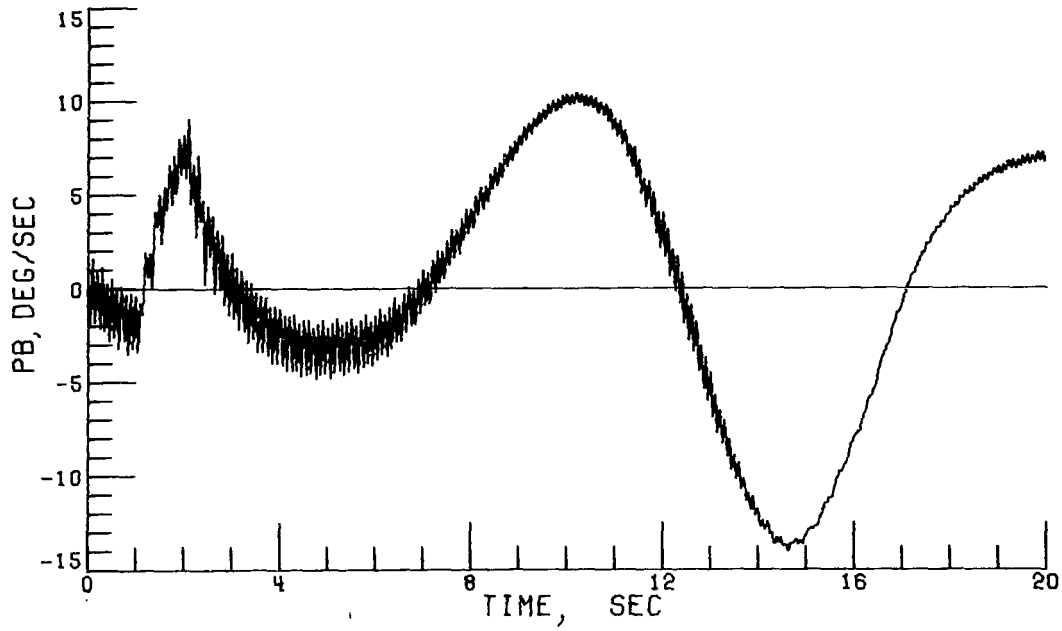

(c) 5b x 5s rotor; 1/20 second.

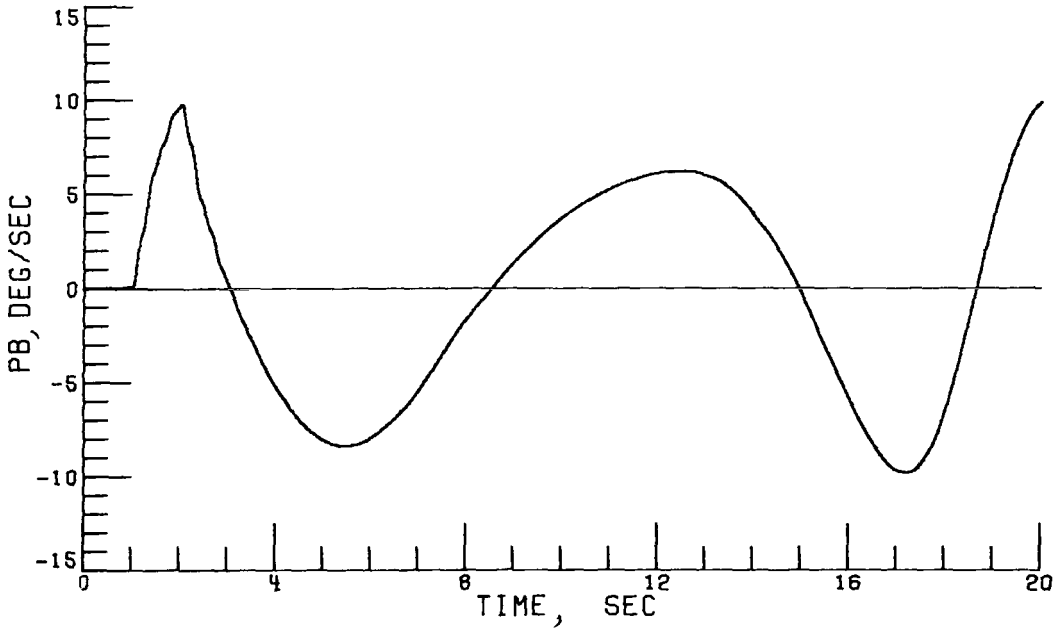

(d) 5b x 10s rotor; 1/240 second.

Figure 19.- Continued.

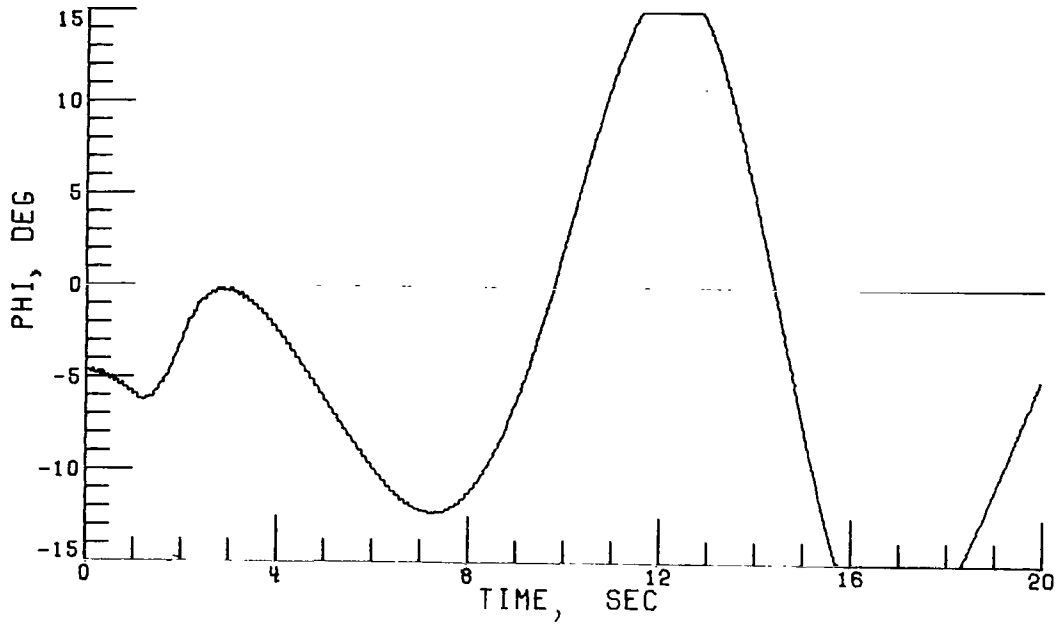

(e) 5b × 5s rotor; 1/20 second.

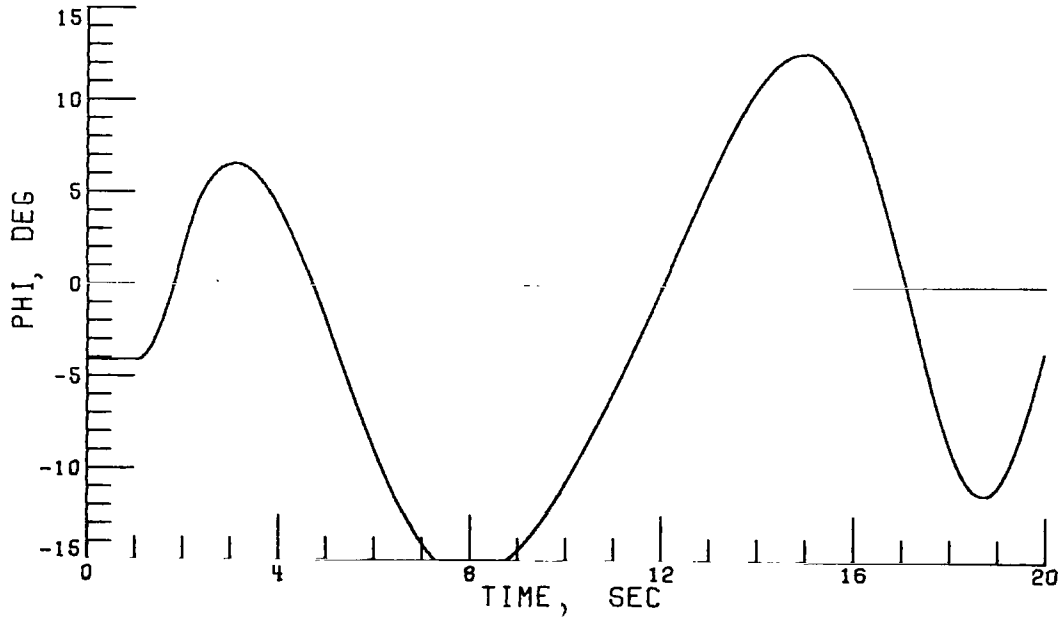

(f) 5b × 10s rotor; 1/240 second.

Figure 19.- Continued.

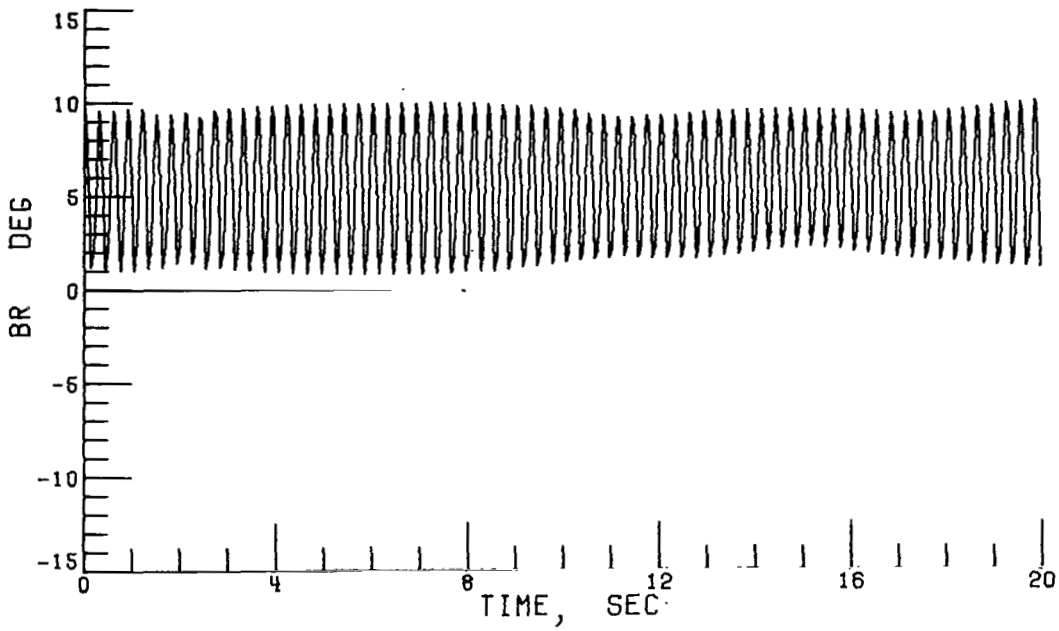

(g) 5b × 5s rotor; 1/20 second.

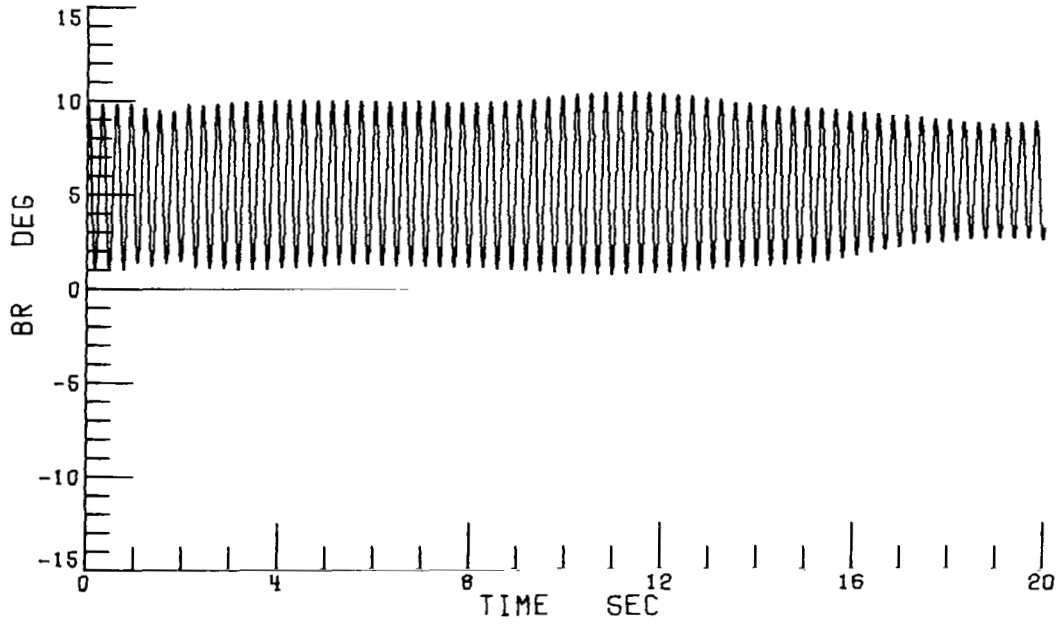

(h) 5b × 10s rotor; 1/240 second.

Figure 19.- Concluded.

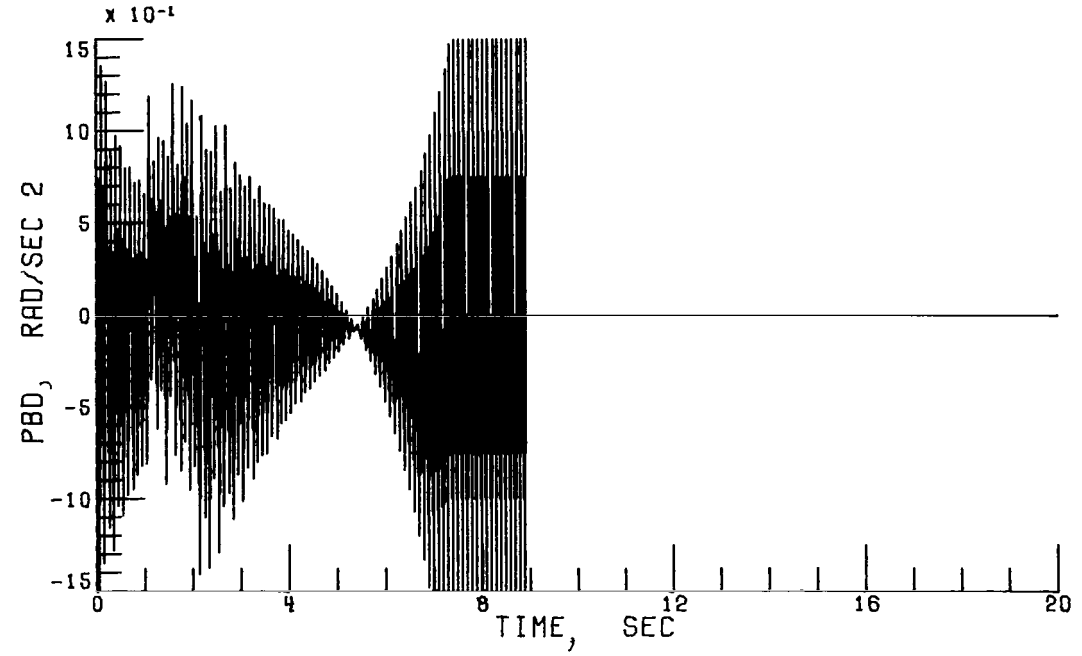

(a) 3b × 3s rotor; 1/20 second.

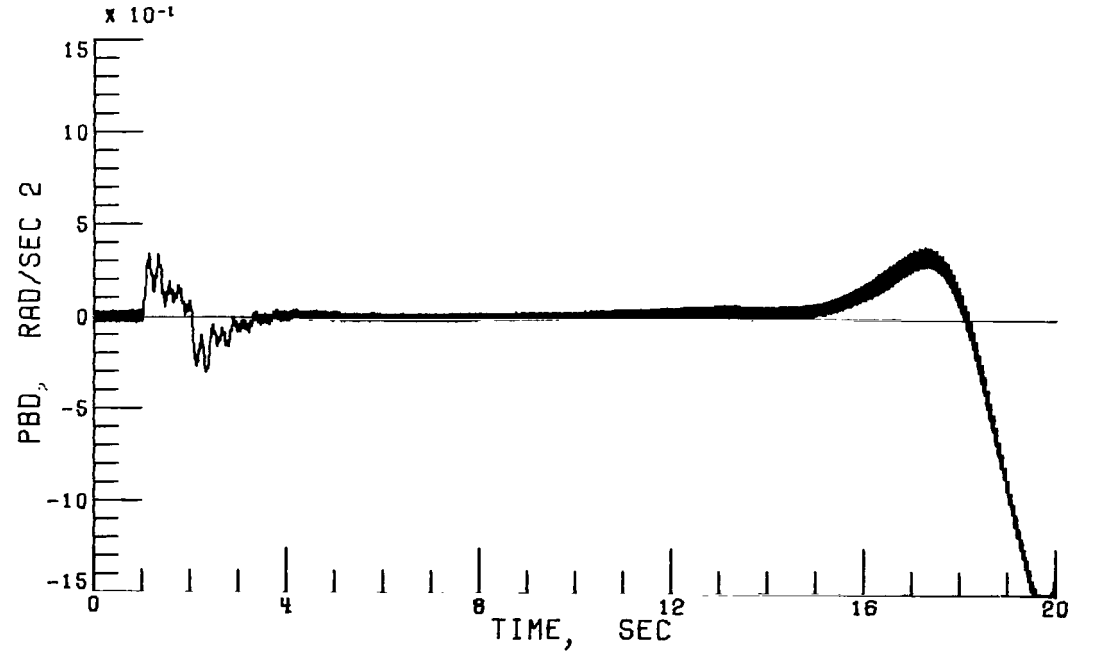

(b) 5b × 10s rotor; 1/240 second.

Figure 20.- Effect of increasing integration interval to 1/20 second on vehicle dynamic response at 120 knots for a three-blade—three-blade-segment rotor compared with the five-blade—ten-blade-segment baseline rotor with an integration interval of 1/240 second.

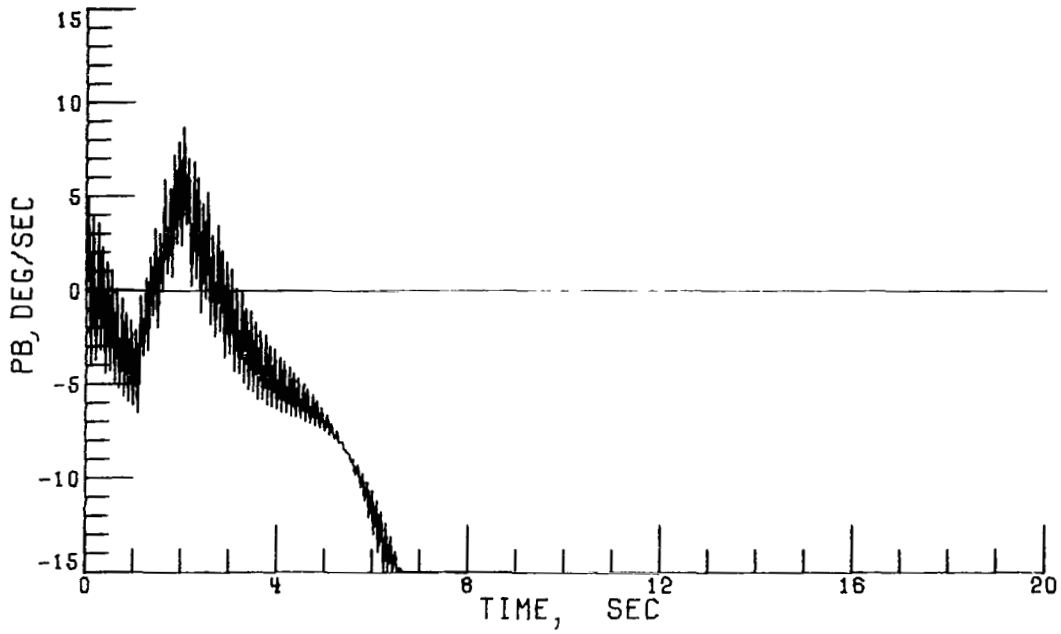

(c) 3b × 3s rotor; 1/20 second.

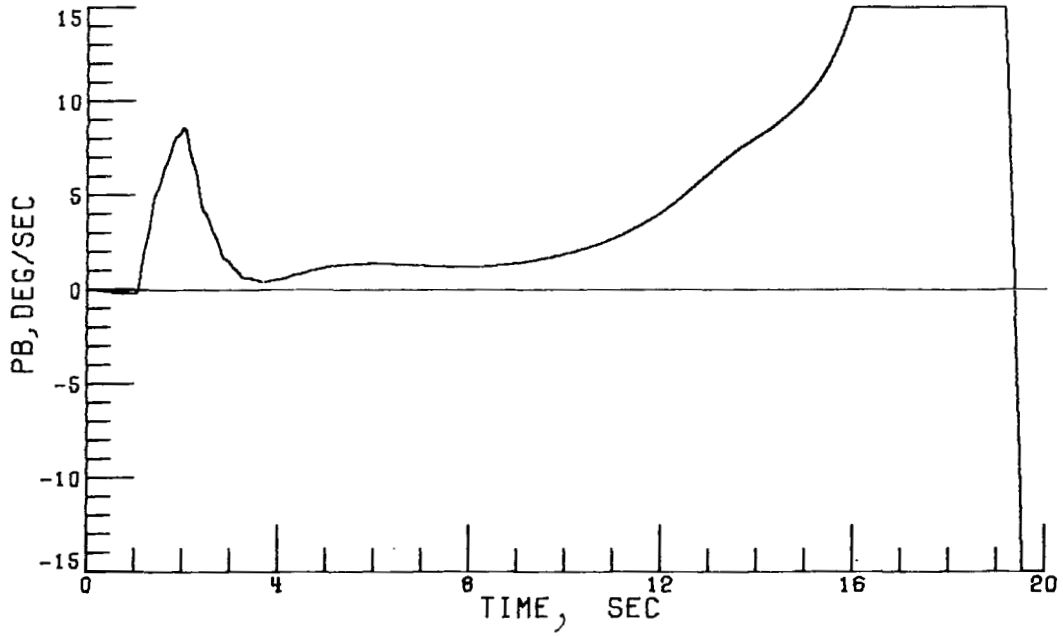

(d) 5b × 10s rotor; 1/240 second.

Figure 20.- Continued.

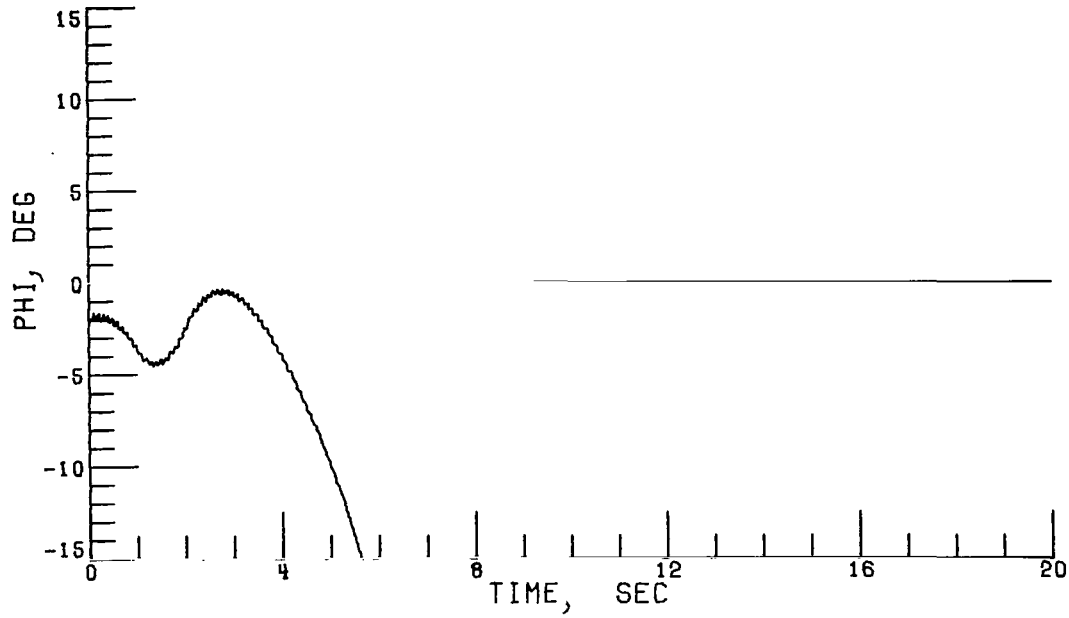

(e) 3b x 3s rotor; 1/20 second.

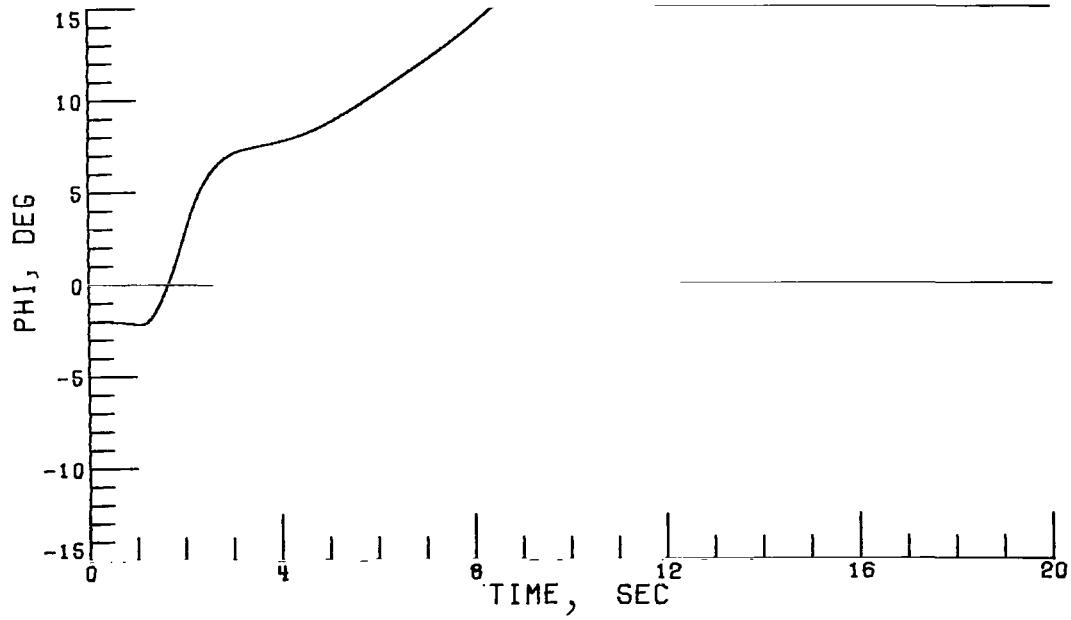

(f) 5b x 10s rotor; 1/240 second.

Figure 20.- Continued.

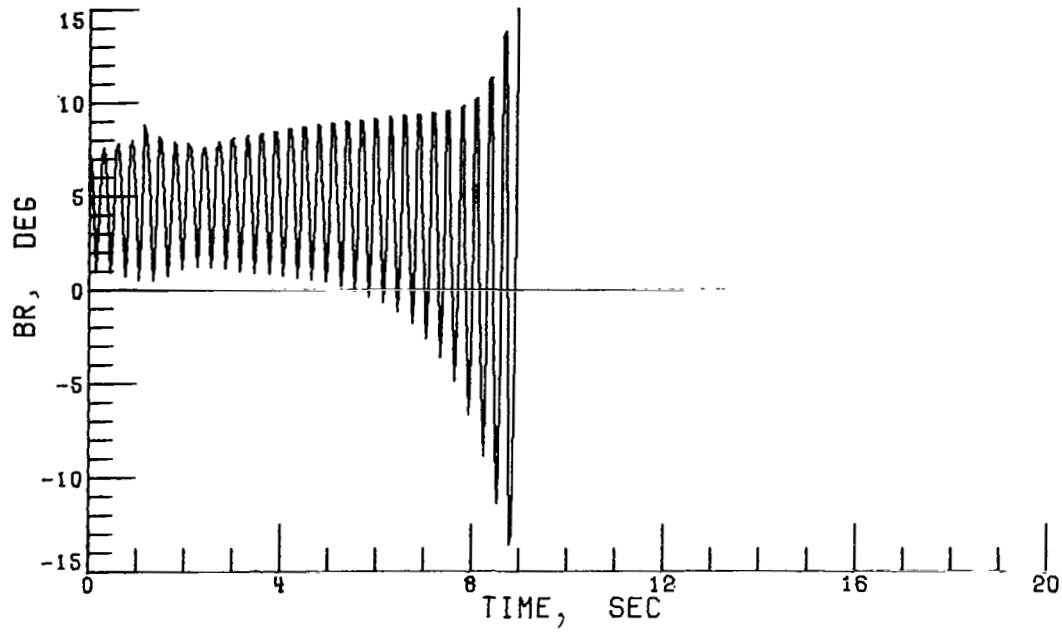

(g) 3b × 3s rotor; 1/20 second.

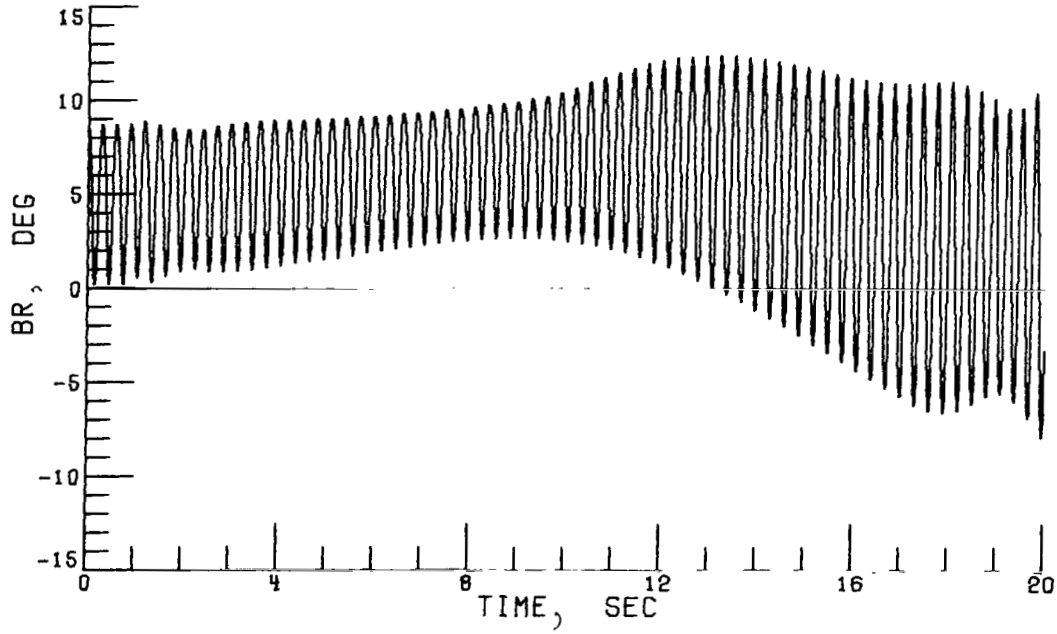

(h) 5b × 10s rotor; 1/240 second.

Figure 20.- Concluded.

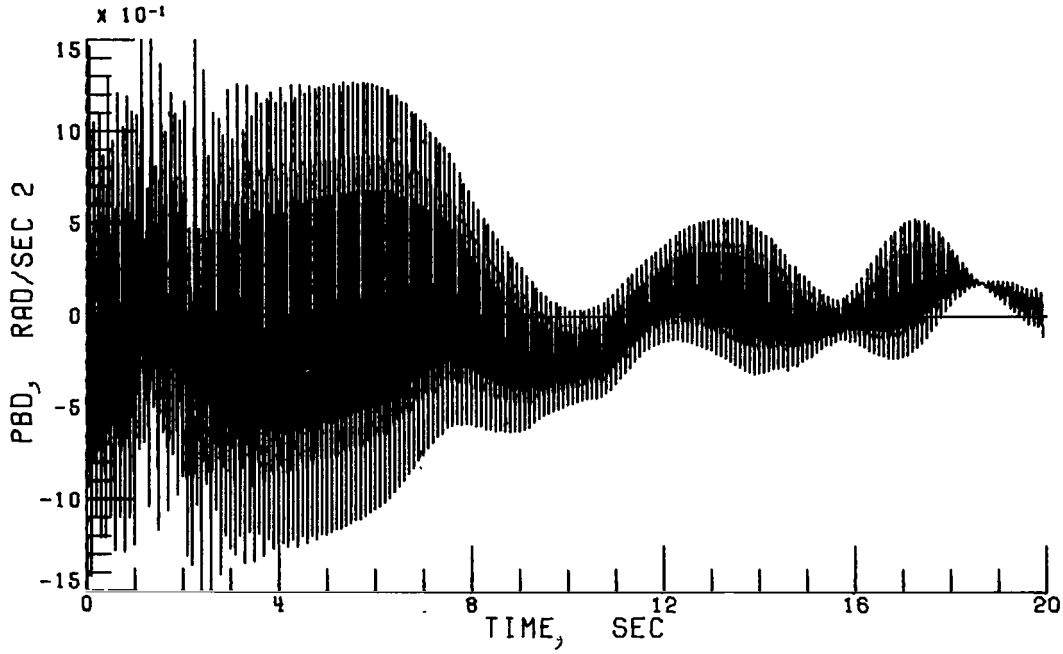

(a) 3b × 3s rotor; 1/20 second.

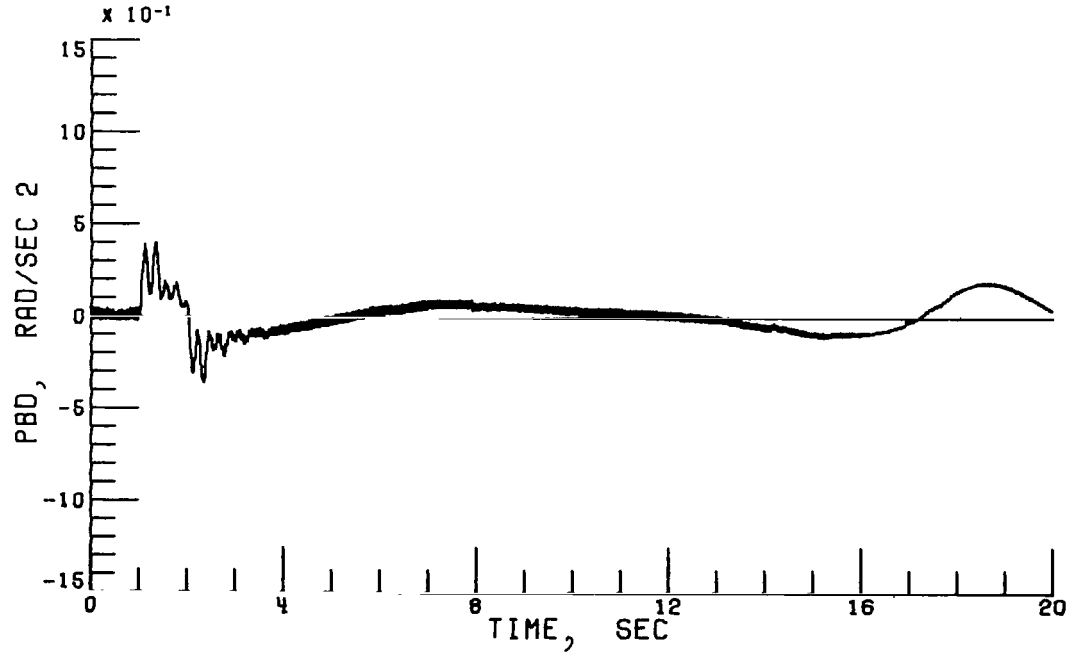

(b) 5b × 10s rotor; 1/240 second.

Figure 21.- Effect of increasing integration interval to 1/20 second on vehicle dynamic response at hover for a three-blade—three-blade-segment rotor compared with the five-blade—ten-blade-segment baseline rotor with an integration interval of 1/240 second.

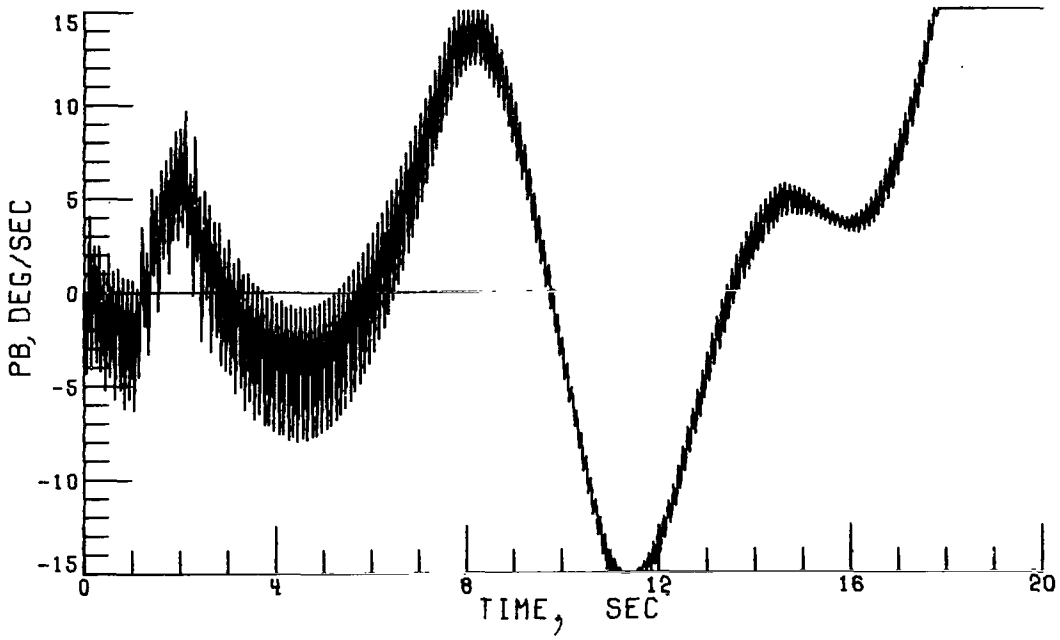

(c) 3b x 3s rotor; 1/20 second.

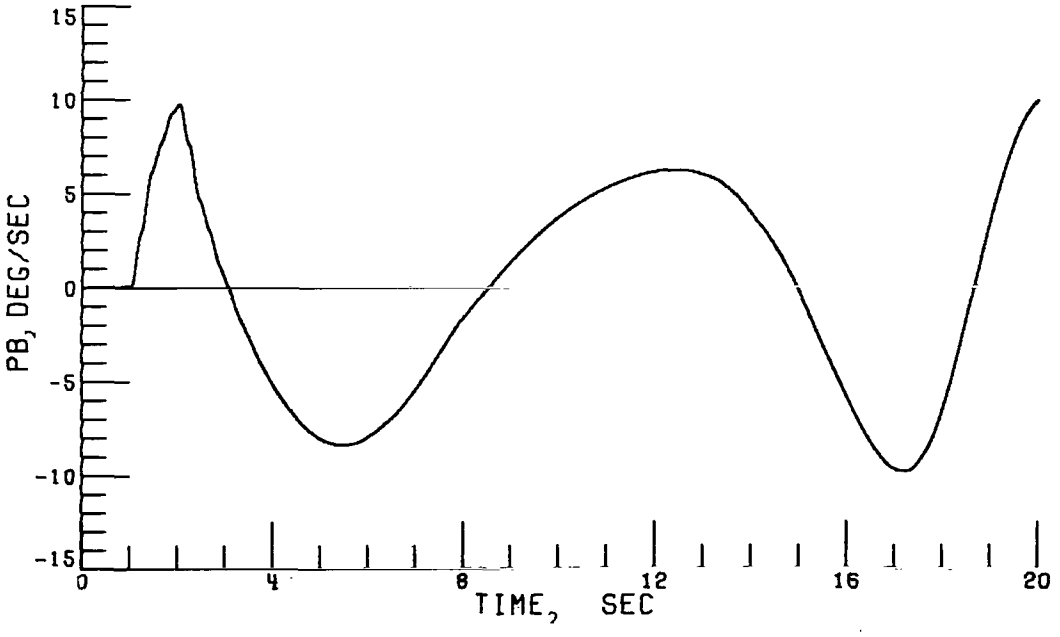

(d) 5b x 10s rotor; 1/240 second.

Figure 21.- Continued.

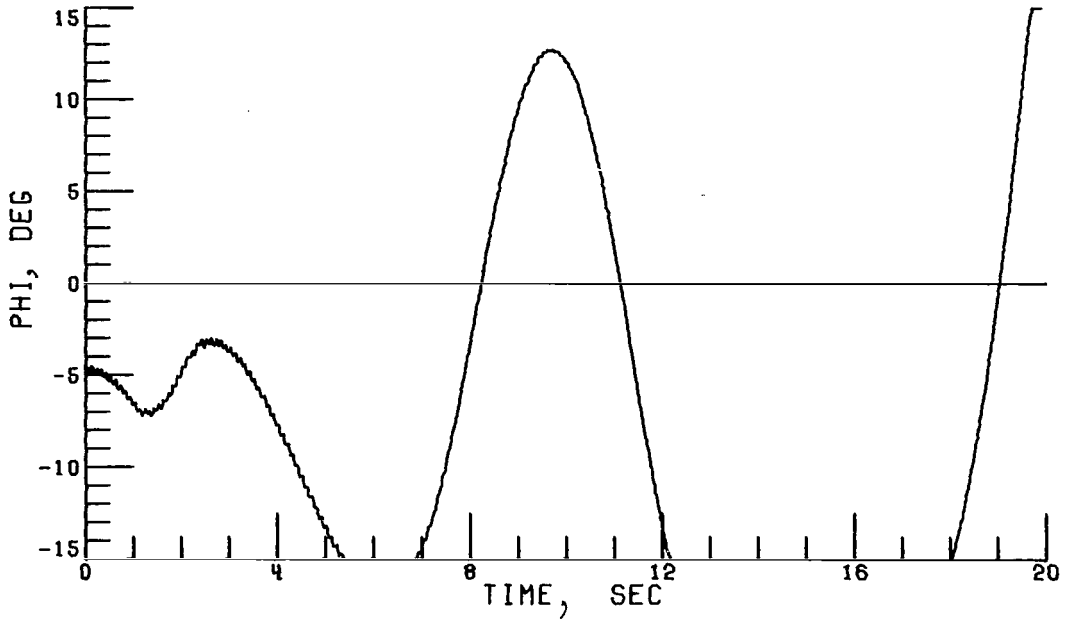

(e) 3b x 3s rotor; 1/20 second.

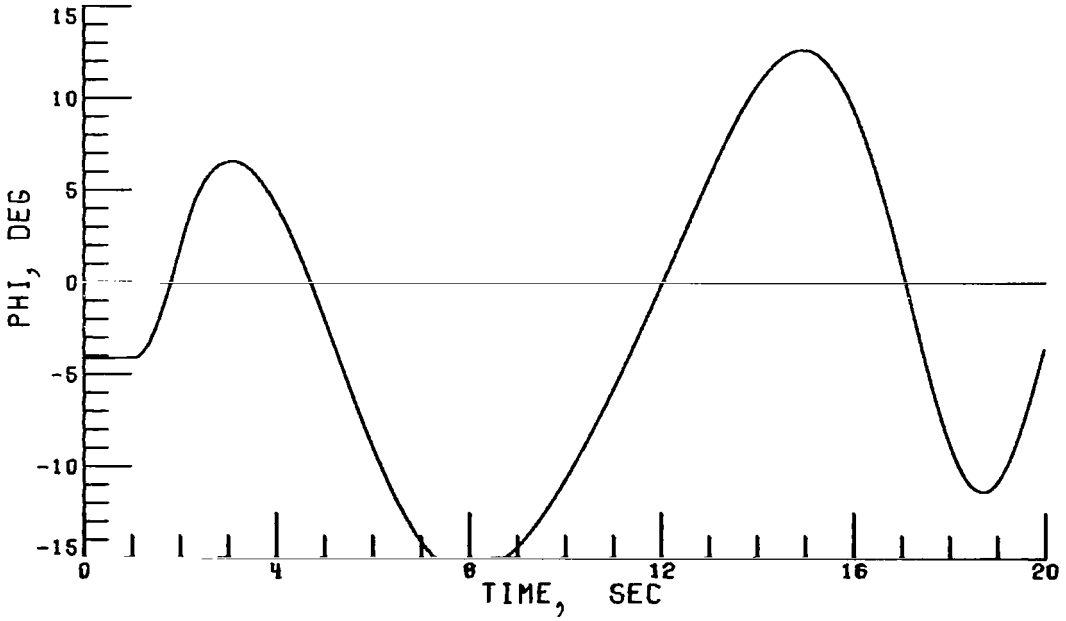

(f) 5b x 10s rotor; 1/240 second.

Figure 21.- Continued.

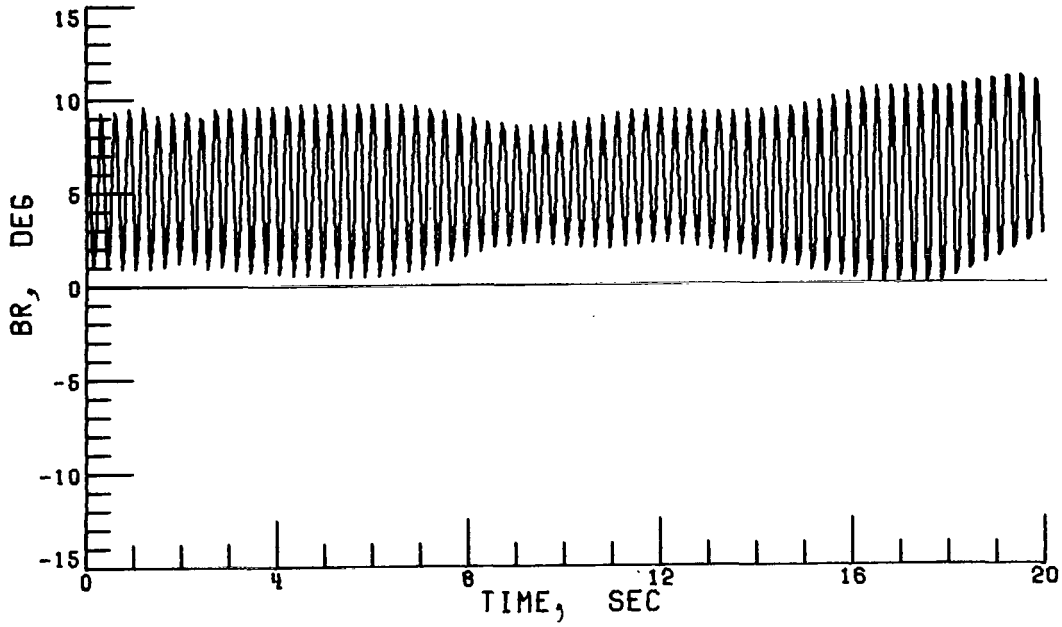

(g) 3b x 3s rotor; 1/20 second.

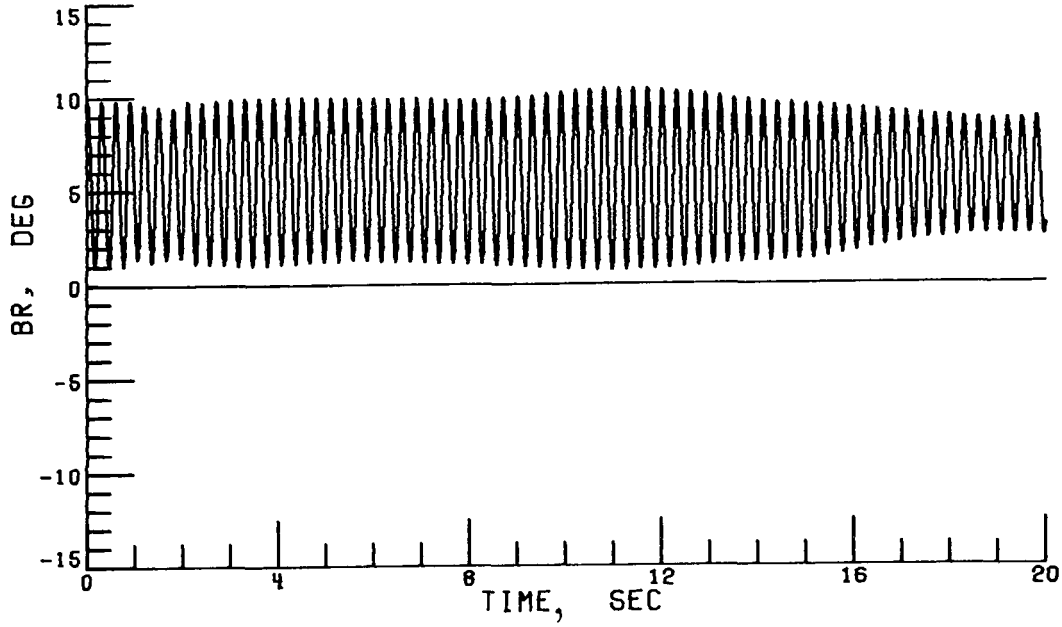

(h) 5b x 10s rotor; 1/240 second.

Figure 21.- Concluded.

NASA-Langley, 1976 L-11083

"The aeronautical and space activities of the United States shall be conducted so as to contribute . . . to the expansion of human knowledge of phenomena in the atmosphere and space. The Administration shall provide for the widest practicable and appropriate dissemination of information concerning its activities and the results thereof."

—NATIONAL AERONAUTICS AND SPACE ACT OF 1958

NASA SCIENTIFIC AND TECHNICAL PUBLICATIONS

TECHNICAL REPORTS: Scientific and technical information considered important, complete, and a lasting contribution to existing knowledge.

TECHNICAL NOTES: Information less broad in scope but nevertheless of importance as a contribution to existing knowledge.

TECHNICAL MEMORANDUMS: Information receiving limited distribution because of preliminary data, security classification, or other reasons. Also includes conference proceedings with either limited or unlimited distribution.

CONTRACTOR REPORTS: Scientific and technical information generated under a NASA contract or grant and considered an important contribution to existing knowledge.

TECHNICAL TRANSLATIONS: Information published in a foreign language considered to merit NASA distribution in English.

SPECIAL PUBLICATIONS: Information derived from or of value to NASA activities. Publications include final reports of major projects, monographs, data compilations, handbooks, sourcebooks, and special bibliographies.

TECHNOLOGY UTILIZATION PUBLICATIONS: Information on technology used by NASA that may be of particular interest in commercial and other non-aerospace applications. Publications include Tech Briefs, Technology Utilization Reports and Technology Surveys.

Details on the availability of these publications may be obtained from:

SCIENTIFIC AND TECHNICAL INFORMATION OFFICE

NATIONAL AERONAUTICS AND SPACE ADMINISTRATION

Washington, D.C. 20546